CHALMERS
UNIVERSITY OF TECHNOLOGY

# Investigation of unintentional island operation during large amounts of inverter based power production

A study of the possibility of unintentional island operation in low voltage networks with large amounts of inverter based power production

Master's thesis in Electric power engineering

Martin Brännman, Emma Stenvall

DEPARTMENT OF ELECTRICAL ENGINEERING

CHALMERS UNIVERSITY OF TECHNOLOGY
Gothenburg, Sweden 2024
www.chalmers.se

Master's thesis 2024

# Investigation of unintentional island operation during large amounts of inverter based power production

A study of the possibility of unintentional island operation in low voltage networks with large amounts of inverter based power production

Martin Bränmman
Emma Stenvall


CHALMERS
UNIVERSITY OF TECHNOLOGY

Department of Electrical Engineering
*Division of Electric Power Engineering*
Chalmers University of Technology
Gothenburg, Sweden 2024

Investigation of unintentional island operation during large amounts of inverter based power production
*A study of the possibility of unintentional island operation in networks with large amounts of inverter based power production*

Martin Brännman
Emma Stenvall



Supervisor: Anders Axelsson, Vattenfall Eldistribution
Supervisor: Mikael Kallin, Vattenfall Eldistribution
Supervisor: Erik Torkildsson, Vattenfall Eldistribution

Examiner: Peiyuan Chen, Associate Professor, Department of Electrical Engineering

Master's Thesis 2024
Department of Electrical Engineering
Division of Electric Power Engineering
Chalmers University of Technology
SE-412 96 Gothenburg
Telephone +46 31 772 1000

Typeset in LaTeX
Gothenburg, Sweden 2024

# Abstract

With increasing efforts to utilize more renewable energy sources, it is becoming more and more popular to install solar panels on buildings and in residential areas. This trend is predicted to continue to grow within the foreseeable future, which brings up questions of how an increased amount of local inverter based power production would affect the contemporary grid and its behavior. There has been concern that an increase of local energy sources, such as solar power, could potentially pose a greater risk of unintentionally transition into island operation if the connection to the utility grid is lost. The aim of this report was therefore to investigate different scenarios in the simulation software Powerfactory and discern the behavior and possible risk of unintentional island operation in different grid models with varying amounts of photovoltaic (PV) modules. All PV modules connected to the Swedish electrical power grid must comply with standards and regulations and their inverters must contain the proper unintentional island protections. The inverter protections come in forms of passive, basic monitoring, protections and active ones, which actively tries to perturb the grid in order to detect islanding events.

This thesis work was conducted by building four different grid models in Powerfactory. The grid models consisted of low voltage grids with varying amounts of PV modules, loads and cables, connected to an external grid which would be disconnected in order to simulate an islanding event. Each model was tested for different potential islanding events on the low voltage side while monitoring voltage, current and frequency values. The protection activation time to detect the potential island was also monitored in seconds, where protection triggers above five seconds were regarded as insufficient detection. For one of the models, a non-detection zone was established in order to visualize the detection limits. From the different grid model behaviors, it was concluded that detection capabilities of the inverter protection was highly dependant on the load imbalance. The reactive power mismatch had a much lower threshold compared to the active power, resulting in a very narrow non-detection zone in regard of reactive power compared to the much higher threshold values of active power in said non-detection zone. It was also concluded that there is not much readily available information about the active inverter protection schemes and further investigation about how they interact with the passive protections are needed.



**Keywords**: Photovoltaic inverters, Anti-islanding protection, Inverter protection, Inverter functions, Island operation, Island protection, Unintentional island operation, Unintentional islanding.

# Acknowledgements

We would like to thank our supervisors Anders Axelsson, Erik Torkildsson and Mikael Kallin at Vattenfall Eldistribution for all of their help, expertise and guidance throughout our Thesis work. We enjoyed every meeting and discussion we had at the office with you guys, hope you found it as giving and enjoyable as we did! It goes without saying that this work would not have been possible without you!

We also want to extend our thanks to our examiner Peiyuan Chen, we would have been lost without the valuable support in PowerFactory you provided. Thank you for all of the supervision and help progressing our work. You have our sincere gratitude for all the help in troubleshooting our models and answering to all our panicked emails.

Additionally, we want to thank Arne Berlin at Vattenfall for meeting with us and discussing island operation and the project in general. It provided valuable insight and perspective we could use in our discussion material.

Another person deserving our gratitude is Thorbjörn Thiringer, thank you for giving us remote access to the computer we run all our simulation work on! It made our day-to-day more flexible, as we could perform the work both in Gothenburg and Trollhättan.

Last but not least, we want to express our thanks to David Frisk, and in extension Magnus Gustaver and Kyriaki Antoniadou-Plytaria. Who's LaTeX Thesis template and add ons to said template made our report writing a lot easier and less stressful.

Martin Brännman & Emma Stenvall, Gothenburg, June 2024

# List of Acronyms

Below is the list of acronyms that have been used throughout this thesis listed in alphabetical order:

| | |
|---|---|
| AC | Alternating Current |
| AFD | Active Frequency Drift |
| DC | Direct Current |
| DG | Distributed Generation |
| DER | Distributed Energy Resource |
| HV | High Voltage |
| LV | Low Voltage |
| MV | Medium voltage |
| MG | Microgrid |
| NDZ | Non-Detection Zone |
| OUV | Over and Under Voltage |
| OUF | Over and Under Frequency |
| PCC | Point of Common Coupling |
| PI | Proportional-Integral |
| PLL | Phase-Locked Loop |
| p.u. | Per Unit |
| PV | Photovoltaic |
| RES | Renewable-based Energy Sources |
| RfG | Requirements for Generators |
| RMS | Root Mean Square |
| ROCOF | Rate of Change of Frequency |
| RPV | Reactive Power Variation |

# Contents

# List of Figures

# List of Tables

# 1
# Introduction

## 1.1 Background

As we are moving towards a more sustainable future, it is becoming increasingly popular to install and utilize solar power. In some cases it is done in combination with energy storage technology, which can range from a few kilowatt (kW) to many megawatt (MW). According to *Energimyndigheten*, there were approximately 252 000 solar cell installations connected to the Swedish electricity grid by the end of year 2023 [1]. Energimyndigheten states that the total sum of installed solar power amounts to roughly 4 000 MW, which corresponds to 3 TWh, and that their short-term prognosis predicts that solar power will amount to 9 TWh by year 2027. This indicates that the steady rise of solar cell installations will continue for a foreseeable future. Which in turn can bring up questions of how this trend will change and affect our contemporary electricity grid.

When it comes to connecting the power park modules to the grid, some suppliers can be rather short in the description of how the equipment behaves and operates against the network. This could become problematic in networks with large amounts of inverter based power production, such as solar power. A risk lies within the possibility of unintentional island operation of parts of the network, where the local energy resources continue to energize the system after being disconnected and isolated from the distribution grid. Events of unintentional island operation can be harmful to equipment due to the uncontrolled and potentially unacceptable voltage and frequency values provided by the local energy source without the connection to the main power grid. This can also represent a hazard to people in the close vicinity who are unaware of the energized parts of the system.

## 1.2 Purpose and Aim

The purpose of this thesis work was to investigate the protection schemes within the grid connected inverters meant to detect and prevent unwanted island operation of Photovoltaic (PV) modules in the low voltage (LV) grid. By using Digsilent simulation software *Powerfactory*, the anti-island protections included in the PV inverters' designs were investigated and tested for different grid model scenarios. The different scenarios of interest included a residential area on the LV grid side with only a few inverters included, and a grid situation favorable for island transitioning with many inverter based generation sources. Other points of interest included

bigger areas of unwanted island operation and their respective behavior. Such as bigger potential islands which encompass more than just the LV grid equipment, for example a medium voltage (MV) cable. The distribution grid in the simulation was to be disconnected after a hypothetical fault in order to check if the existing anti-island protection was sufficient enough to detect the problem, or if said network would start to transition in unwanted island operation undetected. The aim of this thesis work was to gain and provide insight into how plausible the risk of a network to enter unintentional island operation is and how resilient the inverter's base protections are against said event. The study is meant to reflect upon the possible risk of unwanted island operation connected to inverter based generation and to contemplate whether additional protection or precautions are required.

## 1.3 Scope and limitations

The scope of the thesis was limited to investigate three phase inverter functions within the LV grid and/or with some elements from the higher nominal voltage areas. All generation modules were present and inspected within the LV grid. Effectively, the MV grid was not seen as the primary focus of this study. Therefore all PV modules were set according to the Requirements for Generators (RfG), type A, since they only were present in the LV grid and no regulations for the higher voltage and power ratings were applied. All inverters were assumed to correspond to and exist on the "Rikta Rätt" list, meaning that they comply with the requirements of the Swedish power grid. Inverter information and functions were only gathered from manufacturers and sources providing reliable and easily accessible information. In addition, the investigation only considered inverter functions of PV-modules and not that of other generating modules in the area (such as wind power).

The thesis did not investigate the option of black start, as black start is more planned and can not be regarded as unwanted island operation in the same sense. Only disconnections that could create unplanned islanding scenarios were taken into consideration. All tests within the simulations models assumed the external grid would be disconnected due to some opening of a breaker, a three-phase disconnection upstream, in order to observe potential island behavior. Potential islands forming due to other faults were not investigated, due to the point of interest lying within the question of disconnections at specific locations in the grid. The scope did not include faults occurring after or within the potential island as a whole. As the primary focus of the study was to see if the system could transition into unwanted island operation, and not to prolong or assure stable island operation thereafter.

Some of the limitations of this study include modifications of the pre-existing simulation model for anti-islanding protection. A pre-defined Powerfactory model containing the basic anti-islanding protection schemes of voltage, frequency and overcurrent was chosen in order to adapt the functions into other network structures of interest and to avoid building an entirely new model from scratch. Meaning that the more complex protection functions of the inverters, active protections, could not be included in the simulation model due to lack of time. Including the active protection

schemes in the model would have required a significant amount of practice within Powerfactory's own programming language to build new protection functions from scratch. As well as finding manufacturing sources that state exactly how long operation delay the different active protections generally have. Searching via the inverter manufacturers' documentations for operation times and more in depth descriptions of specific active protections didn't provide the necessary insight into their design to be able to incorporate their functions in the simulated environment. Other limitations regarding the simulation is the pure computing capacity needed to simulate the more complicated grid models. Performing tests and simulating around 70 PV inverter modules all with their own protection schemes proved to very time consuming. Spanning from a couple of minutes to a couple of hours of simulation time in order to process more than a couple of seconds of operation. Which meant each test within the more complex simulation models had to be chosen with care in order to progress the work on schedule. This is also the reason why the biggest possible step size within the simulation was used, 0.01 s, in order to reduce computing time. Smaller step sizes added unnecessary simulation time and data points for results that were only studied by three decimals either way, and step sizes bigger than 0.01 s could not converge within the model. Additionally, all the PV-units used in the simulation model were rated with power factor 1 assuming that they provide no reactive support in the LV grid. This assumption was done due to the lack of mentioning of allowed possible reactive support functions in any of the Swedish regulations and settings.

## 1.4 Disposition

The report is divided into four main chapters following the first Introduction chapter containing the general outline of the report. The second chapter is denoted Theory and it contains information about different types of PV inverters, their functionalities and important concepts. The Theory chapter then introduces and explains the general terms and the functions of island operation and protections against unwanted islanding. Lastly, the chapter introduces important regulations and specifications used for operation within the Swedish electricity grid.

The third chapter is the Method chapter, explaining reasoning behind the work and its execution. The Method chapter starts of a description of the Literature study and collection of all the sources used in the Theory chapter. Then it explains the Simulation work, the pre-existing simulation model provided by Digsilent's Powerfactory help and discussion board. The pre-existing converter function and its protection schemes are explained, followed by the explanation of the load setting used for all loads in the models. The basic protection functions were then implemented into each test model. There is a total of four models used, and all of the tests performed in each model are thereafter explained under their respective heading. The first model called 'Basic grid' is based upon the set-up provided by the Powerfactory test model. The second grid model is called 'LV-grid' and is based upon an example of a residential area in the LV grid with corresponding house loads and characteristics. The two remaining models are called 'PV-grid', which was an extension of the

'LV-grid' with more PV-units, and the 'MV cable model' which was an addition on the PV-grid.

The fourth chapter is the Results of all of the tests, once again listed in model order with all of the tests listed under the respective model. Finishing off the report with the Discussion and Conclusion of the study. Appendix A Inverter settings, describes inverters available on the Swedish market and their accompanying protection descriptions. Appendix B Settings, explains settings used in the respective simulation models. And Appendix C is a collection of collected results that are shown in the Result chapter in a more presentable form, for example in a summary table or figure.

# 2

# Theory on inverters and islanding with accompanying regulations

## 2.1 Inverters and inverter functionality

The main purpose of a solar inverter is to convert the DC current produced by the solar panels into AC current, which is used in the electrical grid and in our homes [2]. When it comes to houses or residential buildings, there are four main types of solar inverters [2],[3]. These four types are:

- String inverters
- Microinverters
- Power optimizers
- Hybrid inverters

A string inverter is an inverter which is connected to solar panels connected in series, also called strings. Each string can consist of between six and 20 solar panels, and for installations which are below 20 kW in size, the amount of strings are usually between three to nine [2]. Because of the fact that the solar panels are connected in series, they can all be treated as one unit and this means that anything that reduces the power output for a single panel will heavily impact the power output of the entire string [3].

Microinverters are usually connected to individual solar panels, but can in some cases be connected to multiple ones. When microinverters are used, all solar panels in the installation are usually equipped with their own microinverter. These inverters can also perform power optimization, just like the power optimizers [2].

Power optimizers optimize the power that can be gained from the solar panels. When the power optimizers are utilized, the inverter itself focuses only on converting DC to AC, while the power optimizer handles how the solar panels perform. Some inverters are constructed in a way that they require power optimizers in order to work as intended, but that is not the case for all types. It is only string inverters that utilize power optimizers, as microinverters can do it on their own. However, even if the inverter is not designed to be used alongside a power optimizer, it can usually still be used with one [2].

Hybrid inverters are able to handle the conditions for storing energy in an energy storage unit such as a battery. With a hybrid inverter, there is no need to use

a rectifier in order to store the energy from solar panels, but it is mostly required when string inverters are used [2]. They can also determine how to use the generated power, if it should be sent to the grid, be stored in a battery or be used to power the residential building it is installed on [3].

The first three of these inverter types are also known as "grid-tie" inverters, which means that they are connected to the grid directly [4]. In order to connect to the grid, the inverter needs to operate synchronously with the grid itself. If the inverter detects that the grid has disconnected, it should also disconnect itself as a safety measure [2].

There are two larger categories which inverters are split into. These are grid following, or as previously mentioned grid-tied, and grid forming. Grid following inverters are the most common type of inverter, and can be seen as a current source which relies on the grid to provide a reference point for frequency and voltage [5]. In order to know whether to absorb or inject active and reactive power into the grid, they monitor the magnitude and power angle of the grid. It does this through the use of a phase-locked loop (PLL) [6],[7], which is a system where the output frequency of a signal is compared with the input signal through a negative feedback loop [8]. When the phase difference is zero between the output and input signal, the loop is phase-locked, hence the name. A dual second order generalized integrator (DSOGI) based structure is commonly used for three-phase synchronization, since it also allows for a ready estimation of symmetric components and dampening of the low-order voltage harmonics [9]. Alongside this, a synchronous rotating frame PLL (SRF-PLL) is also used. The instantaneous phase angle can be detected if the rotating frame is synchronized to the grid voltage vector [10].

Grid forming inverters are inverters which can regulate voltage and help support the grid frequency [5], in essence behaving like a voltage source [6]. Depending on how the grid is constructed, the grid forming inverter can operate in a number of different ways, including as a virtual synchronous machine or as droop control [5]. They can also operate on their own, without the support of the grid or an external voltage source. In this category, hybrid inverters and battery inverters can be placed, although these types can usually also operate in grid following mode. A battery or some other kind of energy storage would be required for operating in grid forming mode.

Grid forming inverters are in general more expensive and more technically complicated than the grid following inverters, and are relatively new to being implemented [5]. As the grid forming inverters are a new concept, the regulations have yet to fully define the requirements for them. There has been suggestions proposed for extra regulations of grid forming inverters, amongst them the ability to deactivate and activate the grid forming capabilities and whether or not it should be mandatory for generators of different size classes [11]. Other important factors to establish when it comes to grid forming inverters are simulation models to study behavior, further development of islanded systems, and the further definition of terminology [12].

Besides the different inverter types, there are also many different inverter manufacturers active on the market. Some of the companies selling inverters for PV-modules in Sweden include Ferroamp, Fronius, GoodWe, Growatt, Huawei, Kostal, SMA, SolarEdge, SolaX Power, Solis, Sungrow and Victron Energy [2], [13]. Inverters come in different types and sizes, but also with different protections schemes included in their core design. A short summary of different three-phase PV inverters sold on the Swedish market can be found in Appendix A presented in Table A.1, including their rated powers and protection schemes. Note that the two standards IEC 62116 and EN 62116 are not mentioned in section 2.4 below, even though they are mentioned in the Table A.1, this is due to the fact that they are outside the scope of this report. IEC is the global international standard, EN is the European, and 62116 is the name for a specified test of anti-islanding protections standard for PV inverters. Which describes a physical test procedure for the equipment.

## 2.2 Islanding

The phenomena of islanding occurs when a portion of a network is disconnected from the larger power grid, but has enough production inside of the newly formed islanded section to remain energized after the disconnect. If an islanding event occurs unplanned, it could result in hazardous consequences for both connected equipment and people unaware of said energized section. The distributed energy resource (DER) that keeps energizing the system during an island event may be unable to uphold acceptable voltage or frequency values without the distribution grid, and thus harming connected equipment as a result.

Unintentional island operation of utility-interactive PV inverters can be caused by several conditions, as listed by [14, p. 12]:

- Fault detected by the utility, resulting in opening a disconnecting device, but goes undetected by the PV inverter or protection devices.
- Equipment failure resulting in accidental opening of a disconnecting device.
- Utility switching of distribution system and loads.
- Human error, action with malicious intent or act of nature.

During assessment of unintentional islanding risks of DERs, the risk can be ruled out in three cases as listed by [15]. The first case includes when the aggregated AC rating of all distributed generation (DG) in the potential island amounts to less than some fraction of the minimum real power load inside the potential island. Secondly, when the reactive power supply and demand in the potential island can't be balanced. Lastly, the risk can be ruled out in case of implementation of communication based protection, specifically direct transfer trip or power line carries. However, [15] also mentions cases where the risk of unintentional island operation may merit additional studies. These cases include when the potential island contains large capacitors, while the potential island is tuned such that the power factor is close to 1.0. The other cases include instances when the potential island include a large number of inverters, or a mix of inverters from different manufacturer, or both inverters and

rotating generators.

In order to evaluate whether or not the island will be detected, a non-detection zone (NDZ) can be established [16]. The NDZ is defined by the mismatch in active and reactive power ($\Delta P$ and $\Delta Q$ respectively). The total active and reactive power consumed by the load can be described as:

$$P_{Load} = P_{DG} + \Delta P \tag{2.1}$$

$$Q_{Load} = Q_{DG} + \Delta Q \tag{2.2}$$

where $P_{Load}$ is the active power consumed by the load, $P_{DG}$ the active power produced by the DGs, $\Delta P$ the active power provided by the grid, $Q_{Load}$ is the reactive power consumed by the load, $Q_{DG}$ the reactive power produced by the DGs, and $\Delta Q$ the reactive power provided by the grid. If $Q_{Load}$ is equal to $Q_{DG}$, then there is no reactive power mismatch between the DGs and the load, and the same applies to the active power mismatch if $P_{Load}$ is equal to $P_{DG}$. Once the disconnection of the grid has occurred, the active power of the load is forced to become that of the DGs in the island. As the active power is directly proportional to the voltage [16], the new voltage of the grid becomes

$$V_g = K * V \tag{2.3}$$

where $V$ is the nominal grid voltage and $K$ is

$$K = \sqrt{\frac{P_{DG}}{P_{Load}}} \tag{2.4}$$

If $\mathrm{P}_{Load}$ is greater than $\mathrm{P}_{DG}$ the voltage amplitude will decrease, and if it is less the voltage amplitude will increase. The reactive power in the island is dependent on the voltage amplitude and the frequency according to [16]:

$$Q_{g,load} = Q_{DG} = (\frac{1}{\omega_g * L} - \omega_g * C) * V_g^2 \tag{2.5}$$

where $Q_{g,load}$ is the new value of the reactive power in the island, which is also equal to the reactive power output of the distributed generators, with respect to the changed voltage amplitude $V_g$, $L$ is the inductance and $C$ is the capacitance. $\omega_g$ is the frequency in radians, and can also be written as [16]:

$$\omega_g = \frac{-\frac{Q_{DG}}{C*V_g^2} + \sqrt{(\frac{Q_{DG}}{C*V_g^2})^2 + \frac{4}{L*C}}}{2} \tag{2.6}$$

## 2.3 Anti-islanding measures

There are a number of measures that can be used to detect and prevent unwanted island operation. Some types of anti-island protections are directly used in the inverter designs, so called passive and active protection methods. The passive island

detection methods are built upon the principle of monitoring parameters at the DER connection and turning the inverter off as soon as the parameters violates the range for normal operation. Common parameters monitored for passive island detection include [14, pp. 17–23]:

- Over/under voltage (OUV) and over/under frequency (OUF)
- Voltage phase jump
- Voltage and current harmonics

The active anti-island protection schemes revolves around actively trying to change parameters. For example varying reactive power output, which wouldn't be significantly affected due to the connection to the large distribution grid making said parameter stiffer during normal operation. Observing a significant change in the parameters would therefore mean that the system has entered island operation and trigger the inverter to shut down. Methods of active island detection include [14, pp. 24–36]:

- Impedance measurement
- Detection of impedance for a specific frequency
- Frequency bias
- Frequency jump
- Slip mode frequency shift
- Sandia frequency shift
- Sandia voltage shift
- Mains monitoring units with allocated all-pole switching devices connected in series

Modern inverters are designed with a mix of passive and active protection methods, since they have to posses anti-island protection to be allowed to be connected to the utility grid. One of the active methods, Active Frequency Drift (AFD), works by forcing the frequency of the current to be slightly higher than that of the voltage from the previous cycle [16]. The inverter current is kept to zero from when it reaches its zero-crossing until the voltage reaches its zero-crossing. This will in turn cause a continuous change in the frequency in the island until it reaches the OUF thresholds which would not happen if the grid was connected. Another type of active method is Reactive Power Variation (RPV) or reactive power disturbance. The basis of this method is to inject the reactive reference current $i_{q,r}$ with a low frequency harmonic disturbance [16]. When the grid is disconnected, the voltage will be linearly dependent on the current and the disturbance will be able to affect the voltage frequency. These voltage frequency variations can then be detected in order to detect an island. If the grid is connected, these variations will not be present due to the very stiff behaviour of the grid.

## 2.4 Regulations and guidelines

When it comes to connecting PV-units to the utility grid, there are specific regulations and guidelines to pay heed to. Firstly, all power generation plants connected in the Swedish power grid are separated into different Requirements for Generators

(RfG). Which is a European regulation from 2016 ensuring fair competitive conditions on the internal market for electricity, system security and integration of electricity from renewable energy sources and promotion of a union-wide electricity trade. The different types of power generation plant categories are synchronous power generation modules, power park modules and offshore power park modules. Each category is subsequently graded from type A-D, where the grade corresponds to the modules maximum continuous power and voltage level at its connection point. The different type ratings and limits that applies in all Nordic countries according to the RfG [17], [18] are listed accordingly:

- Type A: $\geq$ 0,8 kW and $<$ 1,5 MW.
- Type B: $\geq$ 1,5 MW and $<$ 10 MW.
- Type C: $\geq$ 10 MW and $<$ 30 MW.
- Type D: $\geq$ 30 MW and/or voltage $\geq$ 110 kV.

As the type list indicates, a facility can be rated as type D independently of power rating if the voltage is 110 kV or greater. Further stated in the RfG, generators of type A have different requirements regarding operation time in different ranges of frequency, which are displayed in Table 2.1 below.

**Table 2.1:** Type A generators operation time requirements for frequency ranges, as stated by the RfG [17].

| Frequency range [Hz] | Operation period |
|---|---|
| 51.0-51.5 | 30 minutes |
| 49.0-51.0 | Unlimited |
| 48.5-49.0 | Minimum 30 minutes, is defined by the system manager for the transmission system. |
| 47.5-48.5 | 30 minutes |

Due to the RfG being a European regulation for a number of countries with different grid conditions, the regulation was made flexible in the sense that each country could write complementing requirements based on their own conditions. The complementing regulation of the RfG for the Swedish electric grid is given by *Energimarknadsinspektionen* in the EIFS 2018:2 regulation. The EIFS 2018:2 regulation specifies the conditions set by the RfG for the Swedish grid with slight adjustments in different definitions of values and ranges. Definitions stated in the RfG that can vary between different European countries include power limit values for the different generation types. Requirements for frequency responses further specified in the EIFS 2018:2 regulation [19, pp. 1–2] includes:

- The power generation unit of type A, B, C and D needs to fulfill requirement of staying connected to the grid and function during frequency rate of change up to 2 Hz/s.
- The power generation unit of type A, B, C and D needs fulfill requirement to provide reduction of active power output as frequency response when frequency exceeds 50.5 Hz.
- The droop constant, the quotient of frequency change and change of output

power expressed in percent, should have the primary setting of value 8 % for power generation unit of type A, B, C and D.
- The maximum reduction of active output power as a result of decreasing frequency below 49 Hz should be 3 % for every 1 Hz, for power generation unit of type A, B, C and D.
- Automatic reconnection of the power generation units of type A, B and C is allowed when the network frequency at the connection point is within the range of 47.5-50.1 Hz. The frequency should be within said range for three consecutive minutes before the reconnection.
- Automatic connection of power generation units of type A, B and C should fulfill the following requirement of increase of active power output dependent on the grid frequency i the connection point:

  $<$ 49.9 Hz: No restriction on the rate of increase of the active power output.

  49.9-50.1 Hz: Maximum increase of 10 % of nominal active output power per minute.

  $>$ 50.1 Hz: No increase of active power output allowed.

Other relevant regulations to pay heed to when it comes to connecting PV-units are regulations regarding accompanying PV inverters. Each inverter has to conform with operation and safety requirements before being connected to the utility grid. A good tool that exists is *Rikta Rätt*, which is a list owned by *Energiföretagen* that aims to ease the documentation process by providing inverters that has been previewed and inspected with the previously mentioned RfG and EIFS 2018:2 regulations in mind [20]. It is further mentioned by Energiföretagen that there is no requirement for an inverter to be listed in the Rikta Rätt-list in order to be connected to the Swedish grid, and being included in Rikta Rätt does not imply any formal approval of said inverter. Energiföretagen describe Rikta Rätt as a tool for private actors and companies to make sure that inverters for PV and energystorage units of type A satisfy the requirements for grid connection. Which is ensured by the list's documentation transparency regarding tests of the requirements on the inverters included in the list.

Other useful guidelines that can be used in regards to connecting generation units to the LV grid is the handbook *Connection of electrical generation to the low voltage grid* (ALP for short in Swedish), which also is published by Energiföretagen. In the ALP-handbook there are recommended values for protection functions for generation units of type A, which are listed in Table 2.2 [21].

**Table 2.2:** Recommended relay-protection values for generation units type A according to the ALP-handbook [21].

| Parameter | Level of function | Function time [s] |
|---|---|---|
| OV (step 2) | 230 V +10 % | 60 |
| OV (step 1) | 230 V + 15 % | 0.2 |
| UV | 230 V -15 % | 0.2 |
| OF | >51.5 Hz | 0.5 |
| UF | <47.5 Hz | 0.5 |
| Unwanted-island operation | 2.5 Hz/s | 0.5 |

# 3

# Modelling of distribution system with solar PV for anti-islanding studies

## 3.1 Literature study

In order to get an understanding how inverters work and which anti-islanding measures exist, a literature study was conducted. To find information about anti-islanding measures and their usefulness, search engines such as Scopus and IEEE explore were used to find peer-reviewed articles. Phrases such as "Photovoltaic inverters", "PV inverters", "Anti-islanding protection" "Inverter protection", "Inverter functions", "Island operation", and "Island protection" were utilized and the articles were filtered based on relevancy to the thesis subject.

To gain familiarity with the PV inverters and manufacturers currently on the market, information about which the most popular ones were was gathered by using the search engine Google and the *Rikta Rätt*-list [13]. Information about the actual inverters was taken from the manufacturers' websites. Datasheets and certificates for relevant inverter models were chosen based upon their *Rikta Rätt*-listings and the availability of their specifications mentioning anti-islanding protection. The selection of inverters were listed in order to create an understanding of the different inverter models' power ratings and anti-islanding protection schemes.

## 3.2 Simulation

The simulation was performed in the software Digsilent Powerfactory, which is a simulation software for electrical grids. In order to test out the anti-islanding functions of the program, a pre-defined model [22] for dealing with islanding events for a wind turbine was used. The model, which will be referred to as the wind turbine model, can be observed in Figure 3.1. The model consists of a wind turbine connected to the low voltage busbar which has a nominal voltage of 690 V, a 20/0,69 kV transformer which connects the wind turbine to the medium voltage grid. On the other side of the transformer there was a 20 kV busbar. Then there is a line segment which leads to the Point of Common Coupling (PCC). At this point there is a general load as well as a shunt reactance, and an element representing the external grid. There was also a station controller used in the model, responsible for

the protection of the converter. The controller itself was a composite model, consisting of multiple different DSL blocks. DSL is Powerfactory's internal programming language where those familiar with the language can program the controller to do the desired functions. The composite model consisted of:

- a converter, in this case associated with a wind turbine.
- a converter controller, which controls the behaviour of the converter.
- a current transformer.
- a voltage transformer.
- a protection model, which regulates all the protection settings and trips the converter if the conditions are violated.
- a voltage reference which keeps the nominal voltage and calculates the positive-, negative- and zero-sequence voltages as well as the maximum permissible voltage.

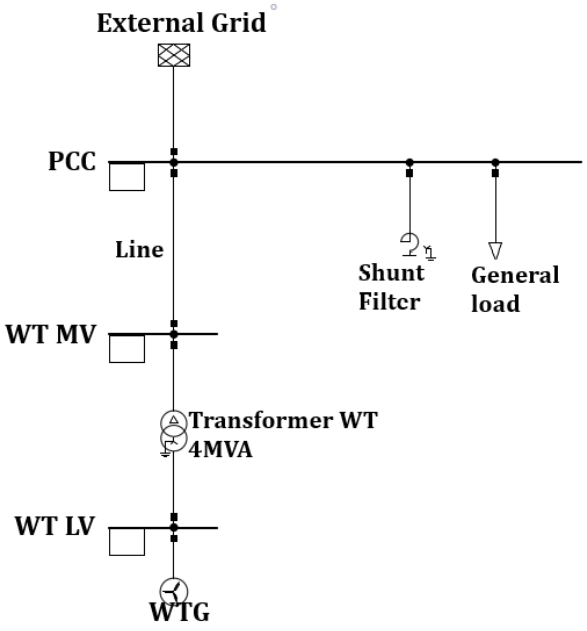


**Figure 3.1:** The pre-defined Wind turbine model, provided by Powerfactory [22], to test anti-islanding functions.

The pre-defined model was chosen due to its functioning controller scheme which meant that a new one would not have to be created from scratch. In order to initialize the model, the steps described in [22] were followed. An EMT simulation was done where the external grid was disconnected after 0.0 seconds and how that affected the grid was observed. When the results had been verified, and the controller was confirmed to be working as it should, the modification of the model began. The different functions and protection schemes utilized from the original Wind turbine model are described in section 3.3, while the changes made to the original model are described in section 3.5 followed by the additional test models. The work was centralized around four different models, referred to as the Basic model, LV model,

PV model and the MV cable model. Each model is based upon the protection schemes from the original Wind Turbine model, and are explained later in this chapter. The tests performed in each grid model are explained after each grid model headline.

## 3.3 Powerfactory converter and converter control

The converter consists of several different DSL models, as mentioned previously. In Figure 3.2 the main DSL model is shown, which consists of three different areas. The first one, the Inverter control unit, consists of the DSL block called "Converter Control", which is its own DSL model in itself, and several input and output signals. The input signals are $V_{dc-positive}$, which is the positive DC voltage, $V_{dc-negative}$, which is the negative DC voltage, $V_{ac-local}$, which is the AC voltage at the measuring point, and $I_{ac-local}$ which is the AC current at the measuring point. The measuring point in this case is at the connection point between the PV module and the terminal. The output signals from the inverter control unit are $u_{1r-in}$, $u_{1i-in}$, and $F_{FAST-PLL}$. $u_{1r-in}$ is the real part of the reference voltage, while $u_{1i-in}$ is the imaginary part of the reference voltage. Both of these signals are sent to the converter itself, the PV module. $F_{FAST-PLL}$ is the frequency which is then sent to the internal protection system.

The second area is called "Protection system" and is comprised of three blocks. The first one, called AC voltage, has an output signal $U_{2r-ABC}$ which is the three phases of the AC voltage, where $U_{2r-ABC}$ is just another name for $V_{ac-local}$. This signal is then sent to both the protection block and the sequence block. The sequence block converts the incoming three phase AC voltage into the positive sequence voltage, $u_{pos}$, and the maximum voltage that the protection should instantly trip for, $u_{max}$. The protection block has five input signals, $I_{ac-local}$, $F_{FAST-PLL}$, $U_{2r-ABC}$, $u_{pos}$, and $u_{max}$. The block then determines based on these signals if the converter can continue to operate or if it shall disconnect to protect the system and the unit itself.

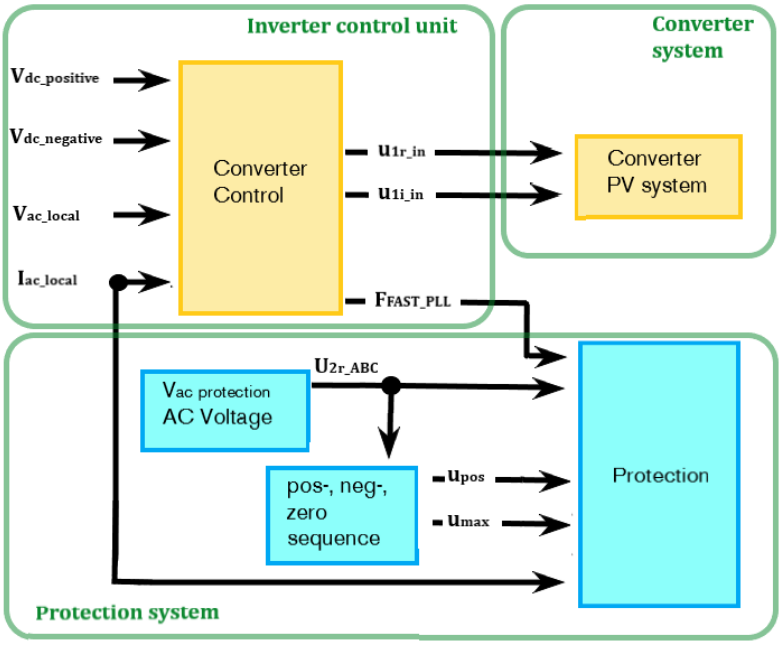


**Figure 3.2:** Block representation of the wind turbine control system from Powerfactory's anti-islanding example.

### 3.3.1 Converter control signals

In Figure 3.3 there are seven different blocks that together make up the control functions of the converter, the previously mentioned Converter Control. The first block, input signals, is where the input signals are collected and sent out to the rest of the blocks. The input and output signals of the converter control is described in Table 3.1.

**Table 3.1:** Input and output signals of the converter control depicted in Figure 3.3.

| Input signal name | Description | Usage and function |
|---|---|---|
| $U_{dc\_ref}$ | Reference signal of the DC voltage. | Further used in the *Input filtering* block. |
| $Q_{ac\_ref}$ | Reference signal of the measured AC reactive power. | Further used in the *Input filtering* block. |
| $P_{ac\_ref}$ | Reference signal of the measured AC active power. | Further used in the *Input filtering* block. |
| $u_a$, $u_b$, $u_c$ | Measured three phase voltage at PV-unit location. | Multiplied with $\frac{1}{\sqrt{2}} \cdot \frac{\sqrt{3}}{\sqrt{2}}$ for p.u. values of phase voltages. |
| $i_a$, $i_b$, $i_c$ | Measured three phase current at PV-unit location. | Multiplied with $\frac{1}{\sqrt{2}} \cdot \frac{1}{\sqrt{2}}$ for p.u. values of phase currents |
| $u_{dc\_pos}$, $u_{dc\_neg}$ | Positive and negative DC voltage values respectively. | |
| **Output signals** | | |
| $u_{r\_ref}$, $u_{i\_ref}$ | Real and imaginary parts of the reference voltage respectively. | |
| $F_{meas}$ | Measured frequency at PV location. | Used as input signal of the *Protection* block. |

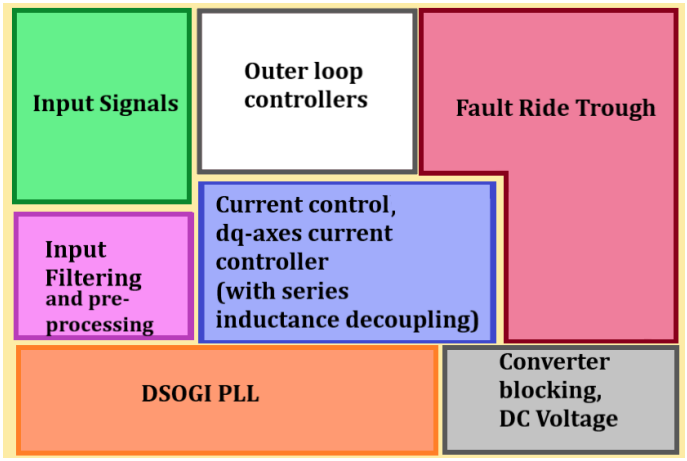


**Figure 3.3:** Block representation of the converter control DSL of Powerfactory's anti-islanding model scheme.

### 3.3.2 Input filtering and pre-processing

For the second block, input filtering and pre-processing, it takes the input signals and runs them through a low pass filter to get rid of high frequency disturbances and distortions so that there are no false positives or false negatives. The time constants of the low pass filters are displayed in Appendix B, Table B.1. The input filtering performs an alpha-beta transformation in order to convert the phase voltages and phase currents into their measured real and imaginary parts, and sends these signals onward. The input filtering and pre-processing block also uses the phase voltages and currents in order to calculate the instantaneous active and reactive power and compares it with the calculated reference apparent power. The ratio between the active and apparent power in p.u is sent further into the controller blocks, and the same happens for the ratio between the reactive and apparent power.

### 3.3.3 Outer Loop controllers

The third block, Outer Loop controllers, regulates the outer loop. It checks if the outer loop is enabled and then, if it is, used the measured reactive power in order to calculate the reference current in q-axis. Depending on the setting, it uses the previously measured active power or the DC-current in order to calculate the d-axis reference current.

### 3.3.4 DSOGI PLL

As for the fourth block, DSOGI PLL which is depicted in Figure 3.4, makes sure to keep a Phase locked Loop. The measured real part of the voltage, here called the alpha component of the voltage, is sent through a loop where the difference between it and the previous value is taken and then multiplied with the square root of two. The same process happens to the imaginary part of the voltage too, but

this is called the beta-component of the voltage. This value is then compared with another value and the difference is multiplied by $\omega$, which is two times $\pi$ times the measured frequency, run through an integrator and is then sent to three different places. The first one is sent back to the beginning, becoming the signals that the initial real and imaginary parts are compared to. The second is to be multiplied with $\omega$ again, run through another integrator, and back to the loop before it was multiplied by $\omega$ the first time. These signals going to the second area are called $qv\alpha_p$ and $qv\beta_p$ respectively. The third is a block which adds the resulting alpha component together with $qv\beta_p$ and the resulting beta component with $qv\alpha_p$. These values are then sent to a block which transforms them from alpha-beta into the dq-axis components through the forward Park transform, which is:

$$d = cos(phi) * \alpha + sin(phi) * \beta \tag{3.1}$$

$$q = -sin(phi) * \alpha + cos(phi) * \beta \tag{3.2}$$

where $cos(phi)$ and $sin(phi)$ are the cosine and sine values of the measured frequency in radians at the time of interest. The q-axis voltage is then run through a Proportional-Integral (PI) controller, in order to get the frequency in radians. The integrator in the PI controller has an initial value which corresponds to two times $\pi$ times the nominal grid frequency (50 Hz) while the gains are listed in Appendix B Table B.1. From this point, the signal is divided by two times $\pi$ in order to get the frequency back in hertz, and also sent through another integrator. The frequency that is measured here, named *Fmeas* in Figure 3.4, is then used in the Protection block seen in Figure 3.2 with the name $F_{FAST-PLL}$. The output of the signal that goes through the integrator is then run through a cosine and a sine function to get the cosine and sine values back and these are then sent back to the dq-conversion block again and to the current control block.

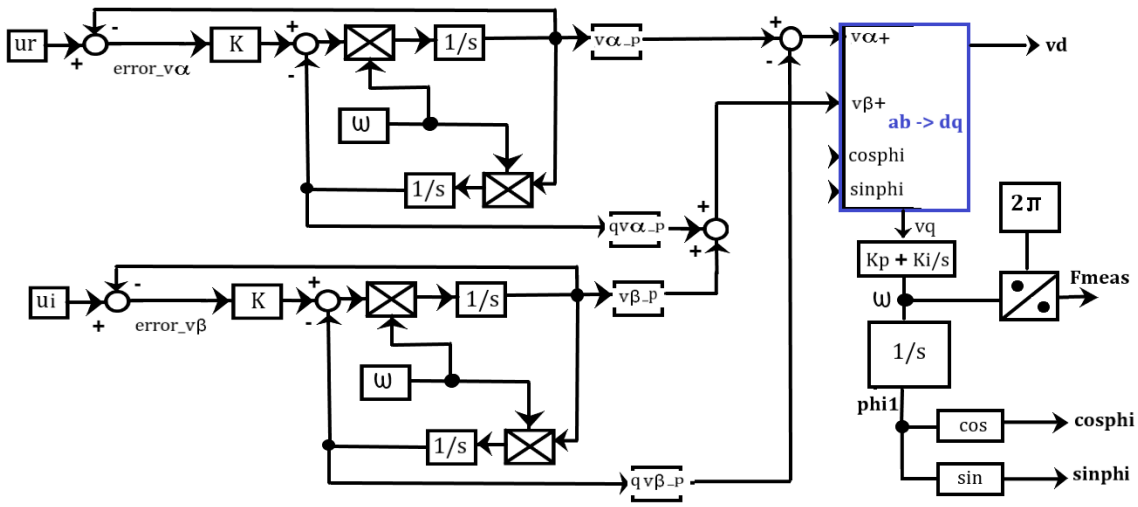


**Figure 3.4:** Block diagram of the DSOGI PLL function block in the converter control. The hollow circles represent summation points, the crossed over blocks multiplication and the block with a division sign represents division.

### 3.3.5 Current control

Current control, the fifth block, operates by first taking the real and imaginary part of the measured voltage as well as the sine and cosine values of the angle and turning them into the dq-axis voltages. The real and imaginary parts of the measured currents are transformed into the dq-axis currents and compared with their respective reference values taken from the Outer Loop Controller block. For the d-axis, the difference between these values is then sent to a PI controller and the output is then compared with the d-axis voltage multiplied with a constant and with the q-axis current which has been decoupled by a series inductance. For the q-axis, the same happens but with the d-axis current being decoupled and the q-axis voltage being multiplied by a constant. These resulting values are then sent alongside the sine and cosine signals into a block that turns the dq-axis signals back into the real and the imaginary parts of the voltage. After going through a limiter, the final output is the real and imaginary voltage reference signals.

### 3.3.6 Fault ride through

The Fault ride Trough block is the sixth block of the converter control, and it checks for faults regarding voltage and current values that should result in the converter's disconnection. The first section of the fault ride through block handles the voltage value coming from the input filtering block and checks so that it is within the OUV values and therefore within the fault ride through threshold. The voltage coming from the input filtering block is the voltage magnitude, and has been created from the real and imaginary parts of the voltage through:

$$u = \sqrt{u_{re}^2 + u_{im}^2} \tag{3.3}$$

with $u_{re}$ being the real part of the voltage and $u_{im}$ being the imaginary part. If the voltage value leaves the acceptable range the fault ride through block activates. The second section of the block monitors the reference values of the d and q currents, and actively keeps the currents at their previous values if the fault ride through activates. If the fault ride through isn't activated, the currents measured from the grid pass through the block without being altered.

### 3.3.7 Converter blocking

The last and seventh block in the converter control is the Converter blocking for the DC voltage. This converter block acts as a DC voltage fault check, and only activates if the measured DC voltage value is negative, effectively turning the converter off. The block monitors the current so that it is flowing in the right direction, meaning that if the current flows into the converter the block engages and starts blocking the converter.

### 3.3.8 Powerfactory converter protection

The Protection block previously shown in Figure 3.2 consists of three different parameters monitored. These parameters are voltage, frequency and current which serve as input signals to the protection trip function which is illustrated in Figure 3.5. If any of the said parameters violates their respective ranges of acceptable values defined by the protection settings, the protection trigger activates and sends a trip signal to the converter which will effectively turn it off.

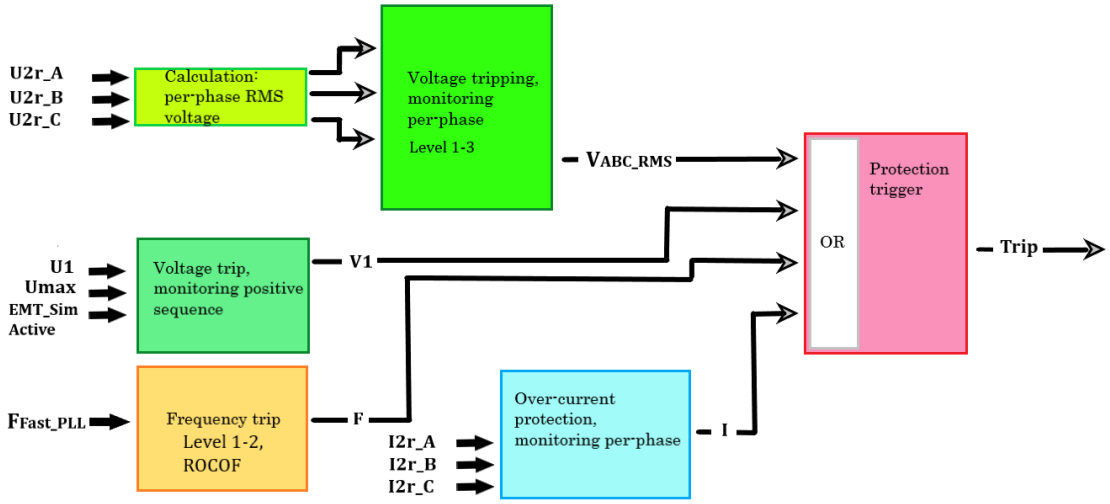


**Figure 3.5:** Block representation of the Protection block of the control system, with its voltage, frequency and current monitoring attached to the protection trigger function.

The Protection block's trigger with respect to frequency takes the measured frequency, as input signal $F_{FAST-PLL}$, which is the same signal as $F_{meas}$ in Figure 3.4, and it was modified to monitor it by two levels corresponding to the OF and UF ranges and function times of the ALP in Table 2.2. The frequency protection monitoring also includes Rate of Change of Frequency (ROCOF), which chosen to trigger for 2 Hz/s in accordance with the EIFS 2018:2 regulation. The current monitoring per phase logic in turn takes the measured current and checks for violations in the form of overcurrent. The limit for the overcurrent protection was set to 50 A, which corresponded to 2-3 times the current values during normal operation. The value was set this high in order to not trip as the important parts of the study was frequency and voltage. Based on simulations, the current remained relatively static and did never have any high increases in its value, meaning that if a lower value had been used, there would not have been a difference in the results. The voltage protection monitoring is based upon the calculation of the RMS-voltage per phase serving as input to the voltage tripping logic. The voltage tripping per-phase function monitors the three phase voltages while making sure said values stays within three different protection levels.

A more detailed illustration of the voltage monitoring per phase block of the protection is shown in Figure 3.6. First, the phase voltages from the AC voltage source,

$U_{2r-ABC}$ are converted to their RMS values. These values are then sent to three stages of protection each. Stage 1 protection is set to a lower value of OUV but with a longer tripping time, in accordance to the ALP step 2 in Table 2.2. Stage 2 protection has a higher tripping threshold but will trigger much faster in accordance to the ALP step 1. Stage 3 has an even higher threshold and trips almost immediately upon detecting a value outside of its allowed boundaries. Due to the stage 3 protection requirements being absent from datasheets and regulations in Sweden, the stage 3 protection was set to values that would never occur and as such putting it out of service. If any of the phases show a value that triggers the protection, a signal will be sent telling the breaker to open and disconnect the converter and PV module. It does not matter if multiple phases all flag for overvoltage, as long as one does, the protection device will activate.

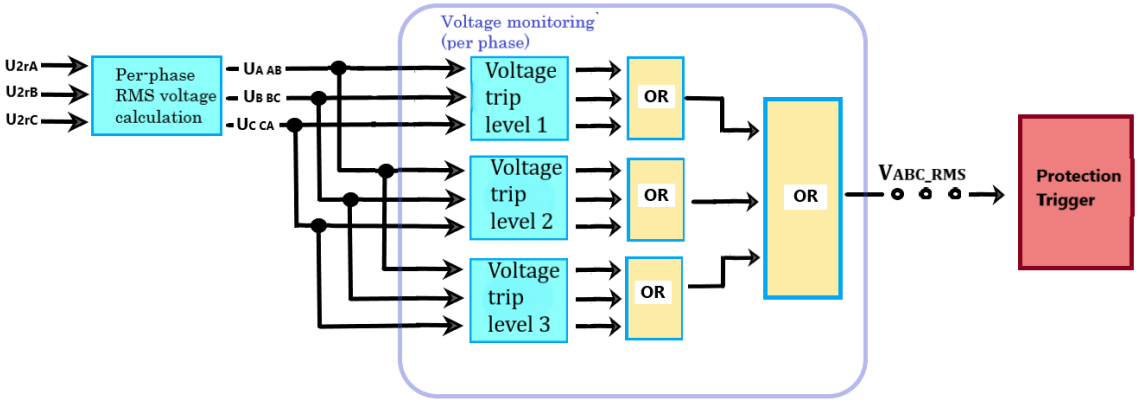


**Figure 3.6:** Block representation of the voltage trip function within the protection block.

The voltage protection also included monitoring of the positive sequence voltage. The signal $u_{pos}$ from Figure 3.2 is here renamed as $U1$ and is measured in per unit (p.u.) voltage. This value is then multiplied with a constant, in this case 400, in order to get the value in volts. The signal is then sent to three different stages of protection. These stages are the same as described in the previous paragraph, but are not connected to the per-phase monitoring and work standalone. The positive sequence monitoring also checks for the maximum allowed voltage that the converter can handle before disconnecting immediately. In the model it was set to 10 p.u, acting as instantaneous detection without time delay, but due to the phase rms voltage limiter being set at 2 p.u this limit will never be reached. The input signal $U_{max}$, previously $u_{max}$ in Figure 3.2, is sent to a block that checks if it is above the predesignated value for the maximum voltage and sends it to another block. This block also receives the input signal $EMT - SimActive$, which checks if an EMT simulation is active or not. If it is active, and a signal that the maximum voltage has been reached, the block instantly sends an tripping signal. If an EMT simulation is not active, this block will do nothing no matter the voltage value.

## 3.4 The PowerFactory load setting

The load models and settings used in the PowerFactory grid models were defined as coefficients of voltage dependence for the active and reactive power P and Q. The voltage dependency of the loads in PowerFactory is based on three polynomial terms as described in *PowerFactory's technical reference document*. PowerFactory uses (3.4) and (3.5) to define the voltage dependence for P and Q [23].

$$\mathrm{P} = \mathrm{P}_0(a\mathrm{P} \cdot (\frac{v}{v_0})^{e_{a\mathrm{P}}} + b\mathrm{P} \cdot (\frac{v}{v_0})^{e_{b\mathrm{P}}} + (1 - a\mathrm{P} - b\mathrm{P}) \cdot (\frac{v}{v_0})^{e_{c\mathrm{P}}}) \tag{3.4}$$

where subscript 0 stands for the operating point values in the load element description window under the Load Flow page. And [1 - $a$P - $b$P = $c$P] and $v$ denotes the p.u. value of the busbar voltage.

$$\mathrm{Q} = \mathrm{Q}_0(a\mathrm{Q} \cdot (\frac{v}{v_0})^{e_{a\mathrm{Q}}} + b\mathrm{Q} \cdot (\frac{v}{v_0})^{e_{b\mathrm{Q}}} + (1 - a\mathrm{Q} - b\mathrm{Q}) \cdot (\frac{v}{v_0})^{e_{c\mathrm{Q}}}) \tag{3.5}$$

where [1 - $a$Q - $b$Q = $c$Q].

By selecting different values for exponents $e_{a\mathrm{P}}, e_{b\mathrm{P}}, e_{c\mathrm{P}}$, $e_{a\mathrm{Q}}, e_{b\mathrm{Q}}$ and $e_{c\mathrm{Q}}$ in the load type's Load Flow page in PowerFactory you can specify different load model behaviors. The exponent values can be selected as either 0, 1 or 2, which stand for constant power, current or impedance respectively. And the coefficients $a$P, $b$P, $c$P, $a$Q, $b$Q, $c$Q can be used to define the relative proportion of each coefficient respectively. The settings for the exponents and coefficients as defined in the General Load Type for the used loads are shown in Appendix B, Table B.4. The used load settings were predefined in the grid data provided by Vattenfall Eldistribution, which is discussed further in section 3.6.

## 3.5 Basic grid model

The Basic grid model was based upon the pre-defined Wind turbine model shown previously in Figure 3.1. The first modification done was to replace the wind turbine with a photovoltaic generator, in order to see if the converter would work with that type of generator, which it did without any issues. In order to test for the scenario when the loads only are present on the low voltage side, the load was moved to the LV side of the transformer and the active power consumption and generation was reduced to levels that would be more suitable in a normal LV grid. The PV-unit was connected to a separate bus from the load on the LV side in order to avoid the problem of the PV-unit exceeding its assigned generation limit of active power. And the line between the load and PV bus was set to zero in order to not represent any losses, and only work as a visual connection point. The nominal voltage of the LV grid was changed to 400 V as that is the nominal voltage in the Swedish low voltage power grid. The PCC and the line segment were then removed as when the load was on the LV side, the PCC and line suddenly had no purpose as if applied to the real world, it would be an empty point at some distance away without any connections. The external grid was instead connected directly to the 20 kV busbar.

The transformer data used in the Basic grid model can be found in Appendix B, Table B.5. All of the changes done in the wind turbine model can be observed in Figure 3.7, which will be referred to as the Basic grid model.

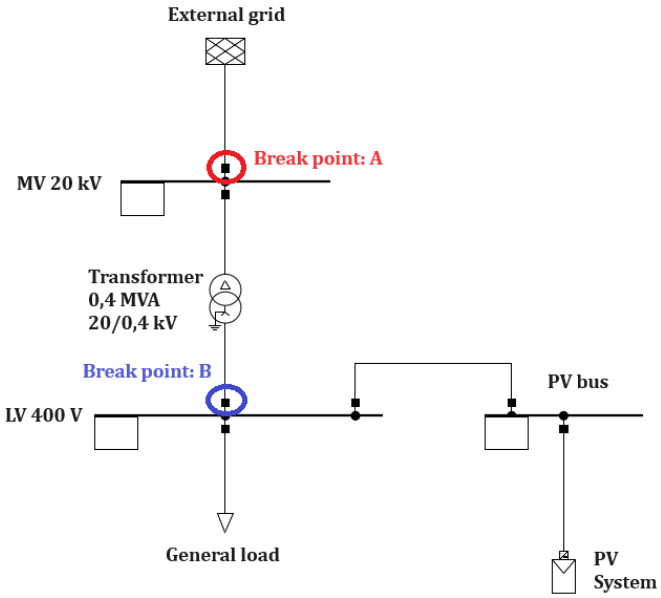


**Figure 3.7:** Basic grid model, one PV-unit connected to a load on the low voltage bus and with connection to the external grid through a transformer.

Afterwards, the protection settings in the DSL blocks were changed to comply with Swedish grid regulations. The used settings for the converter model are presented in Appendix B in Tables B.1-B.3. When the settings had been changed to comply with the Swedish grid voltages and protection settings of frequency and voltage, the model was tested again to make sure that the protection worked as intended for obvious fault conditions. Three different categories of tests were performed in the Basic grid model in order to confirm its behavior and function. Each test is named and listed below with respective explanations and purpose. Starting of with the generation equal load balance tests, followed by load variation tests and lastly testing the impacts of reactive power. The reactive power tests were used to observe how reactive power with different signs affects the possible island formation in the grid. Each test was observed with regard to the three phase voltages and currents, frequency values measured by the PV-unit and its protection. The results for each test are presented in chapter 4 in the form of voltage magnitude and frequency over time in order to show the different triggers of the protection function, which did not include plots of the different currents due to the overcurrent protection never being triggered. Other observations documented include time of protection trigger as well as voltage and frequency values at time of activation of protection. Which were deemed points of interests due to the fact that the protection in itself doesn't act instantly, meaning that the measured parameters keep decreasing or increasing until the protection has activated after a certain time delay. Which leaves the

subject open for discussions regarding if the protection has successfully protected the inverter from harmful operation, or if it possibly doesn't act sufficiently enough.

### 3.5.1 Generation equal load balance tests

To test if the protection measures worked as intended to prevent unintentional islanding, tests were carried out with different settings. There were two possible disconnect points, shown in Figure 3.7, disconnection point A which included the transformer in the possible island and disconnection point B which did not. In addition to testing the Basic grid model of the significance of different disconnection points for each test, the model was also subjected to tests with different load conditions. The first tests were performed with an active power consumed by the load and generated by the PV module at an equal value of 10 kW, which represented the first generation power equal load tests. The generation equal load balance tests were of interest since it in theory would result in the most stable islands, the most seamless transition, if the grid would be unaffected by losses or disturbances during the disconnection from the external grid.

### 3.5.2 Load variations tests

The Basic grid model was then subjected to tests were generation and load weren't equal, starting of with a mismatch between the generation and load of ±1 % followed by tests with ±10 % and ±25 %. These tests were performed by keeping the PV modules generation at 10 kW while varying the load by increasing and decreasing it with the corresponding percentages with respect to said generation of 10 kW. The over and under generation tests served as a base line to determine if the anti-island protection functions functioned as intended in the simulation.

### 3.5.3 Impacts of reactive power

Furthermore, reactive power in the network was varied between no reactive power at all, 0.1 kVAr consumed by the load and 0.1 kVAr injection from the load into the grid in order to determine the effects of reactive power in the model. All tests described previously were performed with 0 reactive power in the load. The reactive power impact test was then carried out with the same settings used in the generation equal load test, with the exception that the load's reactive power was set to +0,1 kVAr (inductive load) and -0,1 kVAr (capacitive load). The impact of reactive power tests in the Basic grid model served as a base line for how reactive power affects the potential islands grid behavior compared to the previous tests with only a variation of active power.

## 3.6 Low voltage grid model

The LV-grid model was provided by Vattenfall Eldistribution and consisted of an external grid which was represented as a large synchronous machine, a 10/0.4 kV transformer, a substation with a 10 kV busbar and a 0.4 kV busbar, 17 cable cabinets,

71 loads which represent houses, and 12 synchronous machines which represented the PV-modules in the LV-grid. The 0.4 kV busbar connected to the LV side of the transformer is referred to as the main bus and had five branches connected to it with the 71 house loads spread out amongst them. A simplified diagram of the LV-grid is presented in Figure 3.8. In the original simulation model, a lot more interconnecting lines and buses exist between the each bus depicted in Figure 3.8, but the figure acts as a condensed representation of the grid in order to make it easy to read. The summed up values of all of the lines depicted in Figure 3.8 are presented in Appendix B Tables B.6-B.11. The transformer type used in the LV-grid model can also be found in Appendix B, Table B.12, as well as the original load data for the house loads in the LV-grid in Tables B.13-B.18.

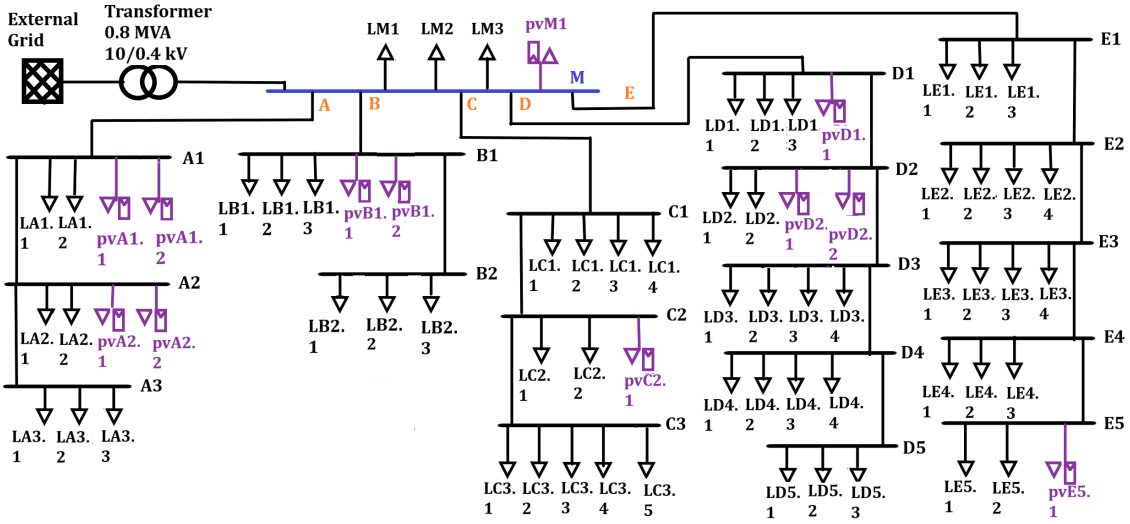


**Figure 3.8:** Condensed diagram of the LV-grid model. Depicting the main bus (M) marked in blue, the five branches (A-E) with house loads (black triangles) and PV-units with their respective loads (purple).

The first thing done was to change all the 12 load bus connected synchronous machines into PV modules with the same active power generation as the synchronous machines they were replacing. The composite models with the converter controls and protection settings were then imported from the Basic grid model and set up for one PV module. The rest of the lines and loads were set out of service in order to test if the composite model could be copied over without causing any issues. After changing the transformer from a Delta-Delta configuration to a DYn configuration, the model worked as intended.

The composite model was then copied again, and a new PV module was assigned to this copy. The line leading to this new PV module and accompanying load was reactivated in order to test if multiple converter control schemes could operate simultaneously. Gradually more composite models were added until all of the 12 PV modules had their own protection scheme which was functioning. The model was then tested for island operation in a similar fashion as the previous grid model. The acceptable time that the protections should be able to detect and trip for

island operation was set to five seconds based on recommendations regarding overall protection from Vattenfall Eldistribution. A total of four different test categories were carried out in the LV-grid model, each test with their purpose and aim are explained below. The four different test categories are described as the generation and load balance tests, NDZ tests, disturbance with car chargers test and the test with the original house load values.

### 3.6.1 Generation and load balance tests

The first tests were performed with the intention to see the LV-grid behavior when the total generation from all of the PV-modules were in balance with the load values. The maximum load values of houses provided in the LV-grid were to large in contrast to the twelve installed PV-modules, so the first adjustment for the balanced tests were to half the house load values in order to make them more manageable. Note that only the active power loads of the house load were used in these tests, rating the reactive power of the loads to 0. Additionally nine more PV-modules were added at certain buses to support and balance the load flow to not overload the lines throughout the grid. The additional PVs and the modified values of the original twelve to amount to a total production of 298.5 kW can be read in Appendix B, Table B.19 and Table B.20 respectively. Two different generation and load balance tests were conducted in the LV-grid, one were the PV-units only compensated for the active power of the house loads (excluding cable effects) and one additional test were the PV-units compensated for the house loads and all of the cables (with respect to cable effects). So the generation and load balance test, with respect to the cable losses, was performed with a small increase of generation as well as a small reactive power consumption originating in one of the loads. The active power compensation of the LV-grid cables were seen as 1.3 kW while the reactive power compensation for the cables were seen as 0.1 kVAr during the load flow of the LV-grid model.

### 3.6.2 Non-detection zone tests

Following the generation and load balance tests, it was of interest to establish a NDZ in order to figure out where the island would operate undetected and where the protections would trigger and remove the island in time. The total generation of all of the 21 PV-units were set to 298.5 kW, and the active and reactive load values were varied with respect to this generation value. This was done by first setting the active power to a fixed value and increasing the reactive power in the network until the protections activated as close to five seconds as possible. Then the reactive power was decreased below zero until the same phenomena appeared. The active power was then gradually increased until a value was reached where it did not matter what the reactive power was, the protection system would activate either way due to UV throughout the grid. For each incremental step, the reactive power was increased and decreased as described previously. When the end point had been reached, the simulation was reset and the reactive power was fixed instead. The active power was increased and then decreased to get the five seconds triggering time, and the

reactive power was then incrementally increased to find the end point, with the active power variation being applied at each step. This was then repeated but with decreasing active power when the reactive was fixed, and with decreasing reactive power when the active power was fixed. The active power was gradually decreased until the overproduction in the grid would activate the protection instantly due to OV, independent of the reactive power value. After drawing the NDZ for the LV-grid with a total generation of 298.5 kW, two tests were performed after in order to see if the NDZ boundaries would change if the total generation of active power by the PV-units was increased or decreased. These tests were performed with an increase of the total generation of 50 %, and then one with a total generation decrease of 50 % with respect to the first total of 298.5 kW.

### 3.6.3 Disturbance with car chargers test

In order to confirm the NDZ drawn from the tests, a test with aim to disturb the island was performed. Keeping the PV-modules generation the same as the previous tests, 298.5 kW, the loads at three different places in the grid were increased at different intervals within the formed island. The three loads were increased with 11 kW each, which activated at one, two and three seconds respectively after the island forming. The 11 kW load increases were chosen in order to simulate three car chargers being connected during the island formation, simulating load variations during the potential island. The exact position of the fictional car chargers can be seen in Appendix B, Table B.19. The disruption test had the aim to observe if a possible disruption of the island formation would correspond with the behavior of the NDZ, depending on if the load variation places the operation point inside or outside of the drawn NDZ.

### 3.6.4 Original house loads test

The last test performed in the LV-grid were with the original load values, twice the amount used in the tests mentioned above and including the reactive power ratings of the house loads. The PV generation was kept with the additional nine PV-modules, amounting to a total generation of 298.5 kW. The run with the original load values were also seen as a test to validate the NDZ, since this load point was well outside of the drawn NDZ boundaries and should not result in a undetected island. The original load values were also a point of interest in the sense of observing if the residential area, with only a few extra PV-units than the original dataset, posed any risk of unintentional islanding with respect to the passive protection schemes. After observing the LV-grid with only 21 PV-units, the question of how the grids behavior would change with more PV-units installed arose. Following the trend of more and more PV-panels being installed, one could wonder how the unintentional islanding behavior will change with more PV-units spread throughout the same grid. This scenario was investigated in the next grid model, the 'PV-grid model'.

## 3.7 PV-grid model

The third test grid is referred to as the PV-grid model and is structured the same as the LV-grid model, with the exception that all the 71 loads in the grid has an accompanying PV-unit. So instead of testing the grid behavior for 21 PV-units as in the LV-grid model, the PV-grid model was observed for a total of 71 PV-units. Meaning that the additional PVs connected to buses in the LV-grid were removed, but all of the extra PVs connected to loads were kept in place. The total active power produced by the PV modules which was used prior to this point, set as 298.5 kW, was then divided by the amount of PV modules in order to get an average value of the produced active power. This value was then selected as the active power production for each new PV module, meaning that every single one of the 71 PV-units in the PV-grid were rated at 4.2 kW. This amounts to a total generation of 298.2 kW in the PV-grid, which was considered close enough to a generation and load balance to be able to compare results with the LV-grid with slightly higher total generation value of 298.5 kW. Island operation tests were performed in this version of the network by disconnecting the external grid, same as in the LV-grid model. The PV-grid model was first tested without any additional modifications, as well as comparing its NDZ with the one drawn for the LV-grid in order to inspect if there are any differences in the four boundary points. The total generation within the PV-grid was raised temporarily, to 298.5 kW instead of 298.2 kW, to be amount to exactly the same generation used in the LV-grid for the NDZ boundary point tests. An observation of varying some of the PV-unit protection settings was also conducted, in order to determine if protection sensitivity has any impact on the island behavior. The grid model was also tested with a balance between consumed and produced active power, which could be compared to the generation and load balance tests performed in the LV-grid model. Resulting in three different categories of tests performed in the PV-model, each of which is explained in more detail below.

### 3.7.1 Comparison of LV-grid NDZ

The first test performed in the PV-grid model was a comparison of the four boundary points of the NDZ with the previous points drawn for the LV-grid model. The PV-grid was set to a total generation of 298.5 kW and the two max/min points for the active power P while Q was set to zero were found, and the corresponding two max/min points for the reactive power Q were found for when P was set to the same value as the generation (298.5 kW). These four points were then compared to the corresponding points of the same generation rating in the LV-grid. This test was conducted to observe if the increased total amount of PV-units spread out throughout the grid would have an impact on the NDZ and the stability of the potential island.

### 3.7.2 Varying inverter settings

After comparing the PV-grid model's boundary points with the previous LV-grid model, the question of protection settings came into question. All of the grid connec-

ted converters follow the regulations and protection requirements for being connected to the Swedish utility grid, but how could potential island behavior vary if these settings are more or less sensitive than others while still being within the acceptable limits? And what protection settings can be deemed to have more impact in certain scenarios? While conducting the NDZ-tests of the previous grid, it became evident that the boundary connected to the OV protection and detection could be regarded as the most flexible boundary in a sense. Operation close to the OV boundary in the NDZ, overproduction scenarios for which the grid has more total generation than load, exhibited a behavior of were groups of PV-units would detect the OV first due to voltage differences in the grid and promptly disconnect. Which would effectively lower the total generation within the grid, lower the voltage for the remaining PV-units still in operation, and result in a smaller island which depending on the size would operate longer than the specified 5 seconds. This behavior was only apparent close to the OV boundary, the other UV boundary in the NDZ exhibited more unison behavior amongst all of the PVs because disconnection of a few PV-units and a voltage drop would just result in instant detection of the whole island. Similarly, the OUF boundaries also showed unison behavior amongst the PVs due to the shared frequency value throughout the grid. This lead to the conclusion that the easiest way to affect the potential island behavior was to change settings related to the OV detection. The most prominent setting affecting OV detection without making changes which would make the converter violate the regulations is the OV detection time delay. The OV protection function time, defined as 0.2 seconds by the ALP, was therefore deemed as a parameter of large impact of the island detection. So the test for varying inverter settings was designed to inspect how the island detection would change if some of the PVs in the PV-grid were significantly more sensitive than the others. Twenty PVs throughout the grid were changed in their protection settings, having their OV (step 1) function time changed from 0.2 seconds to 0.1 seconds, effectively making them act faster than the remaining 51 PVs in OV scenarios. This test was of great interest due to the fact that all inverters in the Swedish grid should be approved following the regulations, but not all inverters act the same. Different manufacturers have different sensitivities, and no one is to say that some inverters can't be more effective or act faster than the regulation requires them to.

### 3.7.3 Generation and load balance test

Following the varying of inverter settings, the PV-model was returned to its original protection settings. With generation and load being rated roughly the same, 298.2 kW and 298.5 kW respectively, this test and the PV-grid behavior could be compared to the previous grids and their generation and load balance tests. The generation and load balance test for the grid was of interest for the same reason as the previous models, finding out how one of the worst cases of unintentional island operation would behave and roughly how long it can persist.

## 3.8 Medium voltage cable model

The last and final grid model is described as the MV cable model, and was based upon the structure of the PV-grid model. The only adjustment made compared to the previous model was that the MV cable model has a MV cable connected right before the transformer 10/0.4 kV transformer. Instead of having the external grid connected to a bus on the 10/0.4 kV transformer's high voltage (HV) side, the MV cable model has the external grid connected to a new 40/10 kV transformer with a 10 kV HV bus connection leading to a MV cable before the connection to the 10/0.4 kV transformer leading down to the LV grid. The changes performed in the MV cable grid are shown in Figure 3.9. The data of the new additional transformer connected on the HV side can be observed in Appendix B, Table B.21, while the MV-cable type and data used for the MV cable model are presented in Table B.22. The purpose of the MV cable model was to monitor the grid behavior for different lengths of MV cable included in the potential island. The aim was to observe how the MV cable's impedance and value would affect this bigger island, and how it would change when comparing the 10 kV cable of 1 km length with 5 km and 10 km respectively. This behavior is of interest regarding questions of the potential island size and how inclusion of higher voltage parts of the grid could affect the island detection as a whole.

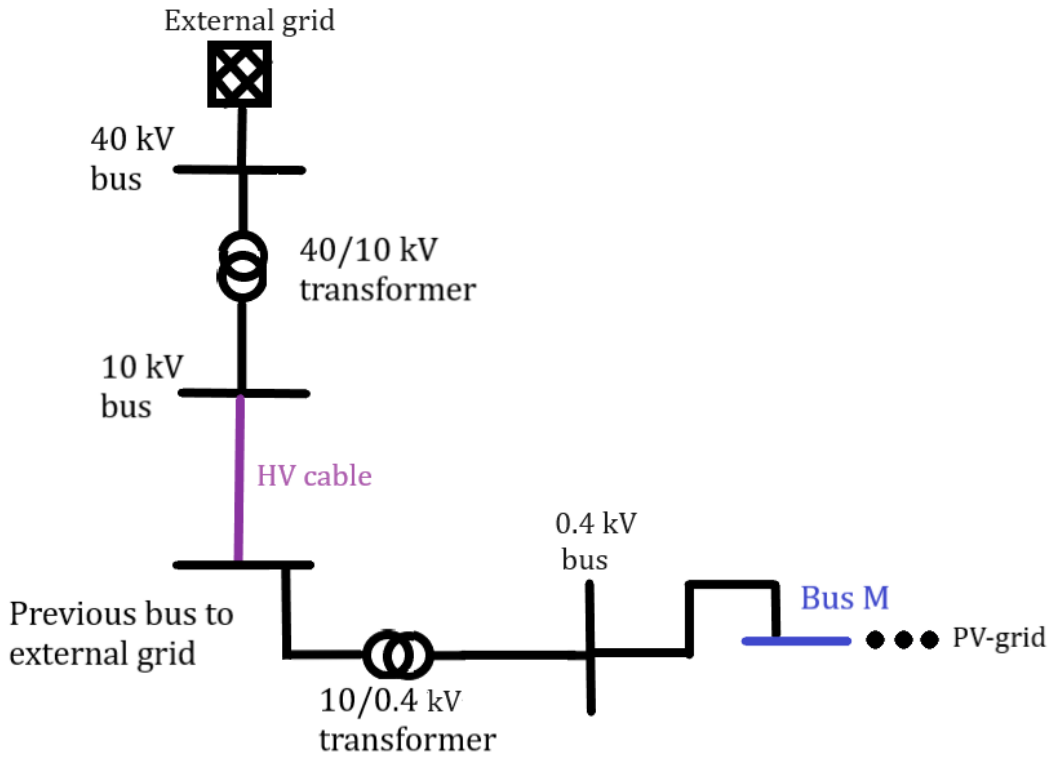


**Figure 3.9:** Medium voltage cable grid model depicting the additional HV buses, transformer and cable connected to the low voltage grid with 71 PV-units.

# 4
# Simulation results

## 4.1 Basic model

The Basic model was used in order to ascertain how well the different passive protections prevented unwanted-island operation observing only one PV-unit connected to a load on the low voltage side. The tests performed on the Basic model are listed in order below, followed by the findings. The first test performed to observe the grid and protection behaviors during unwanted-island operation was the scenario of the load's active power being equal to the generation of the PV-unit. The generation and load balance test was followed by observations of grid behavior if the difference of generation and load differed by ±1 %, ±10 % and ±25 % in active power. Lastly the generation equal load tests were rerun with different values of reactive power for the load, both with +0.1 kVAr and -0.1 kVAr.

### 4.1.1 Generation and load balance

The generation equal load balance test was performed with both generation of the PV-unit and the load being equal to 10 kW and set to 0 kVAr. The frequency and voltage graph for the test with disconnection in break point A can be observed in Figure 4.1. The OF protection activated after 8.39 seconds. The corresponding test for break point B is shown in Figure 4.2, which resulted in a OF protection activation after 22.65 seconds. The PQ flow can be seen in Figure C.1 in Appendix C and indicates that nothing is flowing through breakpoint B, and the external grid is providing power to compensate for the transformer losses through breakpoint A. The breakpoints can be seen in Figure 3.7.

Comparing the result from disconnection in break point B with the previous in break point A shows that the disconnection point has great impact upon the potential island stability. Disconnecting from the external grid in break point B, excluding the transformer from the potential island, left the island more stable and able to persist longer. This is likely to be a direct result of the transformer losses destabilizing the potential island and making the frequency increase faster when included in the potential island.

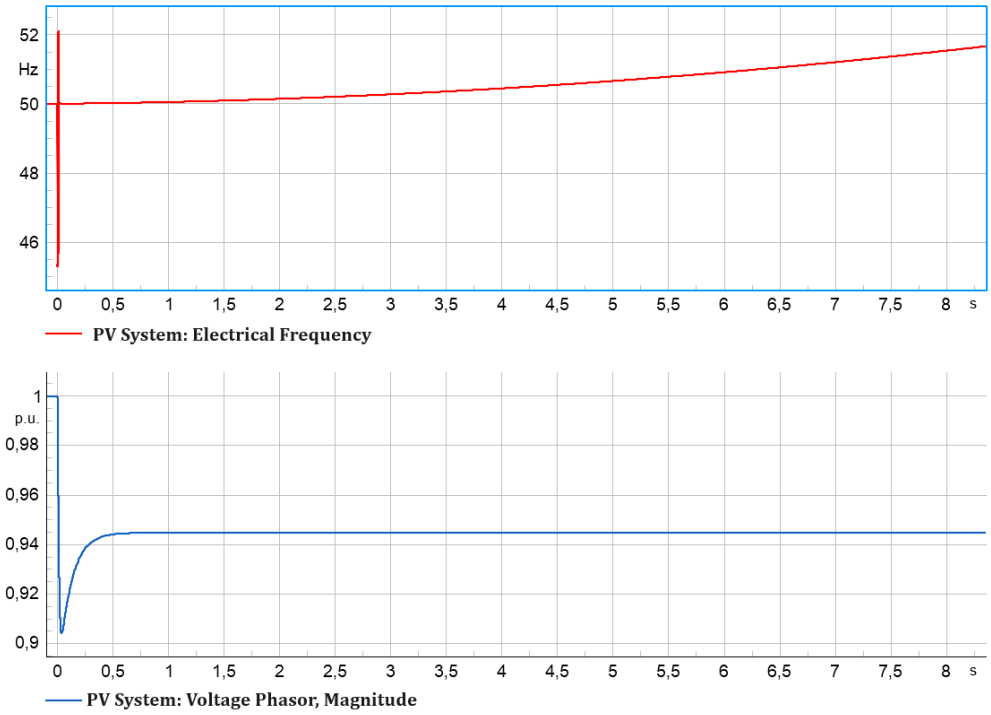


**Figure 4.1:** Frequency in Hz (red) and voltage in p.u. (blue) over time on the x-axis in seconds for disconnection in point A, measured by the PV-unit until the point of protection activation.

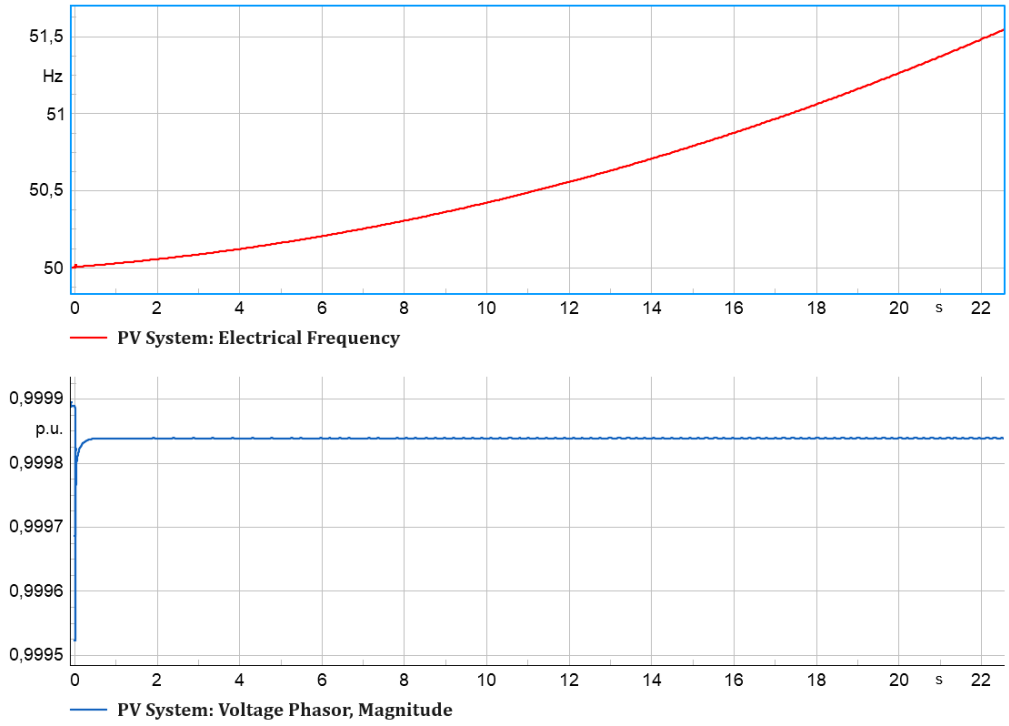


**Figure 4.2:** Frequency (red) and voltage (blue) over time for disconnection in point B, measured by the PV-unit until the point of protection activation.

It is also worth noting that frequency and voltage spikes can be observed in the result graphs, in the graphs above but also the ones shown later in this chapter. These frequency and voltage spikes are due to the disconnection of the different phases once they reach their zero crossing, and can be seen in Appendix C, Figures C.2-C.15. Important to note here is that the direction of the spikes changes depending on if the active power of the load is higher or lower than that of the generation, and the magnitude is dependent on how large the active power mismatch between load and generation is. For the reactive power cases it depends on if there is a capacitive or an inductive load which way the spikes are pointing, and the mismatch determines the magnitude. These spikes are a bit different in the way that they have more of a curvature to their form, especially when it comes to break point B, which can be seen in Figures C.8 and C.9.

### 4.1.2 Difference in generation and load

After investigating the potential island's behavior with regard to size, the impact of the different break points mentioned in the previous section, followed tests with the aim of observing the grid behavior at different imbalances between the generated power and load. The chosen load ratings for these tests were ±1 % over and under the constant PV generation rated at 10 kW, as well as ±10 % and ±25 %. The results from each test, all performed for both break point A and B, are listed in Table 4.1. The frequency and voltage graphs for the tests in Table 4.1 can be found in Appendix C, Figures C.16-C.27.

**Table 4.1:** Summary of the test results with varying active load values, with the PV-unit rated at 10 kW. All measurements are done at the PV-location.

| Load variation with respect to the generation | Active load [kW] | Break point | Protection trigger type | Protection trigger time [s] | Phase voltage at trigger time [p.u.] | Frequency at trigger time [Hz] |
|---|---|---|---|---|---|---|
| -1 % | 9.9 | A | OF | 8.37 | 0.949 | 51.66 |
| | | B | OF | 24.09 | 1,005 | 51.55 |
| +1 % | 10.1 | A | OF | 8.41 | 0.941 | 51.66 |
| | | B | OF | 21,40 | 0,995 | 51.56 |
| -10 % | 9 | A | OF | 8.13 | 0.990 | 51.68 |
| | | B | UF | 49.79 | 1.054 | 47.45 |
| +10 % | 11 | A | OF | 8.58 | 0.902 | 51.66 |
| | | B | OF | 16.07 | 0.953 | 51.61 |
| -25 % | 7.5 | A | OF | 7.48 | 1.072 | 51.68 |
| | | B | OV | 0.22 | 1.172 | 50.03 |
| +25 % | 12.5 | A | UV | 0.22 | 0.803 | 50 |
| | | B | OF | 12.97 | 0.88 | 51.61 |

It is shown in Table 4.1 that the series of tests with ±1 % were similar to the original generation equal load case, with only small differences in protection trigger time. Both the ±1 % and ±10 % tests results in islands persisting much longer than the maximum five second window which has been chosen as an acceptable observation in this study. All of these four tests also trigger for over frequency protection, except for the overproduction case with -10 % load value and break point B, which results in the most stable island that persists for roughly 50 seconds before the protection trigger for under frequency is activated. The origin of this particular UF protection trigger is unknown, since this test showed zero voltage-current angle difference. Further studies would be required to investigate why the frequency drop

occurs and its origin. Lastly, the overproduction case with -25 % load rating and breaking point B as well as the underproduction with +25 % load exhibits almost instant detection of the unwanted islands, due to the sudden increase and decrease of voltage respectively due to the imbalance created in during the disconnections of the external grid. These last four tests show that a disparity as big as 25 % between generation and load can still become a island that goes undetected for more than five seconds depending on if it's a over- or underproduction case, and how big the potential island is (in this case whether the transformer is included or not). These cases show that the 25 % load disparity is enough to instantly detect the island in the overproduction if the island is small enough so that the overvoltage range gets violated (break point B), with a slightly bigger island (break point A) the voltage stabilizes below said overvoltage range of 1.15 p.u. making sure the island can persist a while longer. In the underproduction case with 25 % extra load, one can see that the bigger island created with the transformer included due to disconnection in break point A results in a big enough voltage drop that the undervoltage protection detects said island. Meanwhile the case utilizing break point B results in a small enough island that the voltage stabilizes above the undervoltage range, and keeps going for roughly 13 seconds undetected. One of the observations that can be made from the results presented in 4.1 is that the chosen break point of the disconnection from the external grid has a big impact upon the potential island's stability. Having the disconnection in break point A previously shown in Figure 3.7, makes the potential island include more equipment and elements, affects its stability in the way that the island is detected faster. Having the disconnection in break point B for comparison, which excludes the transformer from the potential island, makes the potential island more stable and therefore results in a longer detection time. This is probably due to the transformer losses, namely core and copper losses, which adds disruption to the island when the transformer is included while using break point A. Using break point B on the other hand does not include extra losses or elements said transformer, resulting in a more stable island than one resulting from break point A.

### 4.1.3 Impact of reactive power

The last tests on the Basic grid model were done with the same settings as the generation and load balance tests, with the exception that the load was rated with 0.1 kVAr capacitive and inductive load. A summary of the results of the four reactive power tests are presented in Table 4.2. The frequency and voltage magnitude graphs are presented in Appendix C, Figures C.28-C.31.

**Table 4.2:** Summary of the test results with varying reactive load values, with the PV-unit rated at 10 kW and active load 10 kW.

| Reactive load [kVAr] | Break point | Protection trigger type | Protection trigger time [s] | Voltage at trigger time [p.u.] | Frequency at trigger time [Hz] |
|---|---|---|---|---|---|
| -0.1 | A | UF | 3.89 | 0.945 | 46.83 |
| | B | UF | 3.31 | 1.001 | 46.7 |
| +0.1 | A | OF | 2.65 | 0.945 | 52.12 |
| | B | OF | 2.46 | 1.00 | 52.19 |

Comparing the previous results of Table 4.1 and Table 4.2, one can swiftly notice the different impacts of active versus reactive power in the grid and the resulting detection time of the potential islands. While the active power in the load could be varied with as much as 2.5 kW up and down and still result in a persisting island for more than five seconds, changing the reactive power of the load with ±0.1 kVAr resulted in quick detection of the island in both cases. This result shows that the potential island in of itself is more easily disturbed by reactive power imbalances in the grid compared to active power imbalances.

The reactive power has a big impact on the island stability due to the effect it has on the angle between voltage and current. Having an inductive load in the grid causes load angle to be positive, resulting in a rising frequency curve after disconnecting the external grid. A capacitive load would likewise cause a negative load angle, current leading the voltage, and result in a decreasing frequency curve after the disconnection of the external grid. The load angle in turn causes the voltage-current angle at the PV inverter to change too, as seen in Figure 4.4 when a capacitive load is connected. The frequency stability is much more easily disturbed due to the reactive power imbalances in the grid compared to the active power imbalances it would take to trigger the voltage protections. The explanation for this might be the use of the two-port equations in case of highly resistive grid impedance. The two-port equations are shown in (4.1)-(4.4).

$$P_1 = \frac{|V_1|^2}{|Z|} sin\theta + \frac{|V_1||V_2|}{|Z|} sin(\delta - \theta) \tag{4.1}$$

$$P_2 = -\frac{|V_2|^2}{|Z|} sin\theta + \frac{|V_1||V_2|}{|Z|} sin(\delta + \theta) \tag{4.2}$$

$$Q_1 = \frac{|V_1|^2}{|Z|} cos\theta - \frac{|V_1||V_2|}{Z} cos(\delta - \theta) \tag{4.3}$$

$$Q_2 = -\frac{|V_2|^2}{|Z|} cos\theta + \frac{|V_1||V_2|}{Z} cos(\delta + \theta) \tag{4.4}$$

Where $P_1$ and $Q_1$ is active and reactive power from supplying bus respectively, $P_2$ and $Q_2$ is active and reactive power from receiving bus, Z stands for the impedance, $\delta$ the transmission angle and $\theta$ is the loss angle defined as $arctan(\frac{R}{X})$. In a lossless case, where the loss angle $\theta$ is very small then the cosine value would be close to its maximum. A small change of delta in this case would result in a very small change in cos($\delta$) and consequently $Q_2$ in (4.4). In the case of a highly resistive grid ($R \gg X$), where $\theta$ becomes large for example 45°, then a small change around that angle would result in a large change of $cos(\delta + \theta)$ and accordingly $Q_2$. This also indicates that a change in load angle would have a much greater impact for the reactive power compared to the active power, which then in turn influences the calculated $u_r$ and $u_{im}$ that the PLL uses to calculate the frequency. If this happens to a large enough degree, or at a certain speed, it is possible that the calculations performed by the PLL will have errors which in turn causes a chain reaction which will further change the frequency.

Which could explain why reactive power imbalance is more strongly tied to the frequency protections, as the active power imbalances is more tied to the voltage protections in these tests. As observed in the tests regarding active power, the active power mismatch triggers the OV protection if the load is small enough compared to the generation that the grid voltage exceeds the OV range. Likewise, the active power has to be sufficiently large compared to the generation in order to trigger the UV protection.

Additionally, which can be seen in Figure 4.3, when the disconnection happened when the load and generation was the same, in this case occurring at 2 seconds instead of 0 in order to increase visibility, the difference in angles between the voltage and current phasors for the PV-system at the PV-bus, see Figure 3.7, jump up to become approximately 0.05 degrees. This in turn causes the PV to output a very slight amount of reactive power, which in turn makes the frequency slowly increase which can be seen in the previous results clearly. When a capacitive load is applied instead of a resistive one, the angle difference now turns negative to around -0,5 degrees. This only means that the current is now leading instead of lagging, and this difference can be seen in Figure 4.4. Important to note here is that the angle difference is changing towards the positive direction as it is moving closer to -0,4 degrees, indicating that the reactive output of the PV inverter somewhat counteracts this initial angle difference.

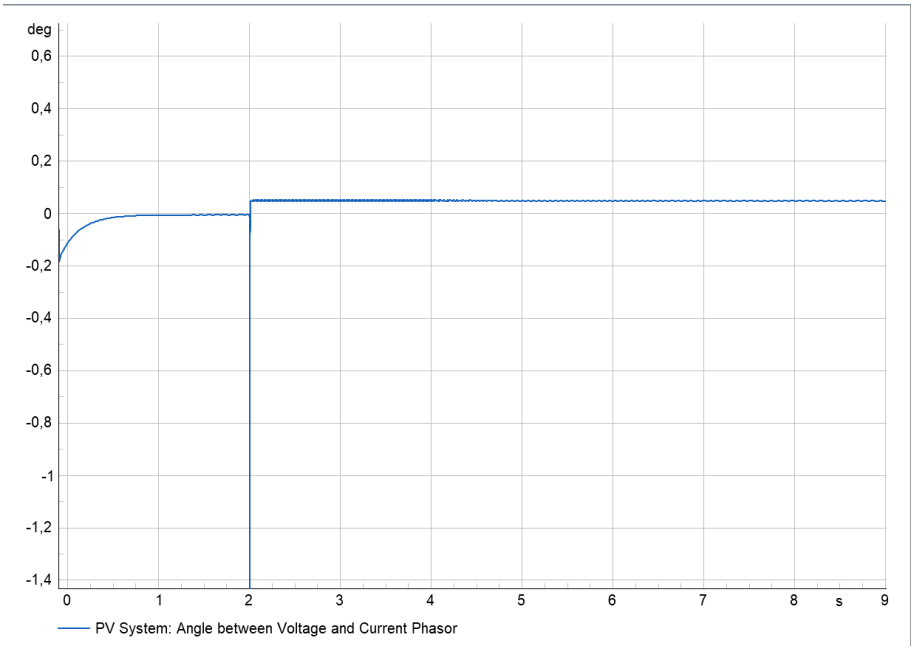


**Figure 4.3:** Angle difference between voltage and current phasors for generation and load balance.

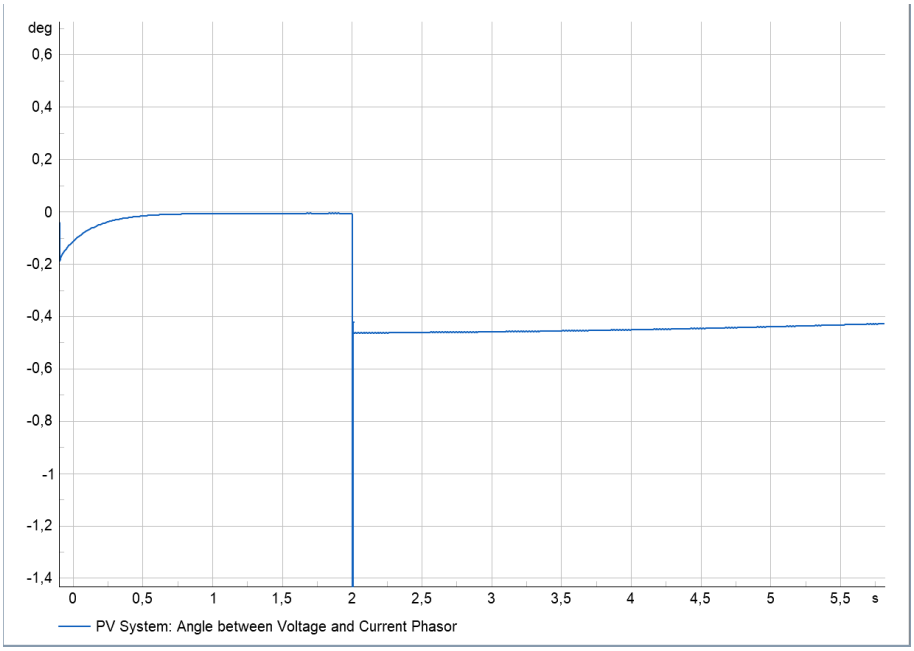


**Figure 4.4:** Angle difference between voltage and current phasors for -0,1 kVAr.

When an inductive load is used, the angle difference increases in the positive direction instead, seen in Figure 4.5. Here the difference also increases with time, going from almost 0,55 degrees to 0,59 degrees. This seems to confirm that the reactive output of the PV inverter has a rather noticeable effect on the system. When the resistive load is changed to be smaller instead, the angle difference remains roughly the same as it was in the balanced case, 0,05 degrees, and can be seen in Figure 4.6. This indicates that the active power mismatch will not affect the angle difference for the PV much at all, and will as such not contribute notably to the frequency increasing or decreasing.

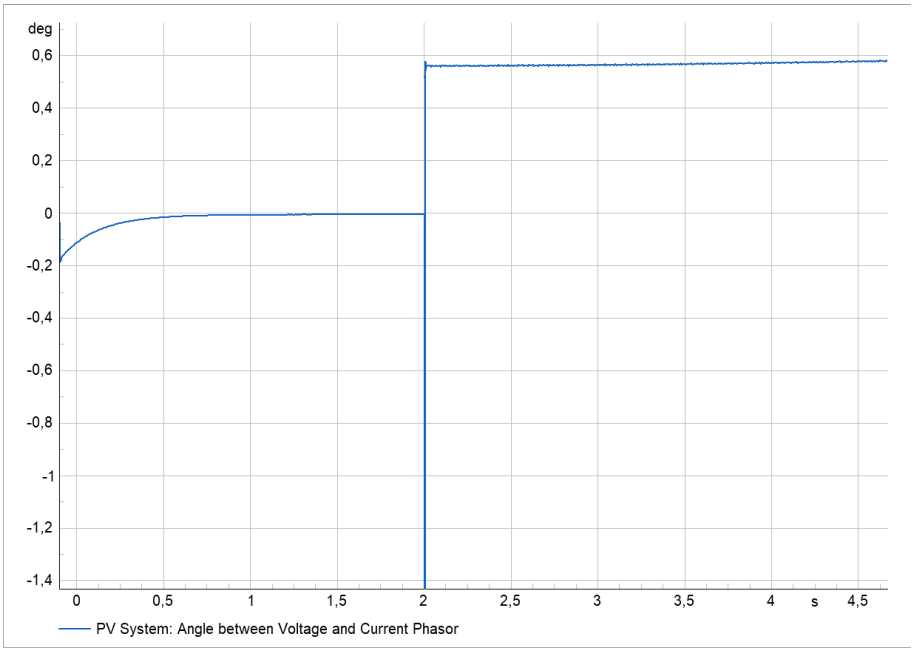


**Figure 4.5:** Angle difference between voltage and current phasors for +0,1 kVAr.

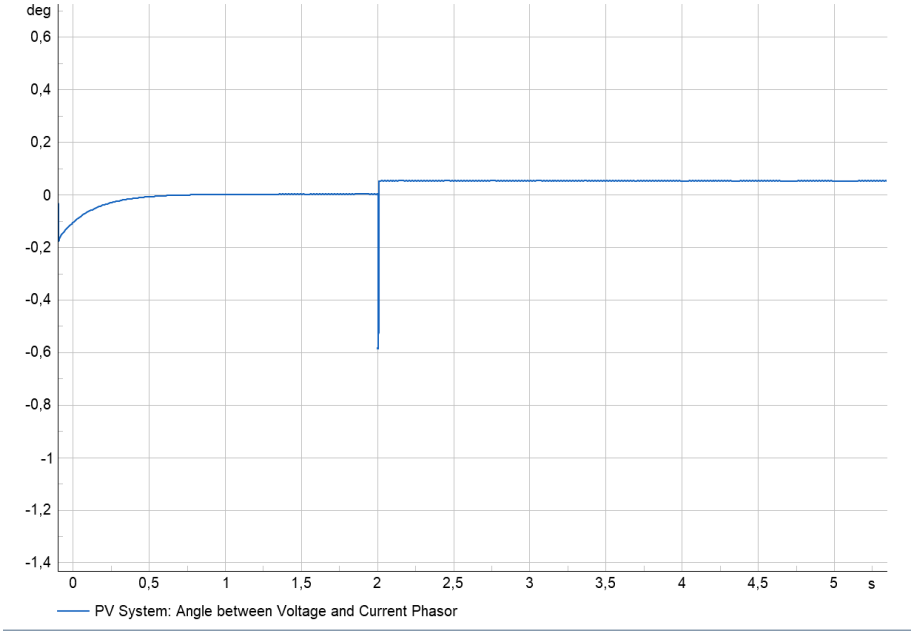


**Figure 4.6:** Angle difference between voltage and current phasors for 9 kW.

## 4.2 Low voltage grid model

The tests explained in chapter 3.6 are listed with respective results below. Starting with the generation and load balanced test, without and with respect to the cable effects. Followed by the NDZ for different active and reactive power values with respect to the total generation of 298.5 kW, and then with a higher and lower total

generation of ±50 %. The last tests were the disruption with additional car charger loads, and lastly the test with the original maximum load values for the houses throughout the grid. A summary of all of the tests performed in the LV-grid model, except for the NDZ tests, are presented below in Table 4.3.

**Table 4.3:** Summary of LV-grid test results, excluding the NDZ tests.

| Test description | Total active load P [kW] | Total reactive load Q [kVAr] | Total PV generation | Protection activation time [s] | Protection trigger type | Voltage at trigger time [p.u.] | Frequency at trigger time [Hz] |
|---|---|---|---|---|---|---|---|
| Generation and load balance (without cables) | 298.5 | 0 | 298.5 | 16.52 | OF | 1.001 | 51.63 |
| Generation and load balance (with cables) | 298.5 | -0.1 | 299.8 | 89.15 | OF | 1.003 | 51.54 |
| Disturbance test (car chargers) | 331.5 | 0 | 298.5 | 17.23 | OF | 0.9476 | 51.61 |
| Original house load values | 596 | 95 | 298.5 | 0.211 | UV | 0.539 | 50.66 |

### 4.2.1 Generation and load balance tests

The generation and load balance test, excluding the cable effects, resulted in an island lasting roughly 16 seconds before the protection triggered for overfrequency values. The frequency and voltage magnitude graphs can be seen in Figure 4.7 below. The test showed that the potential island for the generation and load balance with the 21 PV-units persists longer than the previously mentioned 5 seconds used as a base line in this report.

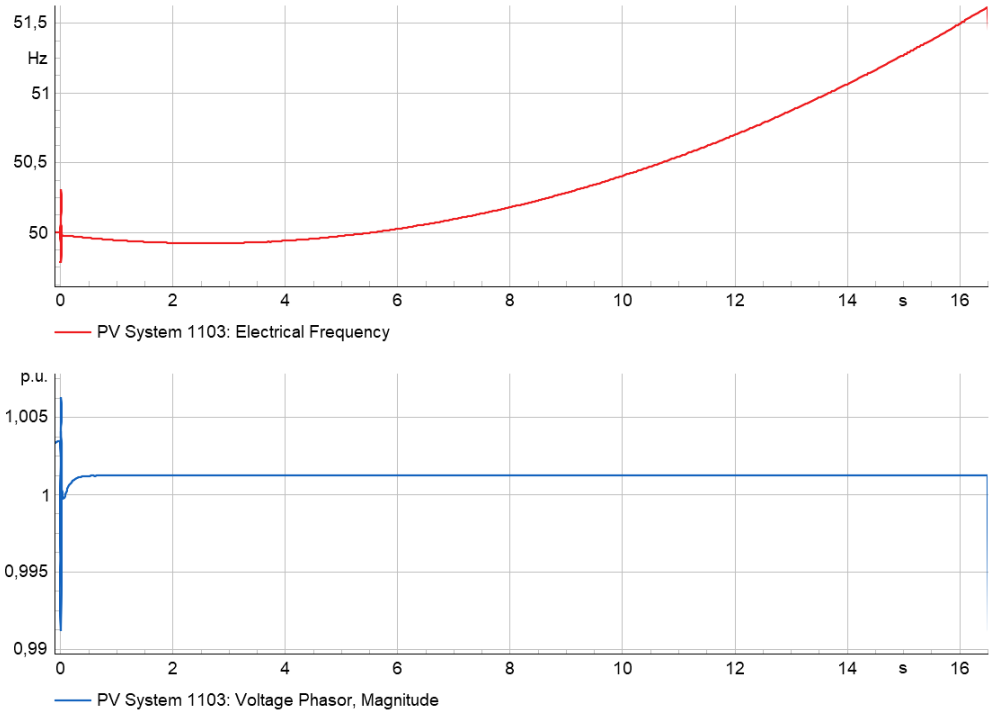


**Figure 4.7:** Frequency and voltage magnitude graphs for the generation and load balance test, excluding cable values, in the LV-grid.

Further extending the test to also include the cable values in the LV-grid, which in

the load flow showed values amounting to 1.3 kW and 0.1 kVAr, proved that the closer you get to true balance of the total grid values the more stable the potential island will become. The resulting graphs of the generation and load balance test with respect to the cable values can be observed in Figure 4.8. Including the cable values in the generation and load compensation resulted in undetected island operation lasting for almost 90 seconds, which compared to the island created in the previous balanced test that only lasted 16 seconds shows a clear escalation of the island stability. Which brings up the question of which parameter affects the potential islands stability the most? And when aiming for zero-tolerance of unwanted-island operation, when does the risk of an island forming and not being detected within 5 seconds of the formation appear? These questions for this specific LV-grid model are answered in the next section, where NDZ of the grid was put to the test.

The unusual shape of these frequency graphs shown in Figure 4.7 and Figure 4.8 is due to the angle differences shown in section 4.1.3, but also due to when the disconnection of the external grid occurred. Something which can be observed in Figure 4.3 is that the angle difference starts out negative before stabilizing before the disconnection occurs. When doing these tests for the LV-grid, the initial angle difference can be observed in Appendix C, Figure C.36 which is for the PV-grid presented later but applies to the LV-grid too and shows that there is an initial angle difference here as well. As the disconnection was done at 0 seconds, which is at the highest part of this difference graph, this error is persistent through the simulation and causes the initial dip followed by the rise, creating a "banana" shape of the frequency graph. Had the disconnection happened at 2 seconds instead, something akin to Figure C.37 in Appendix C would have been observed. This is a significant error, and the detection time would be faster, but it would still be far outside of the 5 seconds that has been specified as unwanted and does not largely affect the upcoming NDZ.

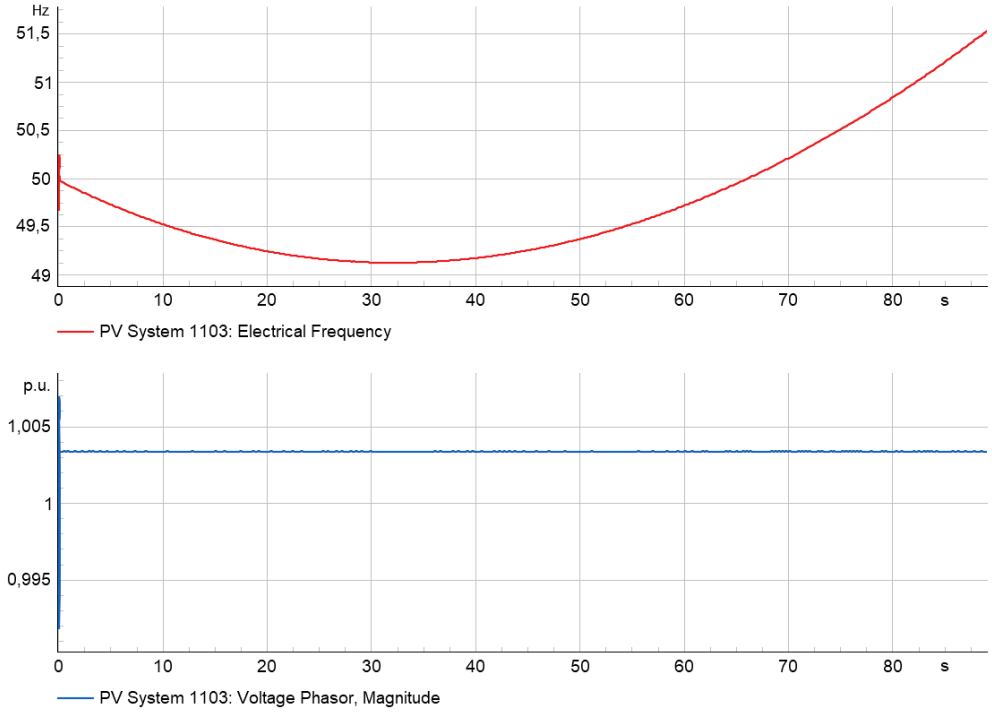


**Figure 4.8:** Frequency and voltage magnitude graphs for the generation and load balance test, including cable values, in the LV-grid.

### 4.2.2 Non-detection zone of varying loads

The NDZ of the LV-grid model is shown in Figure 4.9, where the x-axis is in the change factor of active power P with respect the generation of 298.5 kW and the y-axis is the reactive power Q in percent of the same generation. The orange points represents frequency boundaries, where OF or UF protection triggers, and for which the island exceeds 5 seconds of operating time when moving inside the zone. The points to the right of the center represent an overfrequency while the points to the left represent underfrequency. The grey points represents the voltage boundaries, for which the value of P is large/small enough to instantly detect the island due to the UV (top) or OV (bottom) independent of the Q value. All of the NDZ points depicted in Figure 4.9 are listed in their numerical values in Appendix C, Table C.1.

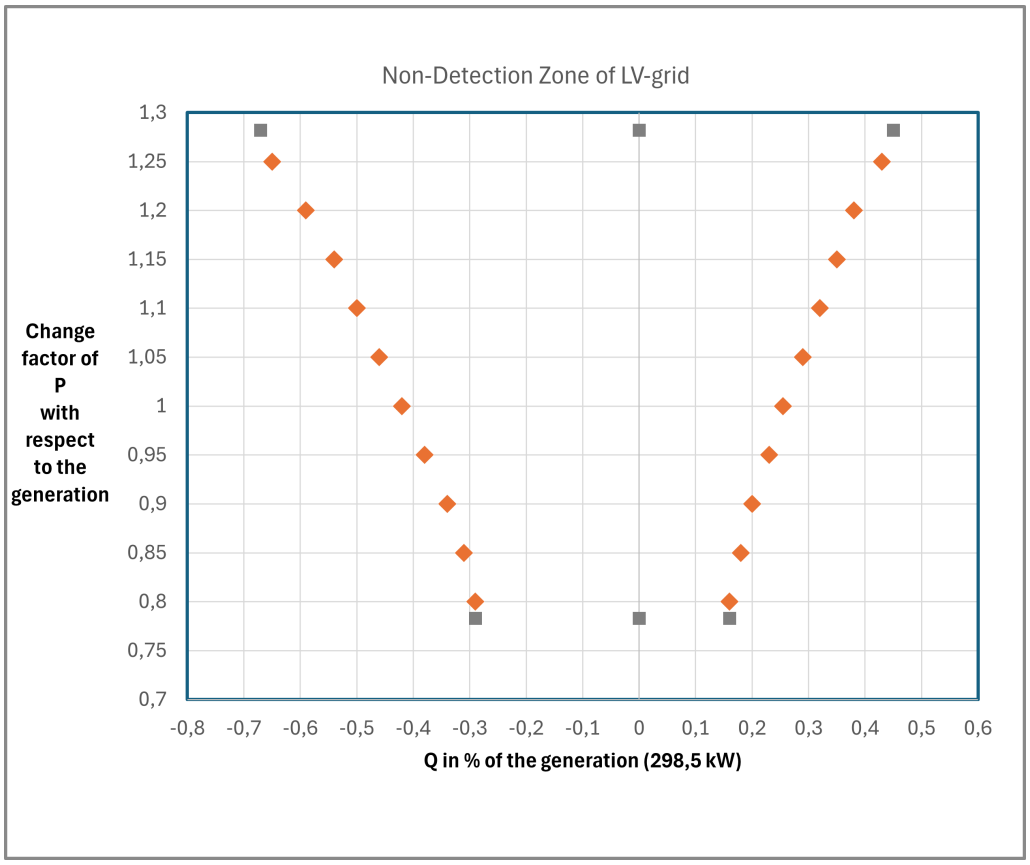


**Figure 4.9:** NDZ of the LV-grid, zone depicting island operation longer than 5 seconds. Active power P change factor of generation (298.5 kW) on the y-axis, reactive power Q in percentage of the generation on the x-axis.

The resulting NDZ of the LV-grid shows that the grid is much more sensitive to reactive power imbalances than active power, since the active power boundaries are located at 28.2 % load over the generation value and 21.7 % load under the generation value. The reactive power boundaries on the other hand are located at -0.42 % and 0.255 % of the generation respectively. The P boundaries in kW correspond to 382.68 kW for the upper boundary and 233.73 kW for the lower one. The Q boundaries in kVAr are 0.761 kVAr and -1.254 kVAr respectively. But these boundaries were only relevant for when the PV-units generated a total of 298.5 kW through out of the grid, so additional tests for increased and decreased total production were carried out to observe if said boundaries would shift. The decreased total production comparison was done for 50 % less generation, meaning 149.25 kW instead of 298.5 kW. Lastly, a test with higher total generation of 50 % extra generation, giving a total of 447.75 kW, were performed for the 4 boundary points of P and Q. Assuming that the NDZ retains the same cone like shape as in the 298.5 kW generation case depicted in Figure 4.9. The zones with different total generation were only tested for the maximum and minimum P when Q is zero and the max and minimum Q points when P is equal to the total generation. The results of these four boundary points for the different total generation values are presented in Figure 4.10, and all of the values for each point if Figure 4.10 are listed in Table

4.4.

**Table 4.4:** Values for the boundary points with varying generation, original points for 298.5 kW of generation (blue), increased generation resulting in 447.75 kW (purple) and points for a decreased total generation resulting in 149.25 kW (yellow).

| Total generation [kW] | Active power P [change factor of the generation] | P [kW] | Reactive power Q [% of generation] | Q [kVAr] | Protection trigger time [s] |
|---|---|---|---|---|---|
| 298.5 | 1.282 | 382.68 | 0 | 0 | 0.230 |
| | 0.783 | 233.73 | 0 | 0 | 0.661 |
| | 1 | 298.5 | 0.255 | 0.761 | 5.023 |
| | 1 | 298.5 | -0.42 | -1.224 | 4.98 |
| 447.75 | 1.276 | 571.33 | 0 | 0 | 0.200 |
| | 0.785 | 351.48 | 0 | 0 | 0.600 |
| | 1 | 447.75 | 0.24 | 1.075 | 4.995 |
| | 1 | 447.75 | -0.43 | 1.925 | 5.034 |
| 149.25 | 1.288 | 192.23 | 0 | 0 | 0.4 |
| | 0.78 | 116.42 | 0 | 0 | 0.4 |
| | 1 | 149.25 | 0.28 | 0.418 | 4.962 |
| | 1 | 149.25 | -0.40 | 0.597 | 4.99 |

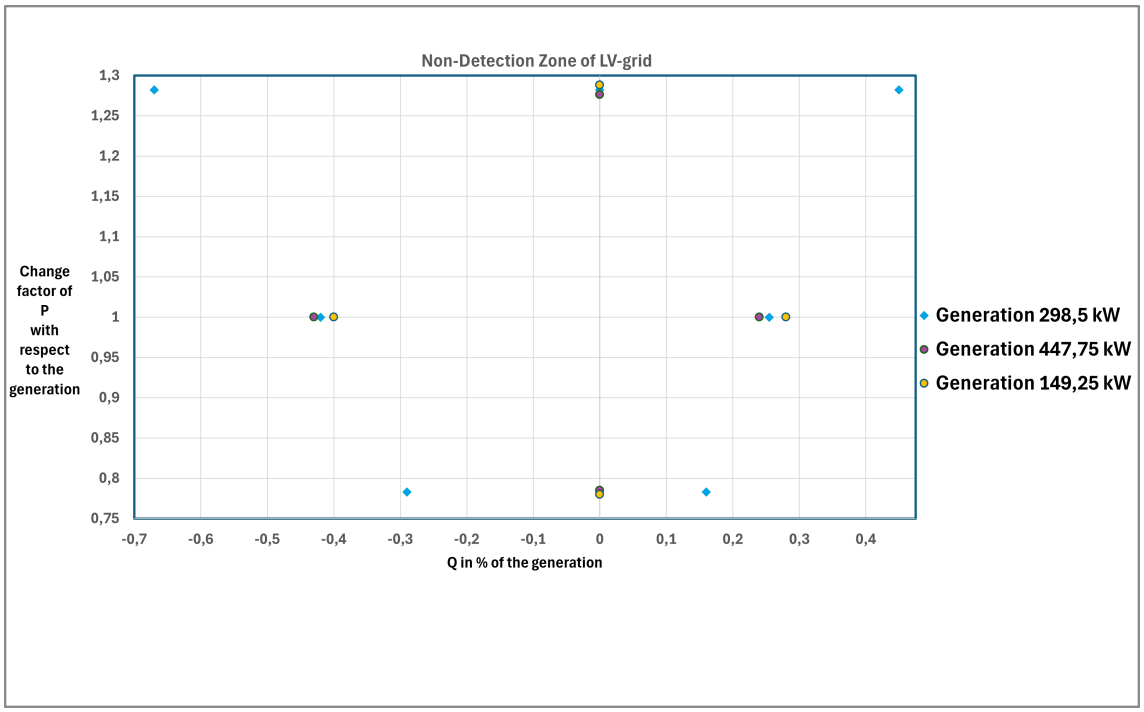


**Figure 4.10:** NDZ of the LV-grid in change factor and percentage values, for total generation of 447.75 kW (purple), 298.5 kW (blue) and 149.25 kW (yellow). Only depicting the maximum P values for Q=0 and the maximum Q points for P equal to the generation.

The points expressed in Figure 4.10 are expressed in change factor and percent of the total generation, the same boundary points can be seen in their respective kW and kVAr values in Figure 4.11.

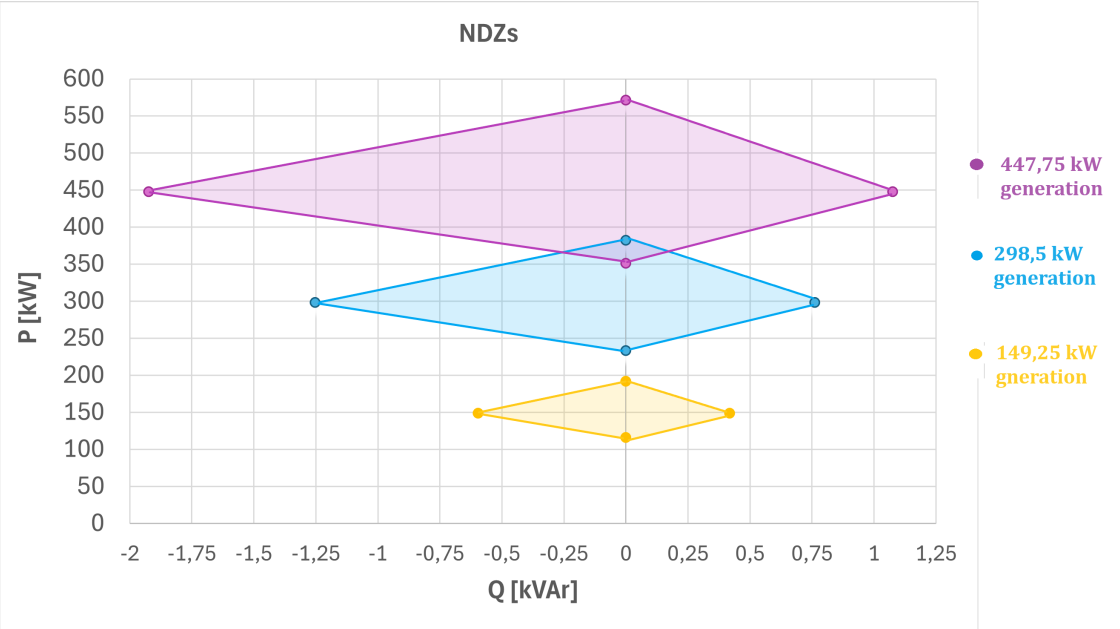


**Figure 4.11:** NDZ of the LV-grid in kW and kVAr values, for total generation of 447.75 kW (purple), 298.5 kW (blue) and 149.25 kW (yellow). Only depicting the maximum P values for Q=0 and the maximum Q points for P equal to the generation.

Both figures representing the four boundary points of P and Q for different total generation values show that the limits while having lower total generation slightly increases the absolute value of the boundaries of the positive and negative P values, and the positive Q value. But the absolute value of the negative Q point becomes slightly smaller. Increasing the total generation on the other hand decreases the absolute value for the positive and negative P values, and the positive Q value in Figure 4.10. But the absolute value of the negative Q value increases. Meaning that we over all get a slightly bigger NDZ for smaller total generation values, except for the negative Q point which decreases slightly. Which is shown in Figure 4.10, in the form of the blue points which represents the original generation value of roughly 300 kW and their relation to the yellow points that represents the smaller generation value of roughly 150 kW. It is also shown in Figure 4.10 that for the larger total generation of roughly 450 kW the purple boundary points become slightly smaller compared to the original 300 kW generation points, except for the negative Q point which absolute value increases. Despite the small boundary shifts the zone itself seems to retain the same shape and characteristic (the cone shape), since the four basic points looks like they retain the same relationship despite the shifts themselves that are very small.

### 4.2.3 Disruption with car chargers

In order to test the NDZ depicted in Figure 4.9 the load was increased after the island formation with 11 kW at 1 second, 2 seconds and 3 seconds, simulating three car chargers being engaged during the island operation. The total load increase of 33

kW being added in the island should be way within the NDZ since it only represents around 11 % increase over the generation if one starts with a generation equals load scenario excluding cable values. The resulting frequency and voltage magnitude graphs for the test can be observed in Figure 4.12. The OF protection triggered after 17.23 seconds, which is a little bit slower than the original 16.5 seconds for the same settings (excluding the activation of the car chargers). Meaning that as long as the load value stays within the NDZ, fluctuations and changes of the load won't trip the anti-island protection and they might even prolong the island operation if the unbalances doesn't become to large.

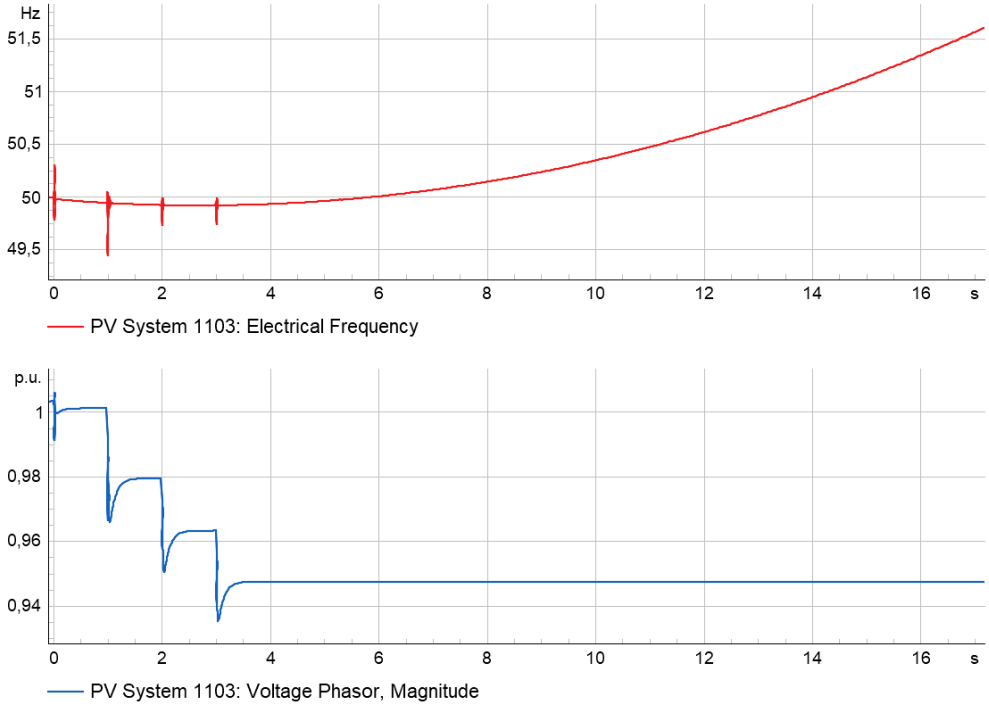


**Figure 4.12:** Frequency and voltage magnitude graphs for the Disruption with additional load test, simulating three 11 kW car chargers being added after 1-3 seconds.Test starts of as the previous generation equal load balance test, not including cable values.

### 4.2.4 Original values

The last test of the NDZ was with the original house loads which had significant active and reactive power values that would exist way outside of the NDZ, even with the extra 9 PV-units over the original 12 spread out in the grid. The tests frequency and voltage magnitude graphs are shown in Figure 4.13, and proves that the original grid values are outside of the NDZ and gets detected almost instantly at 0.211 seconds due to the UV protection. The load imbalance throughout the LV-grid is too big for the original house loads so this specific residential area doesn't run any risk of undetected island formation at the max loads values. Which brings forth the question of how will the grid behave if more PV-units are installed? A question which is investigated in the next section.

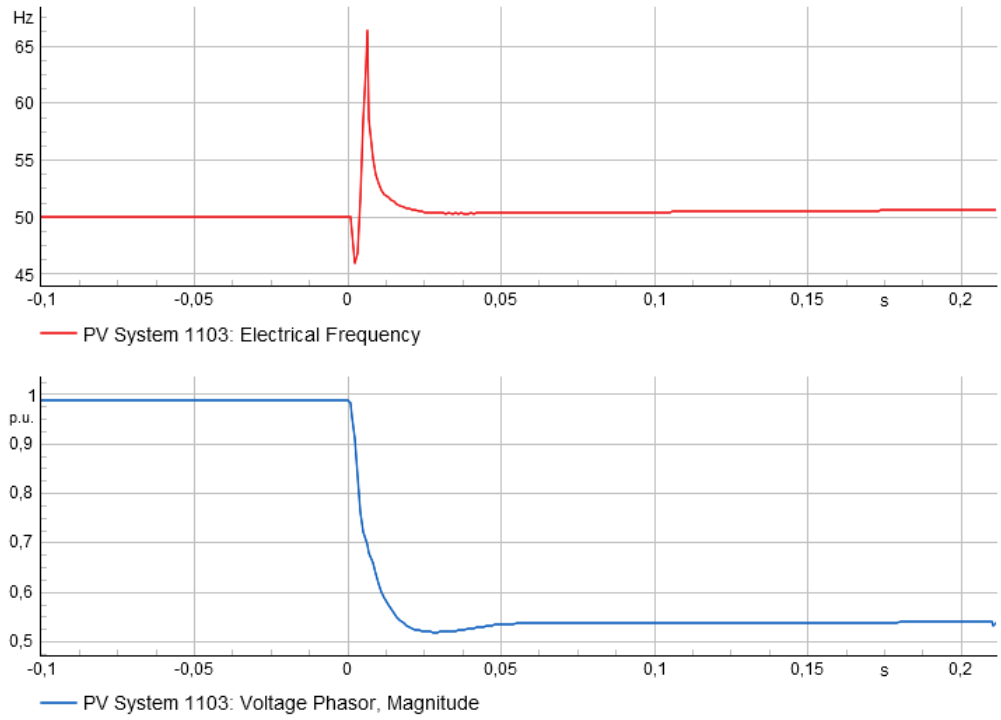


**Figure 4.13:** Test for original house loads in the LV-grid.

## 4.3 PV-grid model

Since the original house load values in the LV-grid creates imbalances during an islanding event due to the large load values, even if the total PV-generation is increased to 298.5 kW, one might wonder how the grid would behave if every house load had their own PV-unit. If every load was supported with an accompanying PV-unit would the NDZ change due to the amount of PV-units in the grid? These questions were answered by utilizing a total of 71 PV-units and setting their total generated power to the same as the previous NDZ test, 298.5 kW. The first test was a comparison of the new PV-grid model and its four boundary points of NDZ and the corresponding boundary points from the previous LV-grid NDZ. After the NDZ comparisons, a test with varying inverter settings was performed. The last test in the PV-grid was a generation and load balance test, with the aim of comparing the grid and its behavior to the previous generation and load balance behaviors in the previous grid models.

### 4.3.1 Comparison of previous non-detection zone

The comparison of the four boundary points, of max/min P while Q equalled zero, and max/min Q for P equal to the generation, with the previous four boundary points for the LV-grid can be observed in Figure 4.14. The figure shows that with the same total generation of 298.5 kW generated by more PV-units compared to the original LV-grid with 21 PV-units, results in the boundary points of Q to shift slightly. The positive Q point increases while the negative Q point's absolute value

decreases slightly. The points of P also shifted a little bit, but not so much to be apparent in the figure. So the original LV-grid points are once again listed in blue in Table 4.5, while the new points for the PV-grid are listed in green.

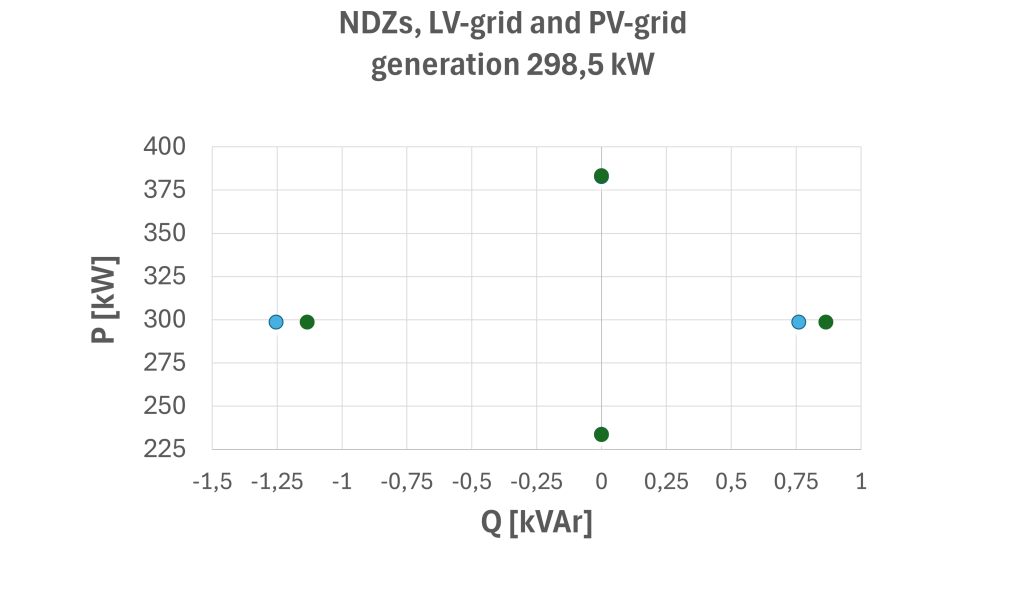


**Figure 4.14:** The four boundary points, of max/min P for Q equals zero and max/min Q for P equal the generation, for the PV-grid (green) and the LV-grid (blue).

**Table 4.5:** Values for the NDZ-tests for the four points of max/min P when Q is at zero and the max/min Q points when P is equal to the total generation. Original points for 298.5 kW of generation (blue) for the LV-grid containing only 21 PV-units, and the same boundary points for the PV-grid (green) for the same total generation but spread out amongst 71 PV-units.

| Total generation [kW] | Active power P [change factor of the generation] | P [kW] | Reactive power Q [% of generation] | Q [kVAr] | Protection trigger time [s] |
|---|---|---|---|---|---|
| 298.5 | 1.282 | 382.68 | 0 | 0 | 0.230 |
| | 0.783 | 233.73 | 0 | 0 | 0.661 |
| | 1 | 298.5 | 0.255 | 0.761 | 5.023 |
| | 1 | 298.5 | -0.42 | -1.224 | 4.98 |
| 298.5 | 1.284 | 383.27 | 0 | 0 | 0.43 |
| | 0.782 | 233.43 | 0 | 0 | 0.43 |
| | 1 | 298.5 | 0.29 | 0.866 | 5.0 |
| | 1 | 298.5 | -0.38 | -1.134 | 5.03 |

Table 4.5 shows the very slight increase of the positive and negative boundary points for P, which isn't evident in Figure 4.14 due to the decimal increase. Comparing the PV-grid points to the previous NDZ-tests of the original, increased and decreased total amount of generation shown in Figure 4.10, one can see that the PV-grid with generation of 298.5 kW shows a similar pattern as the LV-grid with decreased total generation. Meaning that compared to the LV-grid boundary points with the original generation, the PV-grid boundary points for P and the positive Q point expands very slightly meaning their absolute values become bigger. While the negative Q

point's absolute value decreases, moving the boundary point inward unlike the other three points moving outward. It was observed in the load flow while testing the PV-grid that the slight shift of these boundary points is due to the voltage difference throughout the whole grid is smaller. Compared to the load flows observed in the LV-grid, which displayed bus-voltages ranging from 1-1.02 p.u., the PV-grid displayed bus-voltages with 0.99-1 p.u. instead. Which brings the question of the differences between the two grid models, the LV-grid had fewer PV-units installed but with larger values to amount to the same generation value. Which results in bigger voltage differences throughout the whole grid. The PV-grid model on the other had had more PV-units, which were rated at smaller average values to amount to the same total generation value as the LV-grid. Meaning that the PV-grid had smaller bus-voltage differences throughout the grid and the grid distribution as a whole became more uniform. So the voltage boundary in the LV-grid, the max/min P points, are smaller due to the fact that when the grid operates close to the under-voltage boundary, the disconnect of one of the PV-units connected to a bus with lower bus-voltage values results in a cascade event disconnecting all of the PV-units in the grid. Because disconnecting a single PV-unit close to the under-voltage boundary drops the voltage throughout the whole grid under the under-voltage boundary, leading to the detection of the island and disconnection of all PV-units. Meaning that the PV-grid tests have slightly larger boundaries due to the more uniform voltage values throughout the grid. Since the voltage in the grid model was more uniform, operation close to the voltage boundaries were stable a little bit longer before triggering cascade disconnections of the PV-units.

### 4.3.2 Varying inverter settings

After discovering that the pure number of connected PV-units in the grid model can affect the potential island operation, depending on the voltage throughout the grid, the question of small variations in the PV-protections were investigated. Twenty of the 71 PV-units in the PV-grid were changed in the OV (step 1) function time. So instead of having a function time of 0.2 seconds they were set to a function time of 0.1 seconds. Resulting in 20 of the PV-units having more sensitive OV detection and acting faster than the remaining 51 PV-units. The first test with the varying OV detection times was meant to test a value beneath the previous minimum active power boundary, located at 78.2 % of the generation according to Table 4.5, and see if this boundary had been subjected to any change. This test for the mixed OV function times for a load of 72 % of the generation can be seen in Figure 4.15. The frequency graph in Figure 4.15 shows a second spike located at 0.1 seconds after the external grid disconnection at 0 seconds. This second spike is the 20 PV-units with OV (step 1) function time of 0.1 seconds shutting down, while the PV-units with the regular 0.2 seconds setting stays connected due to the voltage drop. Resulting in an island persisting for more than 15 seconds, note that the graph is not simulated until the detection instant.

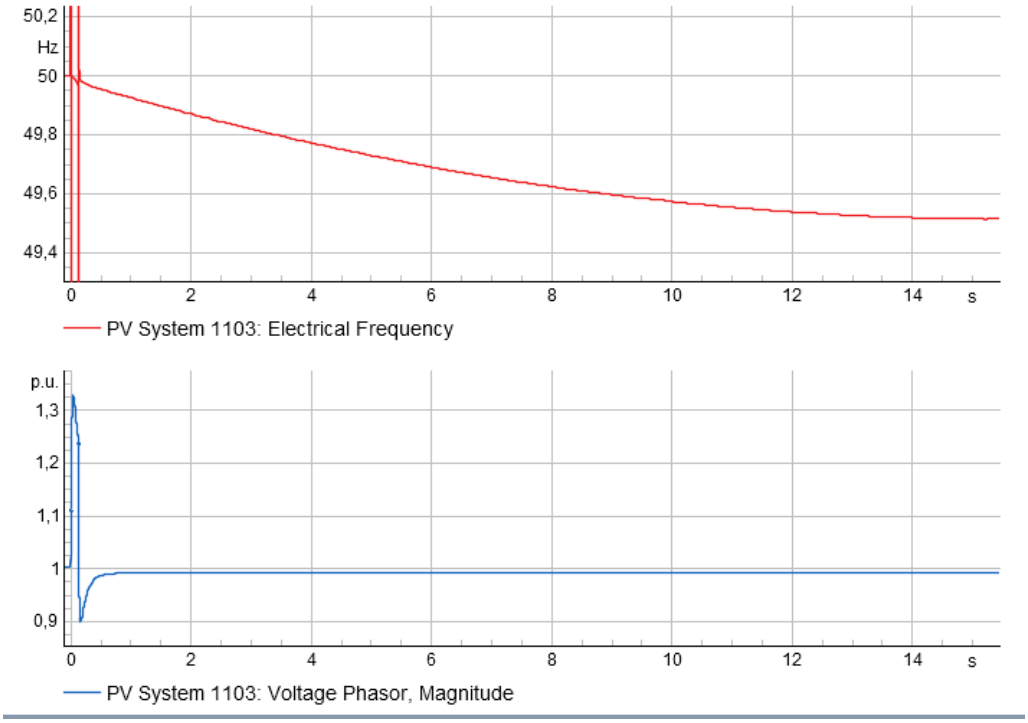


**Figure 4.15:** Test with total generation of 298,2 kW, house loads of total 214.7 kW (72 % of the total generation), and 20 of the PV-units set to 0,1 seconds of function time for OV protection (step 1). Remaining PV-units unchanged.

The significance of the 20 PV-units with a more sensitive setting of OV (step 1) protection, was observed in the test of how these settings would affect the OV-boundary. As previously mentioned in the tests regarding the NDZ boundary points, the minimum active load boundary of P was previously 233.43 kW (or 78.2 % of the total generation). With some of the PV-units having quicker acting OV protection settings, the minimum active load boundary was moved to 155.1 kW ( or 52 % of the total generation). Meaning that the NDZ with varying sensitivity of some PV-units effectively became bigger in the negative spectrum, allowing a bigger unbalance between generation and load before the island becomes detected instantly (before the 5 second mark). The new boundary for overproduction, the minimum active load which would trigger the OV-protection, mentioned above is displayed in picture 4.16 in its corresponding frequency and voltage magnitude graphs. The resulting graphs show the external grid disconnection at 0 seconds, the 20 sensitive PV-units disconnecting at roughly 0.1 seconds , and lastly the remaining 51 PV-units with the regular setting disconnecting at 0.73 seconds. The expansion of the overproduction boundary shows that different sensitivities in the protection settings could be a problem, since different settings results in different connection times. So if enough PV-units have a rather sensitive setting of their protection, they can effectively 'save' the island from detection in the over production cases. Since during over production in the grid, the OV-protection will be the protection trigger detecting the island, and if a couple of PV-units disconnect faster than the others the total generation would go down and result in a voltage drop. If the voltage drop then results in a grid voltage in the accepted voltage range, the remaining PV-units wouldn't disconnect

and would keep energizing the grid until said range is violated.

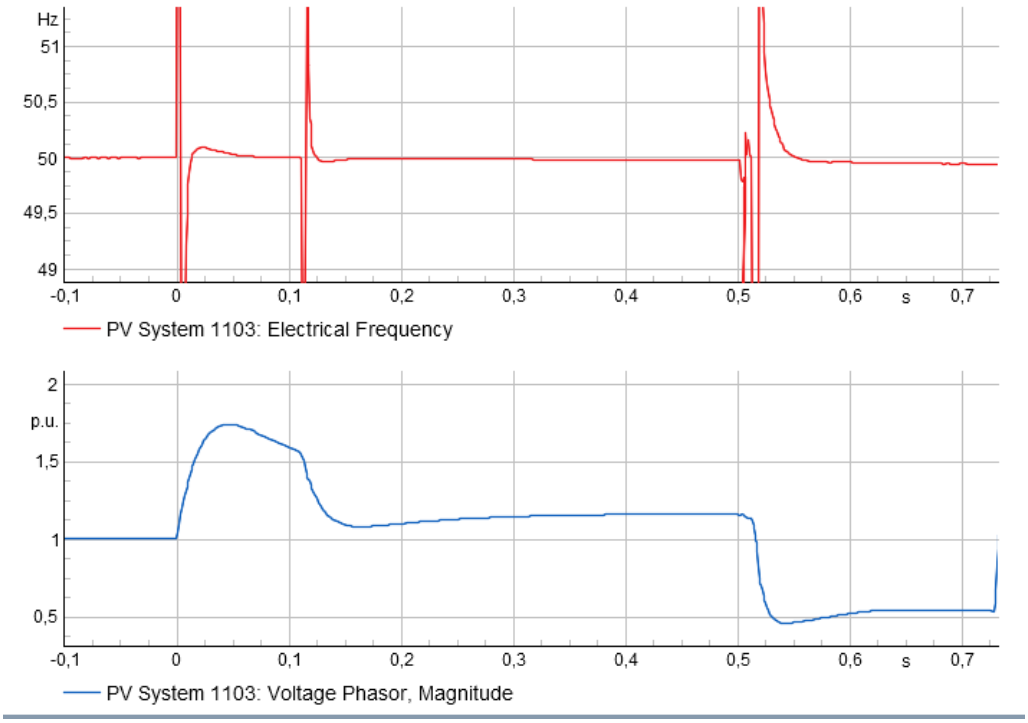


**Figure 4.16:** Test resulting in the voltage boundary from over production in the PV-grid with 20 PV-units with more sensitive settings. Generation set to 298.2 kW, load rated at roughly 155 kW (52 % of the generation).

### 4.3.3 Generation and load balance

The PV-grid was also tested in the sense of generation and load balance, to asses its behavior during a significant island operation time window. The generation value was rated at 298.2 kW while the load was set roughly the same, equal to 298.5 kW. The frequency and voltage magnitude graphs displayed in Figure 4.17 show that this balanced island was detected after almost 81 seconds due to OF trigger.

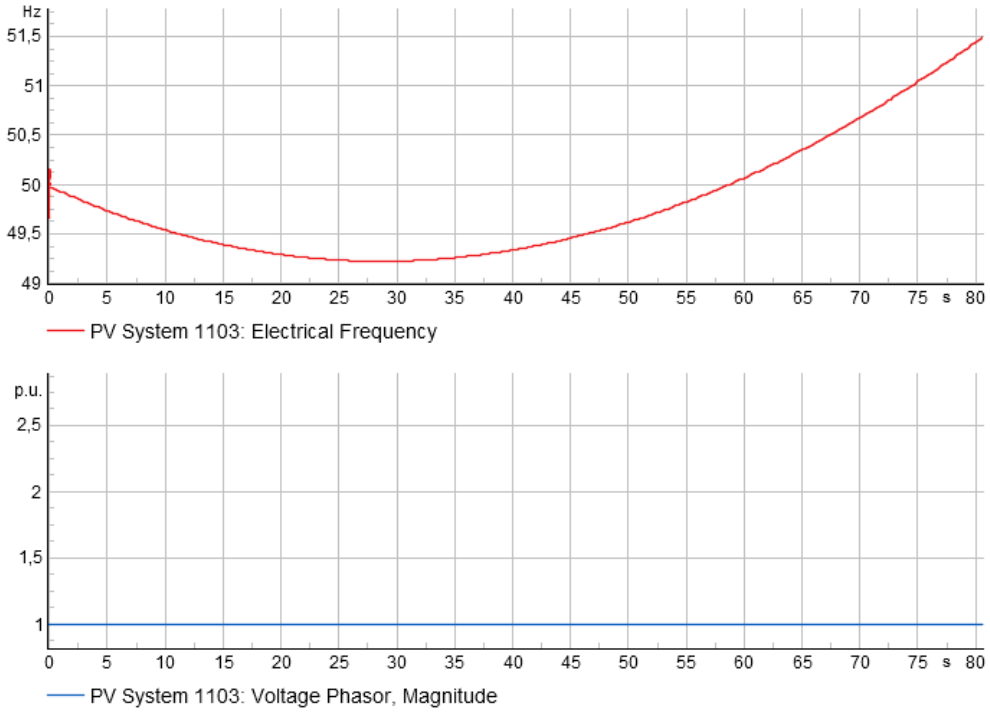


**Figure 4.17:** Generation and load balance test for the PV-grid, with generation 298.2 kW and load equal to 298.5 kW, displaying the frequency and voltage magnitude graphs.

A important notation about this generation and load balance test in the PV-grid, is that its results were expected to be more similar to the first generation and load balance test in the LV-grid. Which was the balance test without the cable values included in the compensation, which resulted in the island being detected after 16 seconds. But this generation and load balance test in the PV grid, which from the start had slightly higher load value compared to generation and no compensation for the cable values, proved to have a behavior much more strongly related to the LV-grid balance test with respect to the cable values which had an island operation time of 89 seconds. The PV-grid test had the same frequency behavior as the LV-grid balance test in Figure 4.8, and a stable voltage at 1 p.u. Which leads to the conclusion that the same grid, but with more PV-units leading to a more uniform voltage spread throughout the whole grid, would result in a more stable island operation disregarding of the cable values. Since the cable impacts throughout of the grid becomes smaller when the distribution is more evenly spread.

Regarding the general frequency curve shape displayed in Figure 4.17, amongst others, the frequency is displayed as decreasing in the beginning and to later adapt a increasing value instead. This curved shape is believed to be a result of the angle difference between the current and the voltage upon initializing the model. The angle difference can be seen in Appendix C, Figure C.36 and as observed, the largest mismatch happens at 0 seconds in the simulation. Due to the tests being conducted with a disconnection from the grid at 0 seconds, this angle difference is present in every result. If the disconnection from the external grid is performed at a

later time when the angle difference is lessened and close to zero, such as after two seconds, this dip in frequency at the start disappears which can be seen in Appendix C Figure C.37. However, in both cases the time until detection vastly exceeds five seconds. When doing sample tests from points in the previously mentioned NDZ with the disconnection time being at two seconds instead of zero, the time until detection was basically identical. This possible source of error was subsequently deemed to not overly affect the final results, especially considering the fitting or validity of the NDZ.

## 4.4 Medium voltage cable

The MV-cable grid model was built from the previous PV-grid model, having PV-modules at every load but with the addition of a MV-cable between the external grid and the LV grid. The three tests of the MV-cable are in the form of different lengths of said MV-cable, 1 km, 5 km and 10 km respectively. The results are displayed in order below. All of the three tests were performed with with the total generation of the PV-units set to 298.2 kW, and the house loads rated to a total of 298.5 kW and 0 kVar in active and reactive power respectively.

### 4.4.1 1 km medium voltage cable

The test with a 1 km MV-cable connected to the LV-grid with 71 PV-units resulted in a load flow displaying that the MV-cable generated 14.5 kVAr reactive power, meaning that it was a 14.5 kVAr capacitive load. The disconnection from the external grid resulted in the island being detected after 0.85 seconds due to ROCOF. Indicating that the reactive power imbalance from the island in the LV grid including the MV-cable became large enough to trigger the ROFOC protection, thus detecting the island almost immediately. The earliest detection of the island would be after the ROCOF protection time delay of 0.5 seconds. The frequency and voltage magnitude graphs for the 1 km test are shown in Figure 4.18.

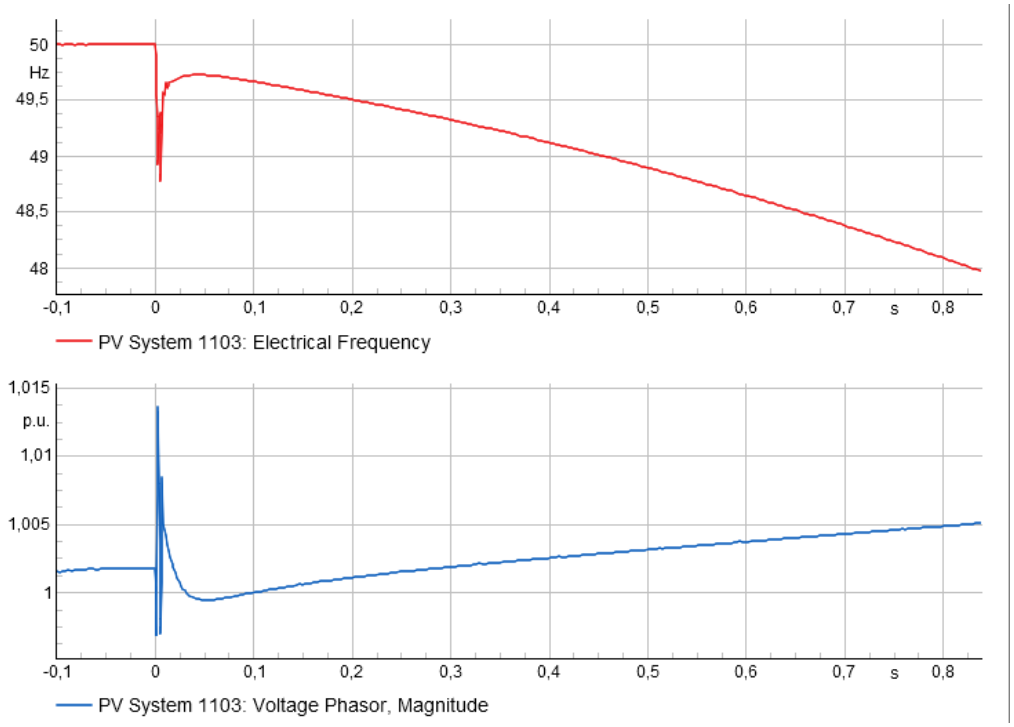


**Figure 4.18:** Frequency and voltage magnitude graphs of a 1 km MV-cable connected between the external grid and the low voltage grid with a generation of 298.2 kW spread amongst 71 PV-units.

### 4.4.2 5 km medium voltage cable

The load flow for the 5 km long MV-cable showed that the MV-cable amounted to an capacitive load of 71.6 kVAr. The corresponding frequency and voltage magnitude graphs for a 5 km long MV-cable are shown in Figure 4.19. The 5 km length MV-cable resulted in island detection after 0.505 seconds due to ROCOF. Which implies that the island is detected at the earliest possible moment for the ROCOF protection, slightly faster than the 1 km cable due to the bigger reactive power imbalance that the 5 km cable creates.

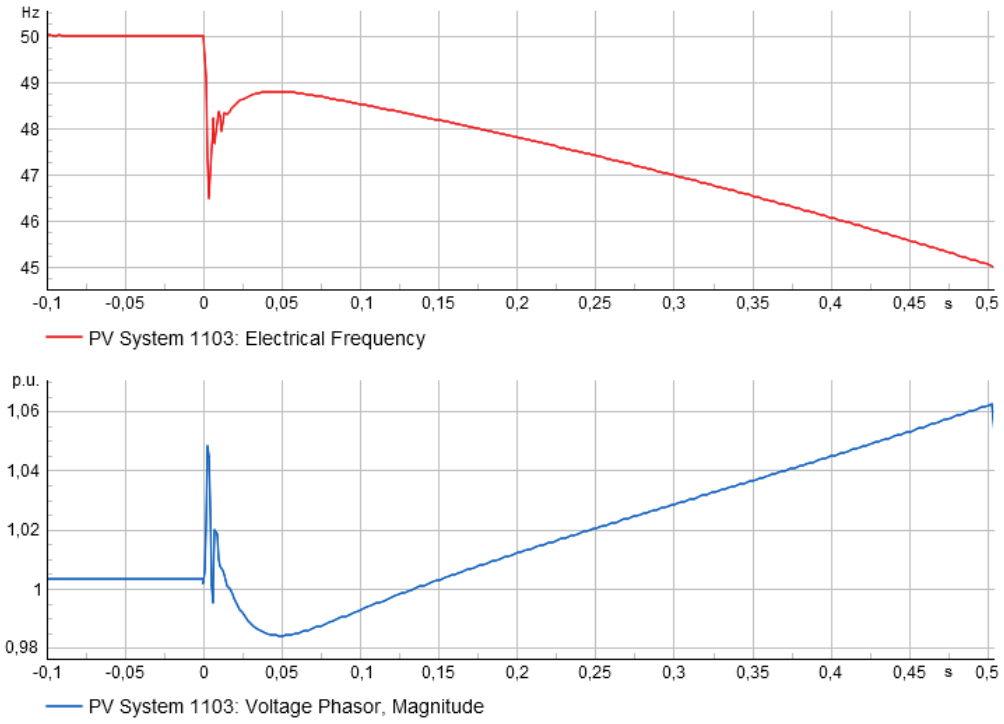


**Figure 4.19:** Frequency and voltage magnitude graphs of a 5 km MV-cable connected between the external grid and the low voltage grid with a generation of 298.2 kW spread amongst 71 PV-units.

### 4.4.3 10 km medium voltage cable

The last test which represented the MV-cable length of 10 km displayed the MV-cable as a 145.8 kVAr capacitive load during the grid load flow. The island was detected after 0.505 seconds due to ROCOF, the earliest possible disconnection just like the 5 km MV-cable. Showing that it doesn't matter how long the MV-cable is exceeding 5 km length since the reactive power imbalance triggers the protection instantly after disconnection from the external grid. The frequency and voltage magnitude graphs for the 10 km MV-cable are shown in Figure 4.20, and has the same profile as the 5 km graphs except for the instantaneous spike values during the external grid disconnection which are larger.

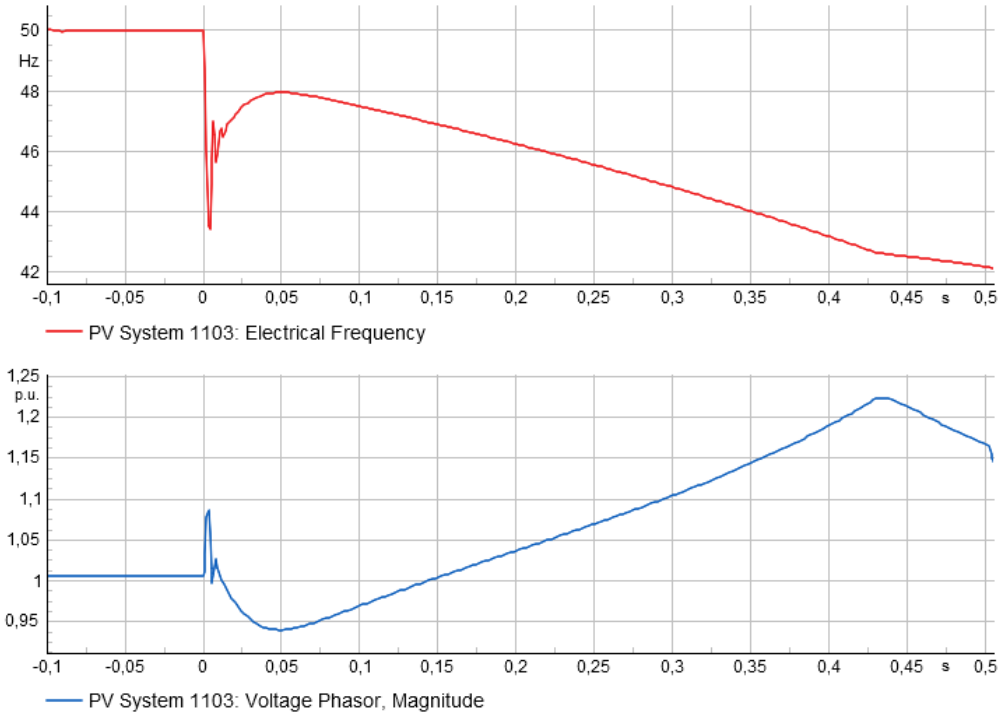


**Figure 4.20:** Frequency and voltage magnitude graphs of a 10 km MV-cable connected between the external grid and the low voltage grid with a generation of 298.2 kW spread amongst 71 PV-units.

# 5
# Discussion

Something that can be noted from the results is that in all of the cases, the active power discrepancy can be quite far from the nominal value without the island protection stepping in within the desired 5 seconds. In fact, the active power will only make the inverter disconnect when it causes the voltage to drop enough to activate the undervoltage protection, or rise enough to activate the overvoltage protection. This time would also not get to the desired 5 seconds when drawing the NDZ, but would instead reach approximately 220-450 ms depending on the actual load conditions in question. There was a higher tolerance for increasing the load compared to the production than for reducing the load compared to the production, which indicates that islands that are created in a heavily loaded grid have a higher probability to create a problem than in a lightly loaded grid. This could have something to do with the load-voltage dependence effect. Meaning that as the voltage drops, the loads are reduced too which results in a slightly smaller load increase that it otherwise would have been. Also important to note here is that for a grid with an uneven voltage distribution, meaning that some areas have a slightly higher or lower voltage compared to the rest, the islanding problems can become worse in the case of overproduction. Some of the inverters could detect a higher voltage and disconnect, bringing the voltage down as the production goes down and thereby creating an island which will not be detected within the desired time window by the remaining inverters still connected.

In contrast, the reactive power required to make the over- and underfrequency protection activate is very small. It only required 0.26 % of the production as reactive power in order to make the underfrequency protection activate, which is 0.76 kVAr when the produced active power was 298.5 kW. For overfrequency it took -0.42 %, or -1.25 kVAr before the time limit was reached. A reason why there is a discrepancy in the absolute value of these reactive powers could be that the cables have a reactive component to them, and as such there isn't actually a complete reactive balance before the tests were ran. Seeing as the reactive limit is very small for what can be allowed within the set island detection time, the cable type could create a relatively big impact. It also shows that a reactive balance is very important in the case of a successful islanding event, as a small discrepancy will be discovered quickly and the anti-islanding protection will activate well within its desired time frame.

A possible source of error within the chosen simulation model is the controller behavior in of itself, more specifically in regards to how it behaves in regards to calculating frequencies. As noted in Figure 4.3 when the disconnect occurs, the angle difference jumps up slightly for no apparent reason as the load and generation are in balance

with each other and no external elements are affecting them. It is unknown as to why this happens, but a possible implication is that the frequencies increase much faster than they otherwise would and thus provide results which do not line up with potential real life situations. More studies and time would have to be devoted to finding out what exactly in the converter controller that makes it behave this way, if it is the PLL or another component that creates this error, if it is in fact an error.

An important aspect to take into consideration is that no active anti-islanding protection schemes have been implemented in the model, while they exist in most inverters sold on the Swedish market. This is both because the manufacturers do usually not list which active protection measures they use and which settings they use for them, and also because of the model itself we tested. No active anti-islanding protection was included in the base model from Powerfactory which we based our own model on, and we do not have the experience or understanding of how to create those DSL blocks in a reasonable amount of time. It is very possible that with active anti-islanding protection schemes, the amount of time it would take to detect an island would be reduced significantly and the non-detection zone would be reduced by a lot. However, we could not make any tests on if or how much they would change.

For the non-detection zone in itself, each zone is only valid for that specific setup (load and generation values). As can be seen in the results, for a different generation level and varying amounts of PV modules, the boundaries of the zone changes slightly. This is quite a small change, but nonetheless a change. It also depends heavily on the time scale set for the test. As five seconds was chosen as the time that the island operation should not exceed, that means that all the tests were done with that time in mind. Had the time instead been set to ten seconds the zone would have been smaller since less reactive power would have been needed. Had it instead have been set to two seconds, the zone would have increased as more reactive power would have been required to push the frequency beyond the limits stated by the ALP within said time.

Something interesting that was found out was that the ROCOF never triggered in any situation in the basic grid or the low voltage grid. The initial frequency spike that comes when the island is formed is not large enough to trigger it, or rather does not last for a long enough time to trigger it. The settings were set a little bit more strict that the requirements according to the ALP were, although that did ultimately not matter in the end. It did however trigger when doing the tests with the high voltage cables, as that reactive component was large enough to reduce the frequency enough in a short amount of time. What this shows is that the ROCOF does not detect minor disturbances, only the larger ones which also affect the reactive power in the system. Since the ROCOF is labeled as the specific "anti-islanding protection" in datasheets, if the island is relatively balanced something else is needed in order to detect the island, ROCOF is not enough to complement the passive protections NDZ. Maybe the settings needs to be even more sensitive, but that would likely make it trigger for other grid events which it should not detect, and would cause the

inverter to disconnect more often than it should. If the chosen ROCOF protection value of 2 Hz/s would have been set to 2.5 Hz/s as the ALP suggested, then the risk of false protection triggers in the system would decrease. The higher ROCOF value would also mean that the protection would trigger even less often then observed in the tests or with greater time delay as a result of the higher ROCOF limit. Seeing as ROCOF already triggers rarely within this system, having it set to a higher value in a real life system where false triggers are more common might not be a bad idea.

Regarding the specific definition of grid-following and grid-forming inverters, some distinctions can be important to make. All inverters in the model were assumed to be and modeled as grid following inverters, as they are the most widely used inverters for residential usage. However, if there were to be one or more grid-forming inverters in the grid, which is not unthinkable in the future, then there could be a sustained island. Energy storage alongside solar panels are becoming more common, and as such more hybrid inverters and battery inverters are being bought in order to utilize them. In this case hybrid inverters are the interesting ones. The grid-forming inverters' ability to control the voltage and frequency would allow them to keep an island active, which is what they are designed to do. In a residential low voltage grid, the grid forming function is likely turned off by default and just following the larger grid like the rest of the inverters. But, there is always the possibility that it is not turned off. It can be very difficult to keep track of which inverter is what type, and there might need to be stricter control of what kind of inverters are installed and what the grid conditions are in that specific area.

While the tests show the conditions in which an unintentional islanding event can occur, what it does not show is when these conditions would occur. Solar panels need the sun in order to produce power, and the solar irradiation is not uniform even on a rather local scale. Over the year, solar irradiation changes quite a bit, and so does the energy usage in houses. How often these conditions line up in order to create an unintentional island is currently unknown to us. For this to have any real impact on how to design grids in the future, or just make the grids today more resilient against unwanted islanding operation, a study will probably have to be conducted which focuses on which times of the year this will be an issue. Most likely, winters will not be an issue as there are very little solar irradiation in Sweden. Summer, autumn, and spring would be the seasons that we suggest focusing on, mainly from late spring to early autumn.

On an even shorter time scale, solar irradiation changes during the day too. There is no sun during the night, and as such there will be no generation during the nighttime hours. This means that the problem of unwanted islanding would only happen during daytime hours. And for loads, in this case houses, the energy usage in them also changes during the day. This can make it more difficult to line up the generation with the load in a way to make it create an unwanted island. And going back to the very low amount of reactive power that is required to detect the island, a neighbourhood could almost certainly consume more than the threshold if it operates certain appliances.

In order for an islanding event to occur, there has to be an upstream fault that cuts off the connection to the larger grid for an area. If this area includes a substation or otherwise a transformer, these will have their own protections to deal with faults that occur. If they activate as intended, a potential island would be contained to the low voltage side of the transformer. If the fault however happened one level above this, in a 40 kV grid instead of a 10 kV grid, then the transformers protections might not trigger correctly. Then there would be an infeed from the low voltage grid into the 10 kV grid instead an a larger island would form. However, this island would be detected very early due to the reactive components of the cables, which have a lot bigger impact in these types of grids, and would not in general be considered a problem. Although, in the unlikely event that there is some sort of battery which can regulate or in other ways help with reactive power balancing in the substations themselves or out in the grid, then the island could of course remain for longer. This could potentially also be the case if there are grid-forming inverters in the low voltage grid, depending on how much reactive power they can consume or generate.

Now, even if the island is detected and the protection devices trigger as fast as possible, at around a little over 200 ms, in cases with a lot of generation and little load the voltage would increase a lot in the small timeframe that it can. Let us say that it is a warm and sunny summer day, the solar panels are producing as much power as they can but the residents are not home because they are on vacation. The solar panels are still on because they want to sell the excess power generated. Suddenly, a fault happens upstream which disconnects the substation from the larger grid. The voltage in the newly formed island now reaches a very high level before all the protection devices activate and shut down the power production. This high voltage could potentially be an issue that needs to be taken into consideration. A voltage that reaches too high values has the potential to damage or outright destroy electrical equipment. The question at hand would then be whether or not this high voltage is acceptable for roughly 200 ms or if this is too long and equipment will be destroyed as a consequence.

## 5.1 Ethical aspects

There are certain ethical and ecological aspects that can be discussed regarding this thesis work and the topic of anti-island protection. If unwanted island operation is a significant risk, then additional protection in the power system has to be installed to protect and to mitigate said risk. This protection costs money and resources, which has to be taken from somewhere, probably from the power company in charge of the grid in question. As the resources aren't infinite, that means that the company has to prioritize where to spend their efforts. If more of it has to go towards anti-islanding protection, some other part of the power grid might have to be neglected which can negatively affect both the power grid itself and its consumers. Thus, if it can be shown that unwanted islanding operation is very unlikely to occur and this protection is not needed, then resources can be allocated to other areas which could

improve the power grid and the quality of the delivered product.

It is important to keep in mind that if there is even a slight chance of unwanted island operation going undetected and potentially harming equipment or people in its vicinity, it is morally right to equip the system with the proper protective measures against it. So the question turns to the implemented passive and active protections utilized in the inverter, does the active protections compliment the passive ones to such a degree that no additional protection is needed? Or is over laying protection needed, such as island indicators in the substations that can warn against unwanted island operation when measurements show that the low voltage side is still energized.

There are often two points of view when discussing the topic of unwanted island operation. One view is that the necessary conditions for the island formation is so overly specific and sensitive that the unintentional island operation risk is negligible. The other point of view is grounded in the unease that the theoretical possibility itself, how ever small or unlikely, still represents a source of concern. Which brings us to the ethical aspect hiding behind this subject, is it feasible to leave the network at risk to enter unintentional-island operation or should time and resources be spent to mitigate this risk? Trying to answer this question can become very tricky without the knowledge of how likely an event of this type is to occur. This risk of unintentional island operation seems to become more prominent with time, due to the recent trends within the power grid. Which includes more DERs such as PV-units or the possibility of installing more batteries and energy storages even within the low voltage grid itself.

# 6
# Conclusions and future work

When it comes to islanding events, the reactive power mismatch is the most important factor in order to determine if it will be discovered by passive protection schemes within the desired time window. Reactive power affects the frequency in this case due to how the load angle affects the frequency estimation, which subsequently makes over- and underfrequency protection the most likely to trip for a given situation. Depending on if the load in the grid is inductive or capacitive, the voltage-current angle difference will take on a positive or negative value respectively. Which in turn affects the frequency of the potential island resulting in an increasing or decreasing run away of the frequency since a grid following inverter doesn't uphold or try to stabilize its local frequency or voltage values. In this specific low voltage grid, the reactive power mismatch would allow for the load's reactive power to be 0.255 % or -0.42 % of the generation rating before disconnection within five seconds. The active power mismatch is more forgiving, being able to handle an increase of 28 % or a decrease of 22 %, with respect to the generation value, before disconnection within 5 seconds. ROCOF is not a suitable protection scheme when checking into small mismatches over a longer time period and is better used when studying large reactive mismatches such as when using long medium voltage cables, or during a much shorter time frame. The risk of a low voltage grid feeding a higher voltage grid in a larger island situation is negligible, unless there is some sort of shunt reactor in the substation, as the reactive power mismatch due to the medium voltage cables is large enough to make the frequency protection disconnect the inverters. The risk of a more stable unintentional-island operation transition in a low voltage grid increases if there is a bigger amount of PV-units with ratings creating a uniform grid behavior regarding the grid's voltage profile, compared to a low voltage grid with fewer PV-units with higher ratings. This is due to the more uniform voltage and current distribution through out of the grid as a whole, if the load is compensated for more evenly then the island protection measures will require more time to detect the possible island. Which is a higher possibility if there are more PV-units installed in the low voltage grid, compared to a scenario were there are fewer PV-units with higher ratings installed. Having fewer PV-units with higher ratings spread out in the same grid wouldn't create a uniform voltage profile throughout the grid since there is a large likelihood the load would be less evenly distributed and therefore create bottlenecks within the grid.

Due to the impending increase of residential solar power installations, it will be important to note what kind of inverter they are using, if it is grid following or grid forming. Creating extra regulations and rules regarding grid forming generators

in general should also be a priority for relevant bodies. More studies into active protection schemes for inverters currently on the market should also be looked into. Which type, the settings, and the operating times are all areas which should be focused on.

## 6.1 Future work

Points of interest regarding future work and studies in the subject would include:

- These studies were conducted with EMT simulations, an additional point for future work could be to conduct the tests with RMS simulations instead while also including the dynamic of the PLL and current controller to see if the detection changes.
- Closer inspection of the active protections schemes utilized in the inverters sold on the market. Observing how they affect the island detection time and how they compliment the passive protection schemes would make it easier to assess the possible need of installing more overlaying protections.
- Additional research of optimal use and utilization of the DSOGI PLL structure in PV inverters. In order to develop a deeper understanding of how and what the voltage and current angle difference in the tests originates from.
- Closer cooperation with inverter manufacturers to get first hand information about the active protection schemes that they use and their function times.
- Further studies of the active and reactive power limits suitable for ROCOF protection triggers, quantifying power magnitudes that utilizes the ROCOF protection in a effective manner.
- Standardization and investigation of grid forming inverters behavior and general settings are also of importance in order to raise awareness of what equipment is present and active in the grid. If there is going to be a larger presence of grid forming inverters in the low voltage grid in the future, for example due to larger utilization of battery and energy storages, there needs to be a distinction between when the grid forming inverter is grid forming or when it is grid following if it all boils down to different settings. How would a grid forming inverter differentiate between unintentional and planned island operation events?
- Other possible studies including observations of which time of the year the unintentional island risk is more prominent due to load variations could also help assess the overall risk.
- Conduct physical testing of different inverters in a controlled and real-world environment instead of a computer simulation. Simulations are generally reliable, but the most reliable test are those done in the field in order to get a first hand experience in how things actually behave.

# References


[1] Energimyndigheten, *Över 250 000 installerade solcellsanläggningar i Sverige*, 3rd Apr. 2024. [Online]. Available: https://www.energimyndigheten.se/nyhetsarkiv/2024/over-250-000-installerade-solcellsanlaggningar-i-sverige/ (visited on 29th May 2024).

[2] A. Hammarstedt, *Vad är en växelriktare för solceller: Funktion, uppgifter och typer*, 7th Sep. 2023. [Online]. Available: https://hemsol.se/solceller/solcellspaket/vaxelriktare/vad-det-ar-och-funktion/ (visited on 20th Feb. 2024).

[3] Airis solutions, *Types of solar inverters*. [Online]. Available: https://airisenergy.us/types-of-solar-inverters/ (visited on 23rd Feb. 2024).

[4] Igoye Energy, *How does a grid tie inverter work?* 11th Aug. 2023. [Online]. Available: https://igoyeenergy.com/how-does-grid-tie-inverter-work/ (visited on 23rd Feb. 2024).

[5] J. Saleem, *Grid Forming vs Grid Following?* 11th Aug. 2023. [Online]. Available: https://energycentral.com/c/iu/grid-forming-vs-grid-followingf (visited on 3rd May 2024).

[6] W. Du, F. K. Tuffner, K. P. Schneider *et al.*, 'Modeling of Grid-Forming and Grid-Following Inverters for Dynamic Simulation of Large-Scale Distribution Systems,' *IEEE Transactions on Power Delivery*, 2020. DOI: https://doi.org/10.1109/tpwrd.2020.3018647.

[7] M. Li and X. Zhang, 'Hybrid dual-mode control for grid-following and grid-forming inverters in high-penetration renewable energy system,' in *2023 International Conference on Power and Renewable Energy Engineering (PREE)*, 2023, pp. 138–143. DOI: 10.1109/PREE57903.2023.10370383.

[8] R. Awati and J. Burke, *phase-locked loop (PLL)*, 1st Jun. 2021. [Online]. Available: https://www.techtarget.com/searchnetworking/definition/phase-locked-loop (visited on 5th May 2024).

[9] P. Rodríguez, R. Teodorescu, I. Candela, A. V. Timbus, M. Liserre and F. Blaabjerg, 'New positive-sequence voltage detector for grid synchronization of power converters under faulty grid conditions,' in *2006 37th IEEE Power Electronics Specialists Conference*, 2006, pp. 1–7. DOI: 10.1109/pesc.2006.1712059.

[10] R. J. Devi and S. S. Kadam, 'Phase locked loop for synchronization of inverter with electrical grid: A survey,' in *International Journal of Engineering Research & Technology (IJERT)*, vol. 4, 2015, pp. 352–358. [Online]. Available: https://www.ijert.org/research/phase-locked-loop-for-

synchronization-of-inverter-with-electrical-grid-a-survey-IJERTV4IS020420.pdf.

[11] H. Abele and A. Gonzalez, *ENTSO-E views on RoCoF and Grid Forming capabilities related amendments of the Connection Network Codes*, 10th May 2023. [Online]. Available: https://www.acer.europa.eu/sites/default/files/events/documents/2023-05/ENTSO-E_presentation_10052023.pdf.

[12] A. Ellis, *Grid Forming Inverters: Requirements and Practical Applications*, 2019. [Online]. Available: https://www.osti.gov/servlets/purl/1639991.

[13] Energiföretagen, *Rikta rätt-listan*, 8th Mar. 2024. [Online]. Available: https://www.energiforetagen.se/493dca/globalassets/medlemsportalen-oppet/rikta-ratt/rikta_ratt.pdf (visited on 14th Mar. 2024).

[14] W. Bower and M. Ropp, 'Evaluation of islanding detection methods for utility-interactive inverters in photovoltaic systems,' Albuquerque, New Mexico: Sandia National Laboratories. SAND2002-3591, Nov. 2002. DOI: https://doi.org/10.2172/806700. (visited on 20th Feb. 2024).

[15] B. Kroposki, 'Prevention of unintentional islands in power systems with distributed resources,' National Renewable Energy Laboratory, 24th Aug. 2016, pp. 30–31. [Online]. Available: https://www.nrel.gov/docs/fy16osti/67185.pdf (visited on 20th Feb. 2024).

[16] R. Teodorescu, M. Liserre and P. Rodriguez, *Grid Converters for Photovoltaic and Wind Power Systems*. John Wiley & Sons, Incorporated, 2011.

[17] *Commission Regulation (EU) 2016/631*, pp. 10-18, 14th Apr. 2016. [Online]. Available: https://eur-lex.europa.eu/legal-content/SV/TXT/PDF/?uri=CELEX:32016R0631&from=RO (visited on 22nd Feb. 2024).

[18] Vattenfall, *Nätanslutning av generatorer (RfG)*. [Online]. Available: https://www.vattenfalleldistribution.se/var-verksamhet/entreprenorleverantor/natanslutning-av-generatorer-rfg/ (visited on 10th Mar. 2024).

[19] Energimarknasinspektionen, *Energimarknadsinspektionens författningssamling*, 5th Dec. 2018. [Online]. Available: https://ei.se/download/18.5b0e2a2a176843ef8f5b74/1608639227153/EIFS-2018-2-om-fastst%C3%A4llande-av-generellt-till%C3%A4mpliga-krav-f%C3%B6r-n%C3%A4tanslutning-av-generatorer.pdf (visited on 3rd Feb. 2024).

[20] Energiföretagen, *Rikta rätt, växelriktare för solceller och energilager*, 23rd Feb. 2024. [Online]. Available: https://www.energiforetagen.se/energifakta/elsystemet/produktion/solceller/rikta-ratt--vaxelriktare-for-solceller/ (visited on 23rd Feb. 2024).

[21] Energiföretagen, *Anslutning av elproduktion till lågspänningsnätet- ALP*, 3rd ed. Energiföretagen Sverige - Swedenergy - AB, 1st Mar. 2020, pp. 17–18. [Online]. Available: https://www.energiforetagen.se/globalassets/energiforetagen/det-erbjuder-vi/e-tjanster/hap/alp-handbok-inlaga-mars-klar-200406.pdf (visited on 14th Mar. 2024).

[22] DIgSILENT, *Do you have an example of an anti-islanding protection system for a renewable generator based on a full scale converter system?* [Online]. Available: https://www.digsilent.de/en/faq-reader-powerfactory/do-you-have-an-example-of-an-anti-islanding-protection-system-

for-a-renewable-generator-based-on-a-full-scale-converter-system.html (visited on 14th Mar. 2024).

[23] DIgSILENT PowerFactory, *Technical Reference Documentation, General Load*. [Online]. Available: https://www.researchgate.net/profile/Cleberton-Reiz/post/Why-does-the-RMS-current-obtained-with-the-EMT-DigSILENT-samples-not-have-the-same-value-as-the-simulated-RMS-current-in-steady-state/attachment/5ef9f15e3909f70001d960f7/AS%3A907761260953600%401593438558096/download/TechRef_GeneralLoad.pdf (visited on 8th Jul. 2024).

[24] Ferroamp, *ANMÄLAN Växelriktare för produktionsanläggning Typ A - Ansökan till Rikta rätt*. [Online]. Available: https://ferroamp.com/wp-content/uploads/2022/09/Blankett_Rikta_ratt-Ferroamp-EnergyHub-Wall-14-kW-1.pdf (visited on 18th Mar. 2024).

[25] Ferroamp, *Certifikat om överensstämmelse med EIFS 2018:2 och SS EN-5049-1*. [Online]. Available: https://ferroamp.com/wp-content/uploads/2021/06/Certifikat20EIFS2018-220och20SS-EN2050549-1-1.pdf (visited on 18th Mar. 2024).

[26] Ferroamp, *EnergiHub Wall 7 & 14 kVA*. [Online]. Available: https://ferroamp.com/wp-content/uploads/2021/06/EnergyHub-Wall_Datasheet_eng_D05_210510.pdf (visited on 18th Mar. 2024).

[27] Fronius, *Anti Islanding Protection Fronius Inverters*. [Online]. Available: https://cdn.starwebserver.se/shops/solelgrossisten-se/files/certifikat-fronius-symo-hybrid-anti-islanding-protection-04-12-2020.pdf?_=1623664766 (visited on 9th Apr. 2024).

[28] KOSTAL Solar Electric GmbH, *Intyg om överensstämmelse EN50549-1:2019/SS-EN 50459-1:2019/EIFS 2018:2/VDE V 0126-1-1:2006*. [Online]. Available: https://cdn-production.kostal.com/-/media/document-library-folder---kse/2023/11/16/11/48/1989_z-en50549-1_sv.pdf?rev=-1&hash=298EC4B25A478DA86CD554DB4415BDCC (visited on 12th Apr. 2024).

[29] SMA Solar Technology AG, *SUNNY TRIPOWER X 12 / 15 / 20 / 25 - Integrerad intelligens för hållbar systemdesign*. [Online]. Available: https://files.sma.de/downloads/HK_STPxx-50_EIFS_2_2018_en-10.pdf (visited on 12th Apr. 2024).

[30] SMA Solar Technology AG, *Technical Information SUNNY BOY/SUNNY BOY STORAGE/SUNNY ISLAND /SUNNY TRIPOWER/SUNNY TRIPOWER STORAGE Parameter settings for compliance with EIFS 2018:2 for type A plants (only for Sweden)*. [Online]. Available: https://files.sma.de/downloads/EIFS_2_2018_Paraeinst-TI-en-16.pdf (visited on 12th Apr. 2024).

[31] SMA Solar Technology AG, *SUNNY TRIPOWER X 12 / 15 / 20 / 25 - Integrerad intelligens för hållbar systemdesign*. [Online]. Available: https://files.sma.de/downloads/STPxx-50-DS-sv-21.pdf (visited on 12th Apr. 2024).

[32] SolarEdge Technologies Ltd, *Intyg om överenssestämmelse EN 50549-1:2019, SS-EN 50549-1:2019*. [Online]. Available: https://knowledge-center.solaredge.

com/sites/kc/files/se-three-phase-inverter-and-storedge-three-phase-en50549-1-certificate-swe.pdf (visited on 17th Apr. 2024).

[33] SolarEdge, *SolarEdge Home Wave Växelriktare Trefas SE3K–SE10K*. [Online]. Available: https://knowledge-center.solaredge.com/sites/kc/files/se-three-phase-inverter-setapp-ds-swe.pdf (visited on 17th Apr. 2024).

[34] SolarEdge, *StorEdge Trefas Växelriktare SE5K-RWS/SE7K-RWS/SE8K-RWS/SE10K-RWS*. [Online]. Available: https://knowledge-center.solaredge.com/sites/kc/files/se_storedge_three_phase_inverter_datasheet_swe.pdf (visited on 17th Apr. 2024).

[35] SolarEdge Technologies Ltd, *Intyg om överenssestämmelse EN 50549-1:2019, SS-EN 50549-1:2019*. [Online]. Available: https://knowledge-center.solaredge.com/sites/kc/files/se-solaredge-home-hub-inverter-three-phase-grid-certificate-swe.pdf (visited on 17th Apr. 2024).

[36] SolaX Power, *X3-Hybrid-serien Användarhandbok*, No.288, Shizhu Road, Tonglu City, Zhejiang Province, China. [Online]. Available: https://malmbergsprod.blob.core.windows.net/web/documents/845eb123-2c3c-4ce9-852c-ba1bbfdc10af.pdf (visited on 15th Mar. 2024).

[37] SolaX Power, *X3-PRO G2-serien Användarhandbok*, No.288, Shizhu Road, Tonglu City, Zhejiang Province, China. [Online]. Available: https://malmbergsprod.blob.core.windows.net/web/documents/ff70d83f-bd55-4999-945f-393f0b167dff.pdf (visited on 15th Mar. 2024).

[38] Shenzhen SOFAR SOLAR Co., Ltd., *User manual Solar Grid-tied Inverter Product Model: SOFAR 3K 6KTLM-G3*. [Online]. Available: https://www.sofarsolar.com/upload/file/20240205/1707118100933046703.pdf (visited on 17th Apr. 2024).

[39] Sungrow, *User Manual PV Grid-Connected Inverter SG25CX-P2/SG30CX-P2/SG33CX-P2/ SG36CX-P2/SG40CX-P2/SG50CX-P2*. [Online]. Available: https://info-support.sungrowpower.com/application/pdf/2023/12/22/SG25_30_33_36_40_50CX-P2-UEN-Ver17-202312.pdf (visited on 12th Apr. 2024).

[40] sunways, *SUNWAYS STT 4 25KTL-P Datasheet*. [Online]. Available: https://www.sunways-tech.com/uploads/file1/20230725/SWS%20Data%20Sheet%20STT%204~25K-P_EN%2020230921.pdf (visited on 17th Apr. 2024).

[41] TommaTech GmbH, *Trio-Plus K-Series User Manual*. [Online]. Available: https://www.tommatech.de/images/down_file/156-tommatech-trio-plus-k-series-user-manual-156-en.pdf (visited on 12th Apr. 2024).

[42] TommaTech GmbH, *Trio-Atom K-Series User Manual*. [Online]. Available: https://www.tommatech.de/images/down_file/153-tommatech-trio-atom-k-series-user-manual-153-en.pdf (visited on 12th Apr. 2024).

[43] TommaTech GmbH, *Trio-Hybrid K-Series User Manual*. [Online]. Available: https://www.tommatech.de/images/down_file/120-tommatech-trio-hybrid-k-series-user-manual-120-en.pdf (visited on 12th Apr. 2024).

# A

## Inverter information

**Table A.1:** Different three-phase inverters on the market with corresponding power ratings and mentions of their protections schemes.

| **Manufacturer (Inverter name)** | **Rated power** | **Anti-islanding protection** | **Sources: Manufacturer's Declarations,** Certificates and Datasheets |
|---|---|---|---|
| Ferroamp<br>(Energy-HubWall) | 7 kW, 14 kW | Relay protection according to ALP: (OUV and OUF)<br>ROCOF | Declaration: [24]<br>Certificate: [25]<br>Datasheet: [26] |
| Fronius<br>(Eco)<br>(Symo)<br>(Symo Hybrid)<br>(Symo GEN24)<br>(Tauro Eco) | <br>25 kW, 27 kW<br>3 kW-17.5 kW<br>3 kW, 4 kW<br>3 kW-10 kW<br>50 kW, 100 kW | Passive protection: mentioned as specified limits for abnormal voltage and frequency values, describing OUV and OUF.<br>Active protection: requirements fulfills IEC 62116, described as reactive current injection with resulting frequency measurement and analysis. | Datasheet: [27] |
| Kostal<br>(Plenticore plus) | <br>3 kW, 4.2 kW, 5.5 kW, 7 kW, 8.5 kW, 10 kW. | Passive protection: OUV and OUF<br>Loss of mains according EN 62116 (LoM) | Certificate: [28] |
| SMA<br>(Sunny Tripower X) | <br>12 kW, 15 kW, 20 kW, 25 kW | Passive protection: OUV and OUF.<br>ROCOF | Declaration: [29]<br>Technical information: [30]<br>Datasheet: [31] |
| SolarEdge<br>(SolarEdge Home Wave, SExK)<br>(StorEdge, SExK-RWS)<br>(SExK-RWB48) | <br>3kW-10kW<br>5 kW, 7 kW, 8 kW, 10 kW<br>5 kW, 7 kW, 8 kW, 10 kW | Loss of mains according to EN 62116<br>OUV and OUF<br>ROCOF | Certificate: [32]<br>Datasheet: [33]<br>Datasheet: [34]<br>Certificate: [35] |
| SolaX Power<br>(X3-Hybrid G4-series)<br>(X3-Pro G2-series) | <br>5 kW - 15 kW<br>8 kW - 30 kW | Passive protection: OUV.<br>Active protection: Active frequency drift. | <br>Datasheet: [36]<br>Datasheet: [37] |
| Sofar Solar<br>SOFAR 3K 6KTLM-G3 | <br>3 kW-6 kW | <br>Active protection: Reactive Power Disturbance | Manual: [38] |
| Solis | | | |
| Sungrow<br>(SGxxCX-P2)<br>(SG30CX-P2)<br>(SG50CX-P2) | <br>25 kW, 30 kW, 33 kW, 36 kW, 40 kW, 50 kW<br>30 kW<br>50 kW | <br><br>Active protection: frequency shift, stated for Australian use for SG30 and SG50. | Manual: [39] |
| Sunways<br>STT-xKTL-P series | <br>4 kW-25 kW | Active protection: Frequency shift | Datasheet: [40] |
| TommaTech<br>(Trio-Plus K-Series)<br>(Trio-Atom K-Series)<br>(Trio-Hybrid K-Series) | <br>8 kW-30kW<br>3 kW-15 kW<br>5 kW-15 kW | Active protection: Active frequency drift.<br><br><br>The Hybrid series uses active frequency offset method. | <br>Manual: [41]<br>Manual: [42]<br>Manual: [43] |

# B

## Settings

**Table B.1:** Converter control settings, table 1 of 2.

| Name | Parameter |
|---|---|
| Uac_rated Rated converter voltage (L-L RMS) [V] | 400 |
| Flag_BLK_Enable | 0 |
| Flag_Outer_Loop_Enable | 1 |
| Flag_IDCTL[Auto] [0/1]<br>0=Vdc, 1=P control | 1 |
| Kp_ID PI gain - d-axis current controller [p.u.] | 0,3 |
| TI_ID PI time constant - d-axis current controller [s] | 0,01 |
| Kp_IQ PI gain - q-axis current controller [p.u.] | 0,3 |
| TI_IQ PI time constant - q-axis current controller [s] | 0,01 |
| XL Reactance - Converter AC series reactor [p.u.] | 0,1 |
| Kp_PCTL PI gain - P control [p.u.] | 0,1 |
| TI_PCTL PI time constant - P control [s] | 0,2 |
| Kp_UDCCTL PI gain - Udc control [p.u.] | 0,1 |
| TI_UDCCTL PI time constant - Udc control [s] | 0,2 |
| Kp_QCTL PI gain - Q control [p.u.] | 0,1 |
| TI_QCTL PI time constant - Q control [s] | 0,2 |
| Udc_min | 0 |
| Kp Proportional Gain | 10 |
| Ki Integrator Gain | 30 |
| K Bandwidth control gain | 1,4142 |
| Uac_nom | 400 |
| Iac_now | value taken from load flow |
| T_Uac Time constant - ac voltage filter [s] | 0,00001 |
| T_Iac Time constant - ac current filter [s] | 0,00001 |
| T_Pac Time constant - active power filter [s] | 0,01 |
| T_Qac Time constant - reactive power filter [s] | 0,01 |
| T_Udc Time constant - dc voltage filter [s] | 0,01 |

**Table B.2:** Converter control settings, table 2 of 2.

| Name | Parameter |
|---|---|
| FRT_DU_UV_Entry<br>Voltage band entry, FRT under-voltage [p.u.] | -0,1 |
| FRT_DU_UV_Exit<br>Voltage band exit, FRT under-voltage [p.u.] | -0,08 |
| FRT_K_GAIN FRT reactive current gain [p.u.] | 2 |
| Consider_Prefault_IQ_Current [0/1]<br>0=do not consider, 1=consider | 1 |
| FRT_Detection_U_Prefault [0/1]<br>Consider fault detection band around<br>pre-fault voltage | 1 |
| T_FRT_U_Prefault<br>Pre-fault voltage averaging time [s] | 1 |
| T_FRT_Detect Fault detection time [s] | 0,005 |
| T_FRT_Exit Fault exit time [s] | 0,01 |
| K_FF Feedforward voltage gain [p.u.] | 0,01 |
| T_BLK | 0,01 |
| T_UBLK | 0,1 |
| Finit Initial Frequency [HZ] | 50 |
| PM_min Minimum modulation index-<br>current control [p.u.] | -2 |
| IDMIN Minimum d-axis current - P control [p.u.] | 0 |
| IQMIN Minimum q-axis current - Q control [p.u.] | -1,1 |
| Qac_REF_GRA_LO | 10 |
| Pac_REF_GRA_LO | 10 |
| PM_max Maximum modulation index-<br>current control [p.u.] | 2 |
| IDMAX Maximum d-axis current - P control [p.u.] | 1,1 |
| IQMAX Maximum q-axis current - Q control [p.u.] | 1,1 |
| Qac_REF_GRA_UP | 10 |
| Pac_REF_GRA_UP | 10 |
| U_max | 2 |
| I_max | 1,1 |

**Table B.3:** Protection settings. Note that the voltage values from UMAX1 to UMIN3 are labeled as kV but are in V, this is how the PowerFactory program was labeled, which was confirmed by testing to be a typo. It is labeled here as the original version in order to give a better understanding if repeating the test.

| Name | Parameter |
|---|---|
| T_F Frequency measurement filter, time constant [s] | 0 |
| FMIN1 Under-frequency, Level 1 [Hz] | 47,5 |
| FMAX1 Over-frequency, Level 1 [Hz] | 51,5 |
| T_FMIN1 Under-frequency trip time, Level 1 [s] | 0,5 |
| T_FMAX1 Over-frequency trip time, Level 1 [s] | 0,5 |
| FMIN2 Under-frequency, Level 2 [Hz] | 0 |
| FMAX2 Over-frequency, Level 2 [Hz] | 99999999 |
| T_FMIN2 Under-frequency trip time, Level 2 | 99999999 |
| T_FMAX2 Over-frequency trip time, Level 2 [s] | 99999999 |
| ROCOF Enable or disable ROCOF [1/0] | 1 |
| df_Rate Max frequency rate of change [Hz/s] | 2 |
| T_ROCOF ROCOF trip time [s] | 0,5 |
| UMAX1 Over-voltage, Level 1 [kV] | 440 |
| T_UMAX1 Over-voltage trip time, Level 1 [s] | 60 |
| UMIN1 Under-voltage Level 1 [kV] | 360 |
| T_UMIN1 Under-voltage trip time, Level 1 [s] | 200 |
| UMAX2 Over-voltage, Level 2 [kV] | 460 |
| T_UMAX2 Over-voltage trip time, Level 2 [s] | 0,2 |
| UMIN2 Under-voltage, Level 2 [kV] | 340 |
| T_UMIN2 Under-voltage trip time, Level 2 [s] | 0,2 |
| UMAX3 Over-voltage, Level 3 [kV] | 2000 |
| T_UMAX3 Over-voltage trip time, Level 3 [s] | 0,05 |
| UMIN3 Under-voltage, Level 3 [kV] | 50 |
| T_UMIN3 Under-voltage trip time, Level 3 [s] | 3 |
| UMAX_Instantaneous Maximum voltage (instantaneous trip) [p.u.] | 10 |
| T_RMS Time window of MAF for RMS calculation [s] | 0,01666667 |
| UPROTECT_PHE_PHPH [0/1] 1:Ph-E Voltage, 0: Ph-Ph Voltage | 0 |
| U_BASE Base RMS voltage [kV] | 1 |
| IMAX_ Over-current protection (internal) | 50 |
| T_IMAX Over-current protection trip time (internal) [s] | 0,002 |
| U_INIT Initial voltage [kV] | 0,4 |

**Table B.4:** Exponent and coefficient settings used for the voltage dependence of the General Load Types in the PowerFactory models, as defined in the provided grid from Vattenfall.

| | |
|---|---|
| Coefficient $a$P | 1 |
| Coefficient $b$P | 0 |
| Coefficient $c$P | 0 |
| Exponent $e_{a\mathrm{P}}$ | 0 |
| Exponent $e_{b\mathrm{P}}$ | 1 |
| Exponent $e_{c\mathrm{P}}$ | 2 |
| Coefficient $a$Q | 1 |
| Coefficient $b$Q | 0 |
| Coefficient $c$Q | 0 |
| Exponent $e_{a\mathrm{Q}}$ | 0 |
| Exponent $e_{b\mathrm{Q}}$ | 1 |
| Exponent $e_{c\mathrm{Q}}$ | 2 |

| Exponent value | Constant |
|---|---|
| 0 | power |
| 1 | current |
| 2 | impedance |

**Table B.5:** Transformer used in the Basic-grid model.

| | |
|---|---|
| Type | Three phase, Dyn11 ASEA |
| Rating | 0,4 MVA |
| HV-side/LV-side | 20 kV/0,4 kV |
| Short-circuit Voltage uk | 6 % |
| Copper losses | 4,8 kW |
| No load losses | 1,2 kW |

**Table B.6:** Cable values from bus M to loads on the main bus.

| Connection from | Connection to | Impedance Z1 [Ω] | R1 [Ω] | X1 [Ω] |
|---|---|---|---|---|
| M | LM1 | 0,00028284 | 0,0002 | 0,0002 |
| M | LM2 | 0,05511278 | 0,055 | 0,0029 |
| M | LM3 | 0,04780189 | 0,0477 | 0,0025 |
| M | pvM1 | 0,08805667 | 0,0879 | 0,0046 |

**Table B.7:** Cable values in branch A.

| Connection from | Connection to | Impedance Z1 [Ω] | R1 [Ω] | X1 [Ω] |
|---|---|---|---|---|
| M | A1 | 0,04761275 | 0,0445 | 0,0168 |
| A1 | LA1.1 | 0,06417982 | 0,0641 | 0,0032 |
| A1 | LA1.2 | 0,08430469 | 0,0842 | 0,0042 |
| A1 | LpvA1.1 | 0,03673029 | 0,036654 | 0,001867 |
| A1 | LpvA1.2 | 0,02021091 | 0,020154 | 0,001067 |
| A1 | A2 | 0,00833847 | 0,0077 | 0,0032 |
| A2 | LA2.1 | 0,07328847 | 0,0732 | 0,0036 |
| A2 | LA2.2 | 0,04947097 | 0,04940992 | 0,00245699 |
| A2 | LpvA2.1 | 0,03302494 | 0,032954 | 0,001667 |
| A2 | LpvA2.2 | 0,0422384 | 0,042154 | 0,002167 |
| A2 | A3 | 0,0094541 | 0,0087 | 0,0037 |
| A3 | LA3.1 | 0,03664424 | 0,0366 | 0,0018 |
| A3 | LA3.2 | 0,04215235 | 0,0421 | 0,0021 |
| A3 | LA3.3 | 0,06047446 | 0,0604 | 0,003 |

**Table B.8:** Cable values in branch B.

| Connection from | Connection to | Impedance Z1 [Ω] | R1 [Ω] | X1 [Ω] |
|---|---|---|---|---|
| M | B1 | 0,02900316 | 0,0267 | 0,0113 |
| B1 | LB1.1 | 0,07879657 | 0,0787 | 0,0039 |
| B1 | LB1.2 | 0,0604647 | 0,06039008 | 0,00300299 |
| B1 | LB1.3 | 0,04585772 | 0,0458 | 0,0023 |
| B1 | LpvB1.1 | 0,32618945 | 0,3257548 | 0,016267 |
| B1 | LpvB1.2 | 0,04594377 | 0,045854 | 0,002367 |
| B1 | B2 | 0,00963846 | 0,0089 | 0,0037 |
| B2 | LB2.1 | 0,03844698 | 0,0384 | 0,0019 |
| B2 | LB2.2 | 0,05676909 | 0,0567 | 0,0028 |
| B2 | LB2.3 | 0,05867172 | 0,0586 | 0,0029 |

**Table B.9:** Cable values in branch C.

| Connection from | Connection to | Impedance Z1 [Ω] | R1 [Ω] | X1 [Ω] |
|---|---|---|---|---|
| M | C1 | 0,01651044 | 0,015088 | 0,006448 |
| C1 | LC1.1 | 0,03664523 | 0,0366 | 0,00182 |
| C1 | LC1.2 | 0,04397427 | 0,04392 | 0,002184 |
| C1 | LC1.3 | 0,03481288 | 0,03476992 | 0,00172899 |
| C1 | LC1.4 | 0,09888833 | 0,09735696 | 0,016656 |
| C1 | C2 | 0,00907413 | 0,008364 | 0,00351901 |
| C2 | LC2.1 | 0,05496636 | 0,0549 | 0,0027 |
| C2 | LC2.2 | 0,04766047 | 0,0476 | 0,0024 |
| C2 | LpvC2.1 | 0,04395509 | 0,0439 | 0,0022 |
| C2 | C3 | 0,0094541 | 0,0087 | 0,0037 |
| C3 | LC3.1 | 0,04215235 | 0,0421 | 0,0021 |
| C3 | LC3.2 | 0,04585772 | 0,0458 | 0,0023 |
| C3 | LC3.3 | 0,08059932 | 0,0805 | 0,004 |
| C3 | LC3.4 | 0,051261 | 0,0512 | 0,0025 |
| C3 | LC3.5 | 0,05496636 | 0,0549 | 0,0027 |

**Table B.10:** Cable values in branch D.

| Connection from | Connection to | Impedance Z1 [Ω] | R1 [Ω] | X1 [Ω] |
|---|---|---|---|---|
| M | D1 | 0,01760567 | 0,0161 | 0,0071 |
| D1 | LpvD1.1 | 0,0898128 | 0,0897 | 0,0045 |
| D1 | LD1.1 | 0,07328847 | 0,0732 | 0,0036 |
| D1 | LD1.2 | 0,03293889 | 0,0329 | 0,0016 |
| D1 | LD1.3 | 0,03293889 | 0,0329 | 0,0016 |
| D1 | D2 | 0,01227676 | 0,011316 | 0,00476099 |
| D2 | LD2.1 | 0,04766047 | 0,0476 | 0,0024 |
| D2 | LD2.2 | 0,05496636 | 0,0549 | 0,0027 |
| D2 | LpvD2.1 | 0,03123457 | 0,03116408 | 0,001614 |
| D2 | LpvD2.2 | 0,0312222 | 0,031154 | 0,001567 |
| D2 | D3 | 0,0094541 | 0,0087 | 0,0037 |
| D3 | LD3.1 | 0,03844698 | 0,0384 | 0,0019 |
| D3 | LD3.2 | 0,03293889 | 0,0329 | 0,0016 |
| D3 | LD3.3 | 0,05496636 | 0,0549 | 0,0027 |
| D3 | LpvD3.1 | 0,051261 | 0,0512 | 0,0025 |
| D3 | D4 | 0,01387808 | 0,012792 | 0,005382 |
| D4 | LD4.1 | 0,07695498 | 0,07686 | 0,003822 |
| D4 | LD4.2 | 0,07695498 | 0,07686 | 0,003822 |
| D4 | LD4.3 | 0,1007743 | 0,1006499 | 0,00500501 |
| D4 | LD4.4 | 0,04214193 | 0,04208992 | 0,00209301 |
| D4 | D5 | 0,01885996 | 0,017384 | 0,007314 |
| D5 | LD5.1 | 0,03664424 | 0,0366 | 0,0018 |
| D5 | LD5.2 | 0,02202748 | 0,022 | 0,0011 |
| D5 | LD5.3 | 0,02933837 | 0,0293 | 0,0015 |

**Table B.11:** Cable values in branch E.

| Connection from | Connection to | Impedance Z1 [Ω] | R1 [Ω] | X1 [Ω] |
|---|---|---|---|---|
| M | E1 | 0,01406981 | 0,0131 | 0,0051 |
| E1 | LE1.1 | 0,0403496 | 0,0403 | 0,002 |
| E1 | LE1.2 | 0,06047446 | 0,0604 | 0,003 |
| E1 | LE1.3 | 0,05867172 | 0,0586 | 0,0029 |
| E1 | E2 | 0,0091 | 0,0084 | 0,0035 |
| E2 | LE2.1 | 0,05496636 | 0,0549 | 0,0027 |
| E2 | LE2.2 | 0,04215235 | 0,0421 | 0,0021 |
| E2 | LE2.3 | 0,05496636 | 0,0549 | 0,0027 |
| E2 | LE2.4 | 0,04585772 | 0,0458 | 0,0023 |
| E2 | E3 | 0,01227721 | 0,0113 | 0,0048 |
| E3 | LE3.1 | 0,02563299 | 0,0256 | 0,0013 |
| E3 | LE3.2 | 0,06598257 | 0,0659 | 0,0033 |
| E3 | LE3.3 | 0,02743574 | 0,0274 | 0,0014 |
| E3 | LE3.4 | 0,07148574 | 0,0714 | 0,0035 |
| E3 | E4 | 0,01403393 | 0,012792 | 0,005772 |
| E4 | LE4.1 | 0,03844698 | 0,0384 | 0,0019 |
| E4 | LE4.2 | 0,04029845 | 0,04026 | 0,00176 |
| E4 | LE4.3 | 0,1348436 | 0,1345501 | 0,008892 |
| E4 | E5 | 0,0141982 | 0,014102 | 0,00165 |
| E5 | LE5.1 | 0,12798269 | 0,12506704 | 0,02604899 |
| E5 | LE5.2 | 0,11134053 | 0,11093008 | 0,00715101 |
| E5 | LpvE5.1 | 0,20634496 | 0,20226808 | 0,03789401 |

**Table B.12:** Transformer used in the LV-grid model.

| | |
|---|---|
| Type | Three phase, Dyn11 |
| Rating | 0,8 MVA |
| HV-side/LV-side | 10 kV/0,4 kV |
| Short-circuit Voltage uk | 5,29528 % |
| Copper losses | 8 kW |
| No load losses | 0 kW |

**Table B.13:** Bus M 'Original house loads', specific load and PV values for test (LV-grid).

| Load name | Peak active power P [kW] | Peak reactive power Q [kVAr] | PV name | Generated power [kW] |
|---|---|---|---|---|
| LM1 | 8 | 6 | | |
| LM2 | 10 | 1 | | |
| LM3 | 14 | 2 | | |
| LpvM1 | 13 | 2 | pvM1 | 2 |

**Table B.14:** Branch A 'Original house loads', specific load and PV values for test (LV-grid).

| Load name | Peak active power P [kW] | Peak reactive power Q [kVAr] | PV name | Generated power [kW] |
|---|---|---|---|---|
| LA1.1 | 10 | 1 | | |
| LA1.2 | 6 | 1 | | |
| LpvA1.1 | 4 | 1 | pvA1.1 | 2 |
| LpvA1.2 | 6 | 2 | pvA1.2 | 6 |
| LA2.1 | 9 | 1 | | |
| LA2.2 | 3 | 0 | | |
| LpvA2.1 | 5 | 1 | pvA2.1 | 7 |
| LpA2.2 | 13 | 2 | pvA2.2 | 14 |
| LA3.1 | 13 | 2 | | |
| LA3.2 | 9 | 2 | | |
| LA3.3 | 7 | 1 | | |

**Table B.15:** Branch B 'Original house loads', specific load and PV values for test (LV-grid).

| Load name | Peak active power P [kW] | Peak reactive power Q [kVAr] | PV name | Generated power [kW] |
|---|---|---|---|---|
| LB1.1 | 10 | 1 | | |
| LB1.2 | 11 | 2 | | |
| LB1.3 | 10 | 1 | | |
| LpvB1.1 | 10 | 3 | pvB1.1 | 7 |
| LpvB1.2 | 5 | 1 | pvB1.2 | 8 |
| LB2.1 | 6 | 1 | | |
| LB2.2 | 9 | 1 | | |
| LB2.3 | 6 | 1 | | |

**Table B.16:** Branch C 'Original house loads', specific load and PV values for test (LV-grid).

| Load name | Peak active power P [kW] | Peak reactive power Q [kVAr] | PV name | Generated power [kW] |
|---|---|---|---|---|
| LC1.1 | 8 | 1 | | |
| LC1.2 | 15 | 2 | | |
| LC1.3 | 4 | 1 | | |
| LC1.4 | 13 | 3 | | |
| LC2.1 | 8 | 1 | pvC2.1 | 5 |
| LC2.2 | 7 | 1 | | |
| LpvC2.1 | 5 | 1 | | |
| LC3.1 | 6 | 1 | | |
| LC3.2 | 9 | 1 | | |
| LC3.3 | 6 | 1 | | |
| LC3.4 | 9 | 1 | | |
| LC3.5 | 10 | 1 | | |

**Table B.17:** Branch D 'Original house loads', specific load and PV values for test (LV-grid).

| Load name | Peak active power P [kW] | Peak reactive power Q [kVAr] | PV name | Generated power [kW] |
|---|---|---|---|---|
| LpvD1.1 | 4 | 1 | pvD1.1 | 2 |
| LD1.1 | 14 | 2 | | |
| LD1.2 | 9 | 1 | | |
| LD1.3 | 5 | 1 | | |
| LD2.1 | 9 | 1 | | |
| LD2.2 | 11 | 2 | | |
| LpvD2.1 | 7 | 1 | pvD2.1 | 7 |
| LpvD2.2 | 7 | 1 | pvD2.2 | 6 |
| LD3.1 | 10 | 1 | | |
| LD3.2 | 6 | 1 | | |
| LD3.3 | 11 | 2 | | |
| LD3.4 | 17 | 2 | | |
| LD4.1 | 11 | 2 | | |
| LD4.2 | 9 | 1 | | |
| LD4.3 | 8 | 1 | | |
| LD4.4 | 8 | 1 | | |
| LD5.1 | 7 | 1 | | |
| LD5.2 | 10 | 1 | | |
| LD5.3 | 6 | 1 | | |

**Table B.18:** Branch E 'Original house loads', specific load and PV values for test (LV-grid).

| Load name | Peak active power P [kW] | Peak reactive power Q [kVAr] | PV name | Generated power [kW] |
|---|---|---|---|---|
| LE1.1 | 6 | 1 | | |
| LE1.2 | 10 | 1 | | |
| LE1.3 | 8 | 3 | | |
| LE2.1 | 8 | 1 | | |
| LE2.2 | 6 | 1 | | |
| LE2.3 | 6 | 1 | | |
| LE2.4 | 10 | 1 | | |
| LE3.1 | 8 | 1 | | |
| LE3.2 | 9 | 1 | | |
| LE3.3 | 10 | 1 | | |
| LE3.4 | 8 | 1 | | |
| LE4.1 | 8 | 1 | | |
| LE4.2 | 11 | 3 | | |
| LE4.3 | 4 | 1 | | |
| LE5.1 | 4 | 1 | | |
| LE5.2 | 9 | 1 | | |
| LpvE5.1 | 6 | 1 | pvE5.1 | 8 |

**Table B.19:** Added PV values in LV-grid, loaction in Figure 3.8, and the loads changed in the disruption with car chargers test.

| Additional PV location | Additional PV rating [kW] |
|---|---|
| Bus C1 | 15 |
| Bus C3 | 15 |
| Load LD3.4 | 14 |
| Bus D4 | 17 |
| Bus D5 | 15 |
| Bus E1 | 14 |
| Bus E3 | 15 |
| Bus E2 | 12 |
| Load LE5.2 | 12 |
| **Car charger location** | **Rating and activation** |
| Load LpvA1.2 | 11 kW increase after 1 second |
| Load LE5.1 | 11 kW increase after 2 seconds |
| Bus D1 | 11 kW increase after 3 seconds |

**Table B.20:** The increased PV values of the original 12 units used in the LV-grid, corresponding to PVs shown in Figure 3.8, amounting to 298.5 kW when added to the Additional PVs

| PV name | Increased PV rating [kW] |
|---|---|
| pvM1 | 18 |
| pvA1.1 | 12 |
| pvA1.2 | 11 |
| pvA2.1 | 14 |
| pvA2.2 | 14 |
| pvB1.1 | 16 |
| pvB1.2 | 16 |
| pvC2.1 | 10 |
| pvD1.1 | 16 |
| pvD2.1 | 15 |
| pvD2.2 | 15 |
| pvE5.1 | 12.5 |

**Table B.21:** HV-transformer used in the HV-cable grid model.

| | |
|---|---|
| Type | 2-Winding, three phase, Dyn11 |
| Rating | 1 MVA |
| HV-side/LV-side | 40 kV/10 kV |
| Short-circuit Voltage uk | 3 % |
| Copper losses | 0 kW |
| No load losses | 0 kW |

**Table B.22:** MV cable data.

| | |
|---|---|
| Type name | NA2YSY 1x240rm 6/10 kV |
| Rated voltage [kV] | 10 |
| Rated current (in ground) [kA] | 0,42 |
| AC Resistance (20 °) [Ω/km] | 0,1292 |
| Reactance X' $[\Omega/km]$ | 0,103672 |
| Susceptance B' [uS/km] | 144,5133 |

# C

## Results

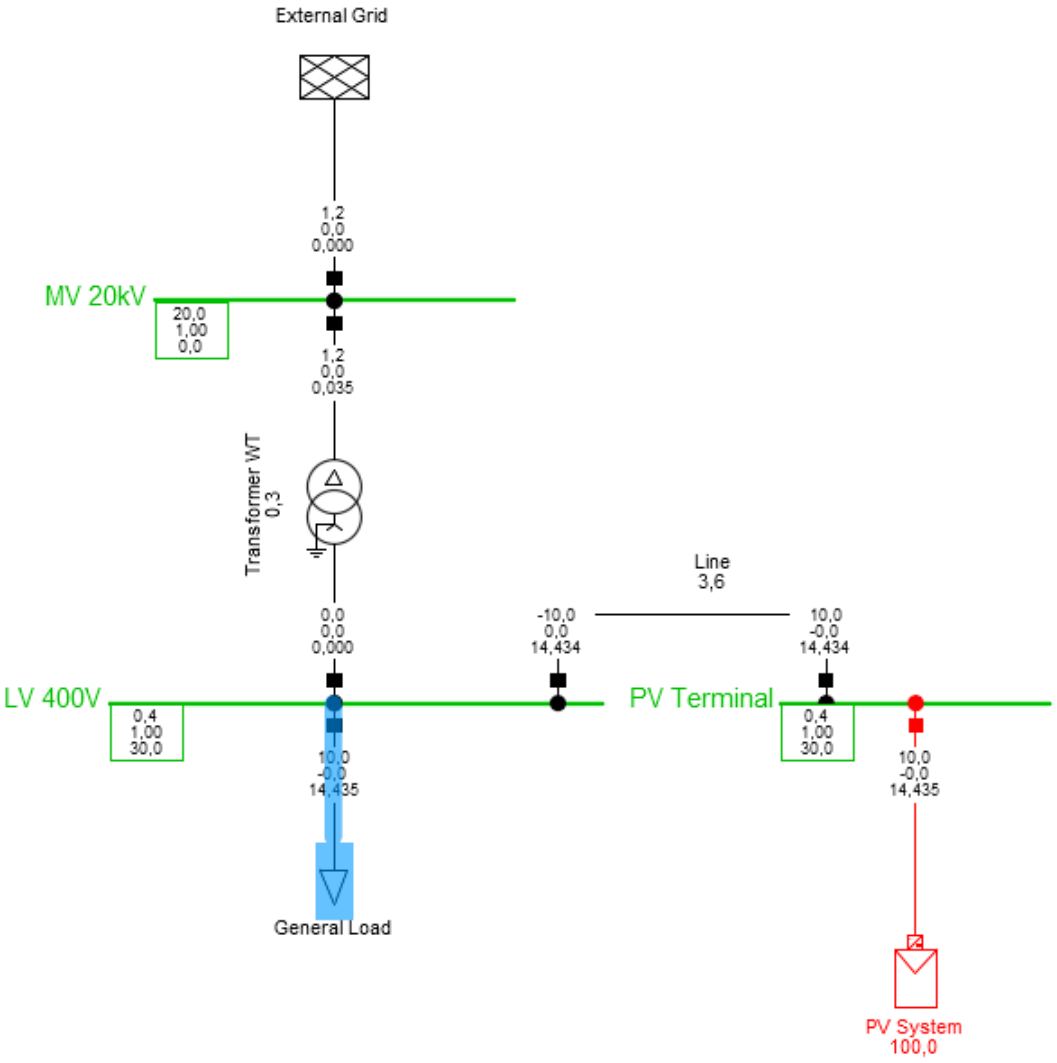


**Figure C.1:** The PQ flow of the basic grid before disconnection. The top number represents P in kW, the middle Q in kVAr and the bottom current in A.

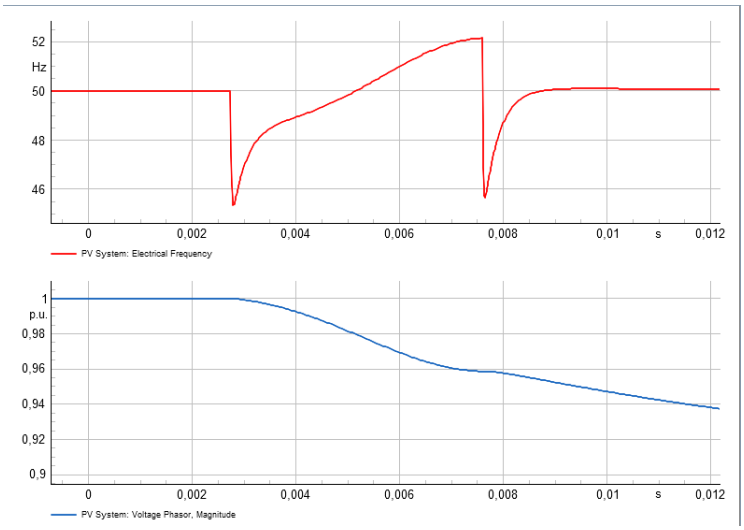


**Figure C.2:** Frequency (red) and voltage magnitude (blue) graphs zoomed in around the frequency spikes for load and generation balance, break point A.

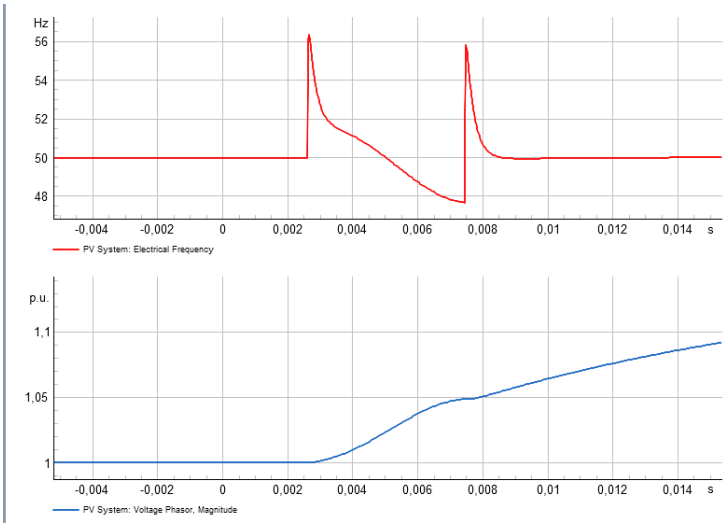


**Figure C.3:** Frequency (red) and voltage magnitude (blue) graphs zoomed in around the frequency spikes for -25 % load with respect to the generation value, break point A.

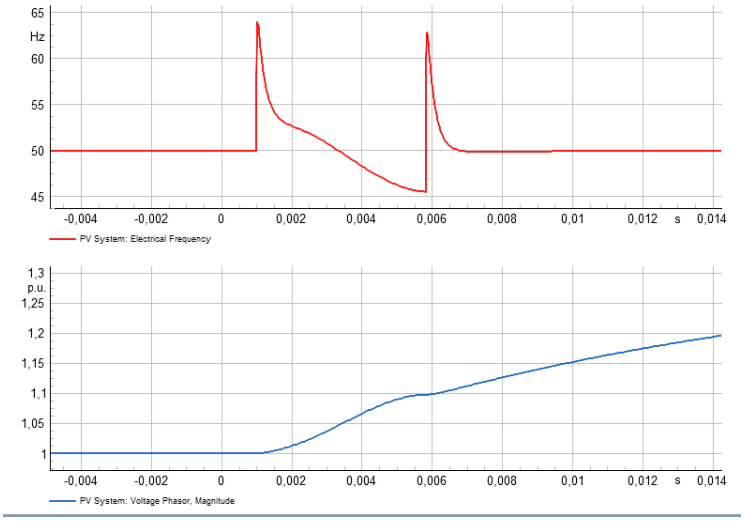


**Figure C.4:** Frequency (red) and voltage magnitude (blue) graphs zoomed in around the frequency spikes for -25 % load with respect to the generation value, break point B.

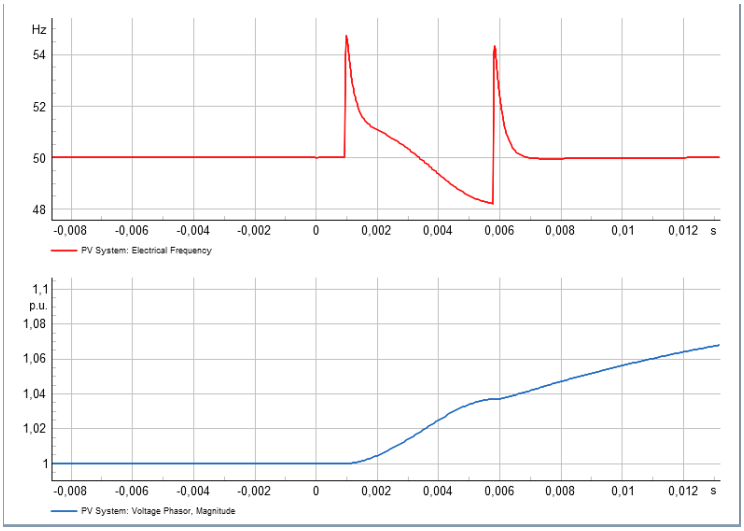


**Figure C.5:** Frequency (red) and voltage magnitude (blue) graphs zoomed in around the frequency spikes for -10 % load with respect to the generation value, break point B.

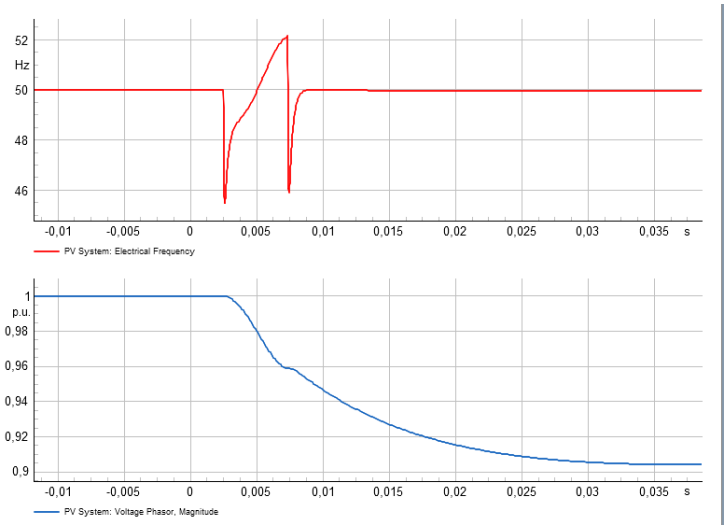


**Figure C.6:** Frequency (red) and voltage magnitude (blue) graphs zoomed in around the frequency spikes for -0,1 kVAr, break point A.

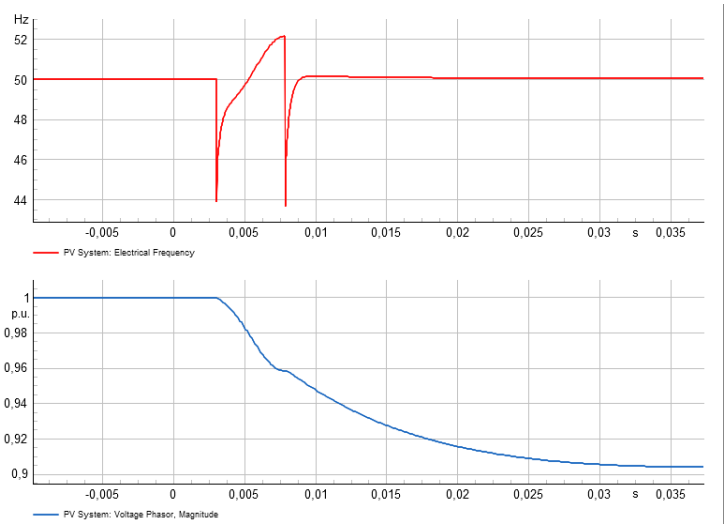


**Figure C.7:** Frequency (red) and voltage magnitude (blue) graphs zoomed in around the frequency spikes for 0,1 kVAr, break point A.

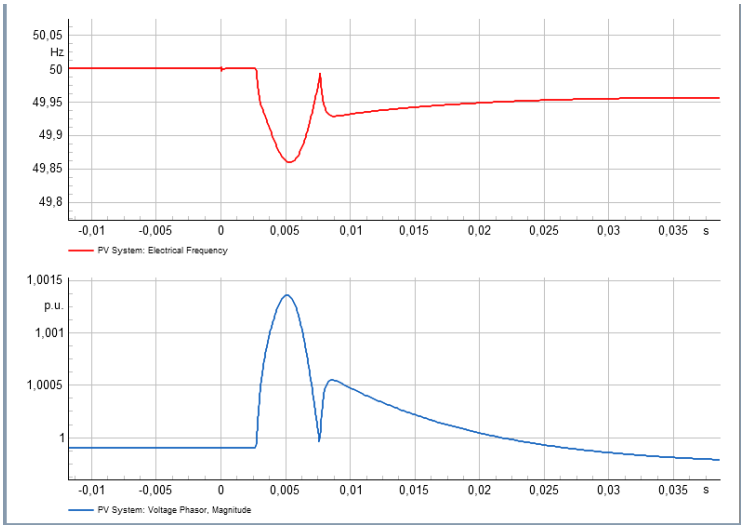


**Figure C.8:** Frequency (red) and voltage magnitude (blue) graphs zoomed in around the frequency spikes for -0,1 kVAr, break point B.

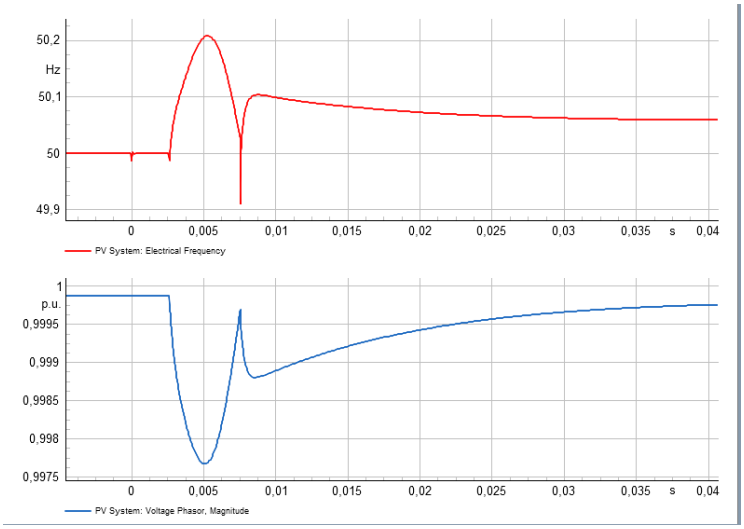


**Figure C.9:** Frequency (red) and voltage magnitude (blue) graphs zoomed in around the frequency spikes for 0,1 kVAr, break point B.

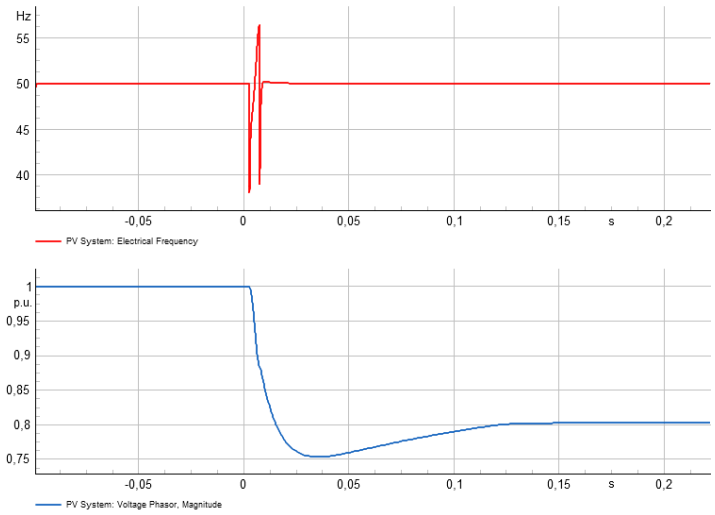


**Figure C.10:** Frequency (red) and voltage magnitude (blue) graphs zoomed in around the frequency spikes for +25 % load with respect to the generation value, break point A.

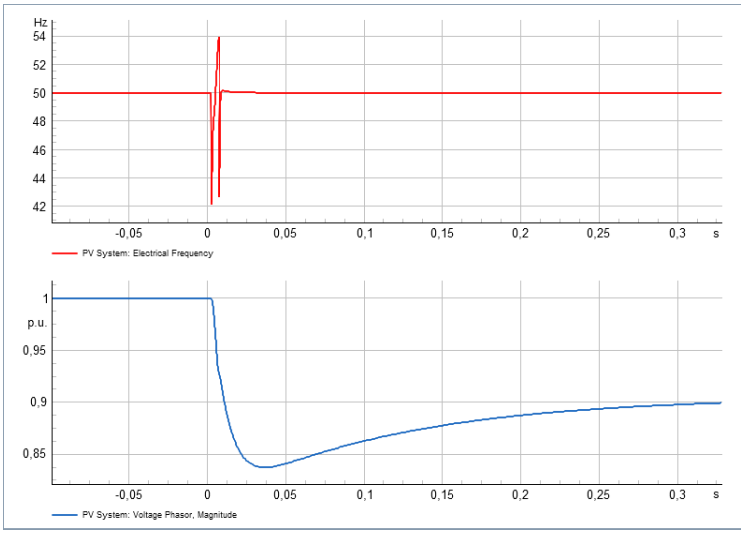


**Figure C.11:** Frequency (red) and voltage magnitude (blue) graphs zoomed in around the frequency spikes for +10 % load with respect to the generation value, break point A.

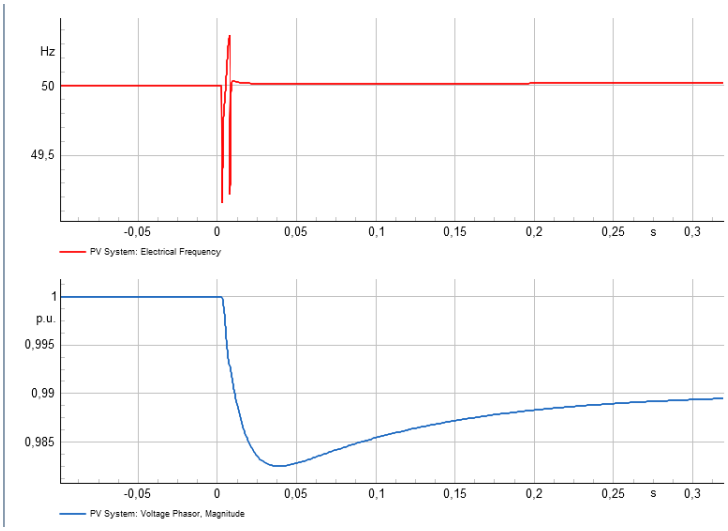


**Figure C.12:** Frequency (red) and voltage magnitude (blue) graphs zoomed in around the frequency spikes for -10 % load with respect to the generation value, break point A.

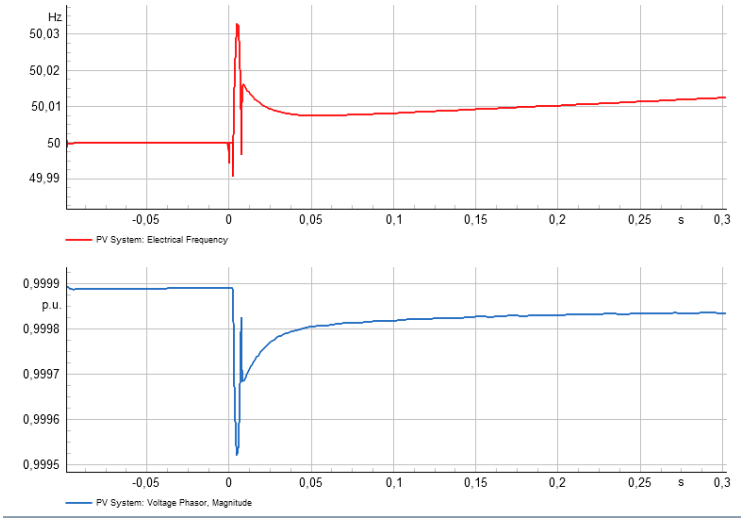


**Figure C.13:** Frequency (red) and voltage magnitude (blue) graphs zoomed in around the frequency spikes for load and generation balance, break point B.

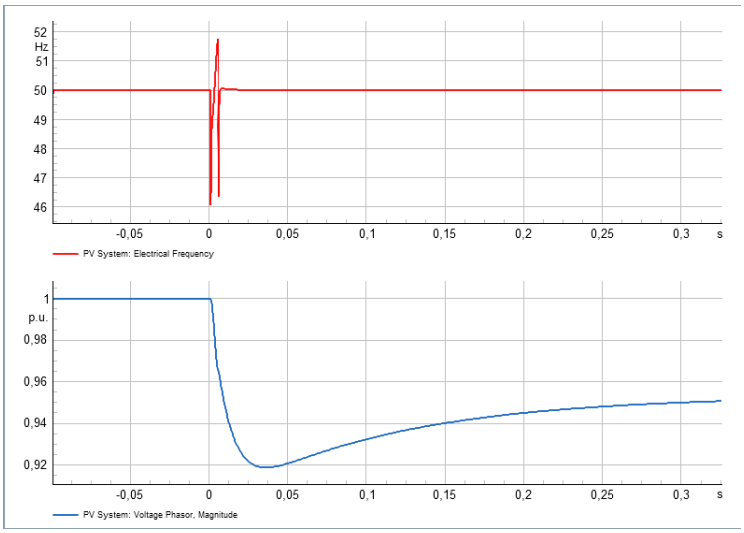


**Figure C.14:** Frequency (red) and voltage magnitude (blue) graphs zoomed in around the frequency spikes for +10 % load with respect to the generation value, break point B.

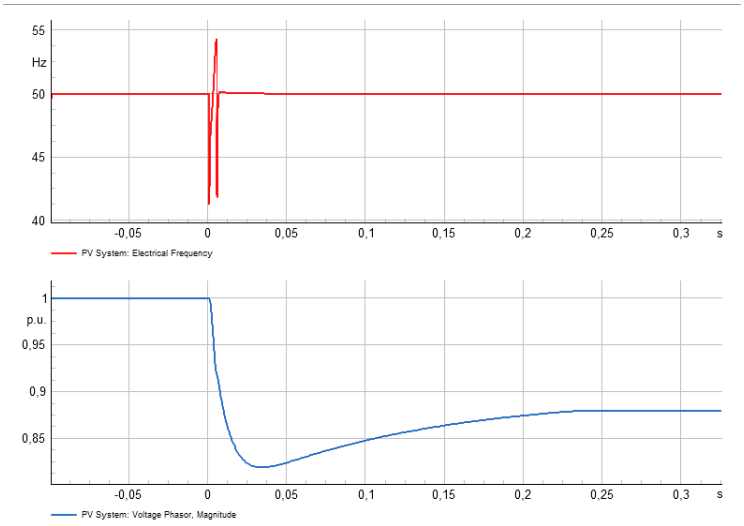


**Figure C.15:** Frequency (red) and voltage magnitude (blue) graphs zoomed in around the frequency spikes for +25 % load with respect to the generation value, break point B.

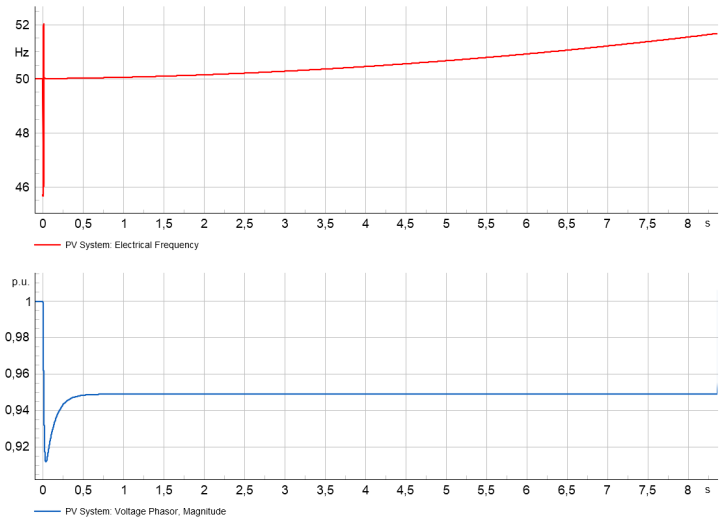


**Figure C.16:** Frequency (red) and voltage magnitude (blue) graphs for test -1 % load with respect to the generation value, break point A.

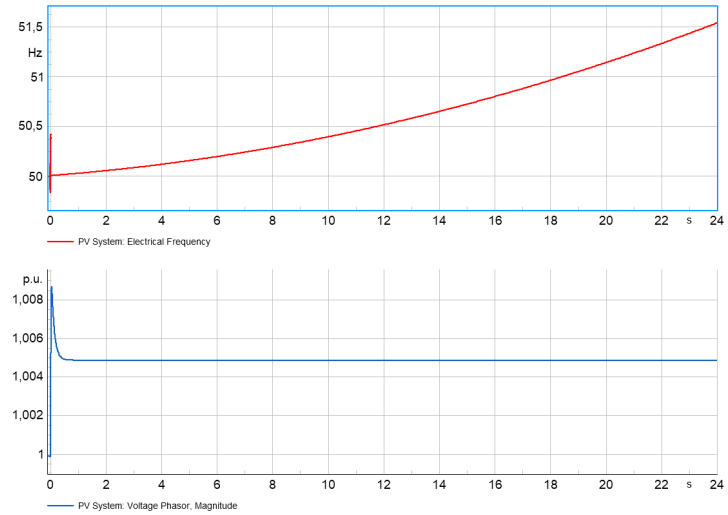


**Figure C.17:** Frequency and voltage magnitude graphs for test -1 % load, break point B.

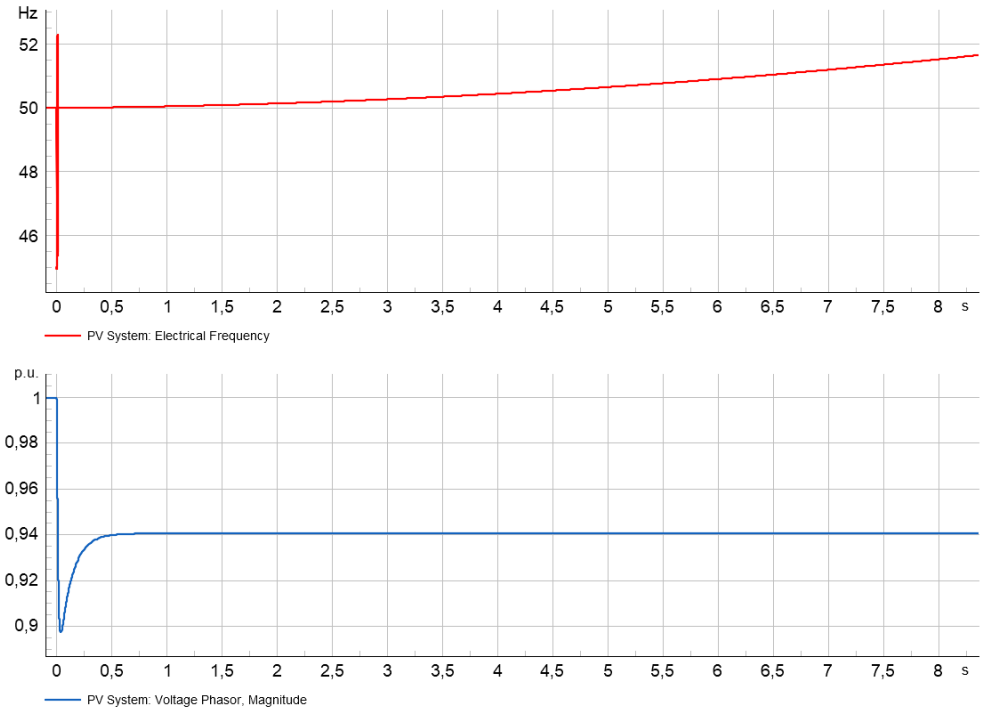


**Figure C.18:** Frequency and voltage magnitude graphs for test +1 % load, break point A.

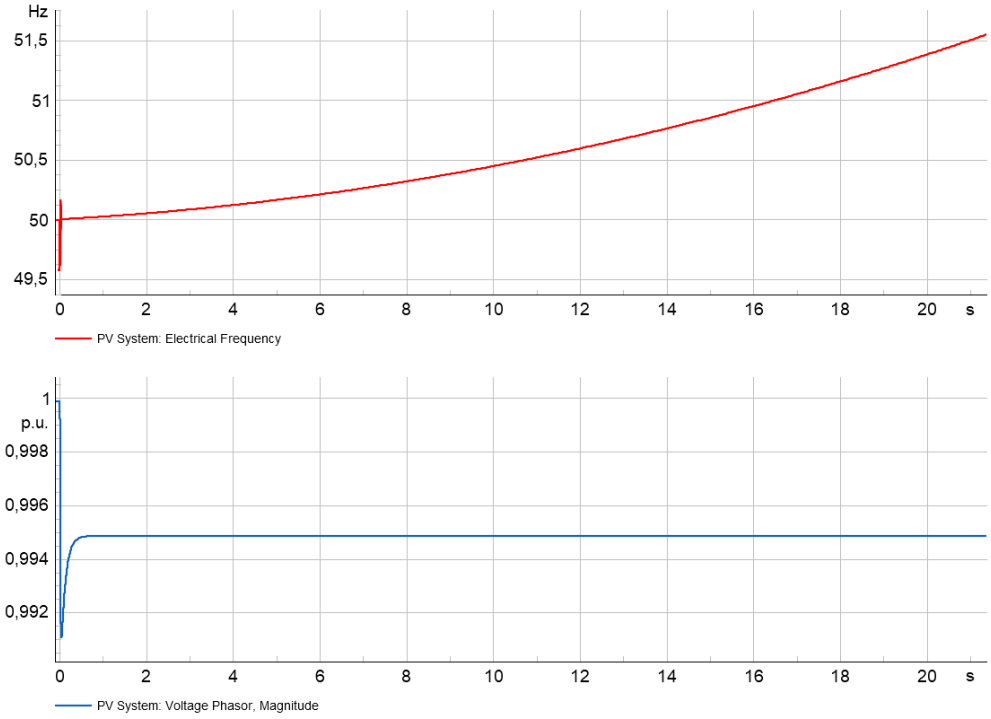


**Figure C.19:** Frequency and voltage magnitude graphs for test +1 % load, break point B.

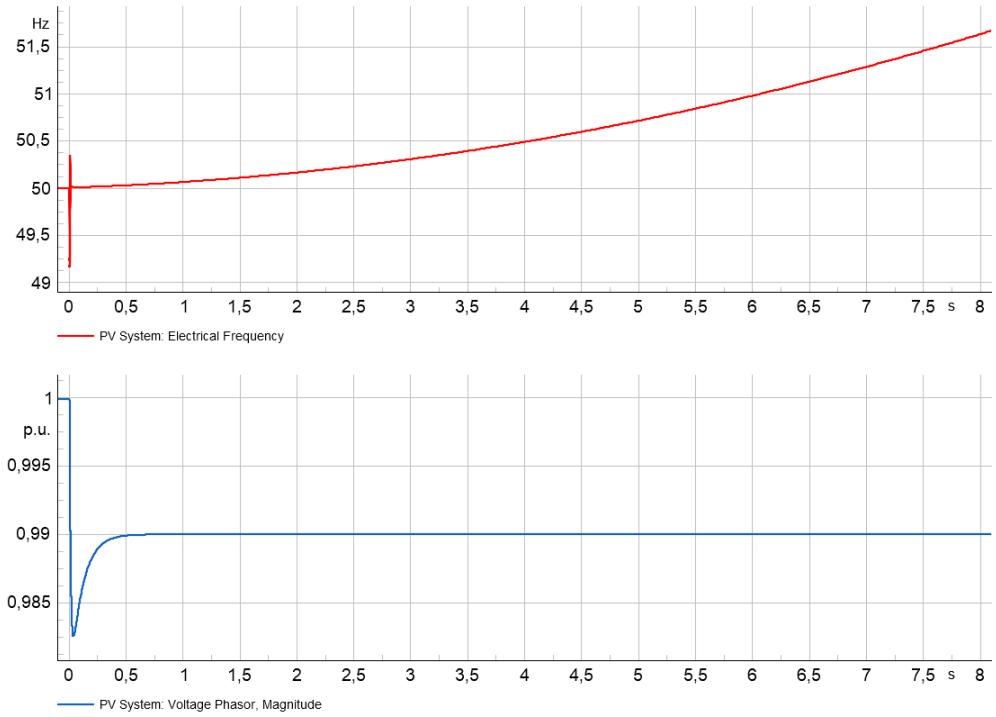


**Figure C.20:** Frequency and voltage magnitude graphs for test -10 % load, break point A.

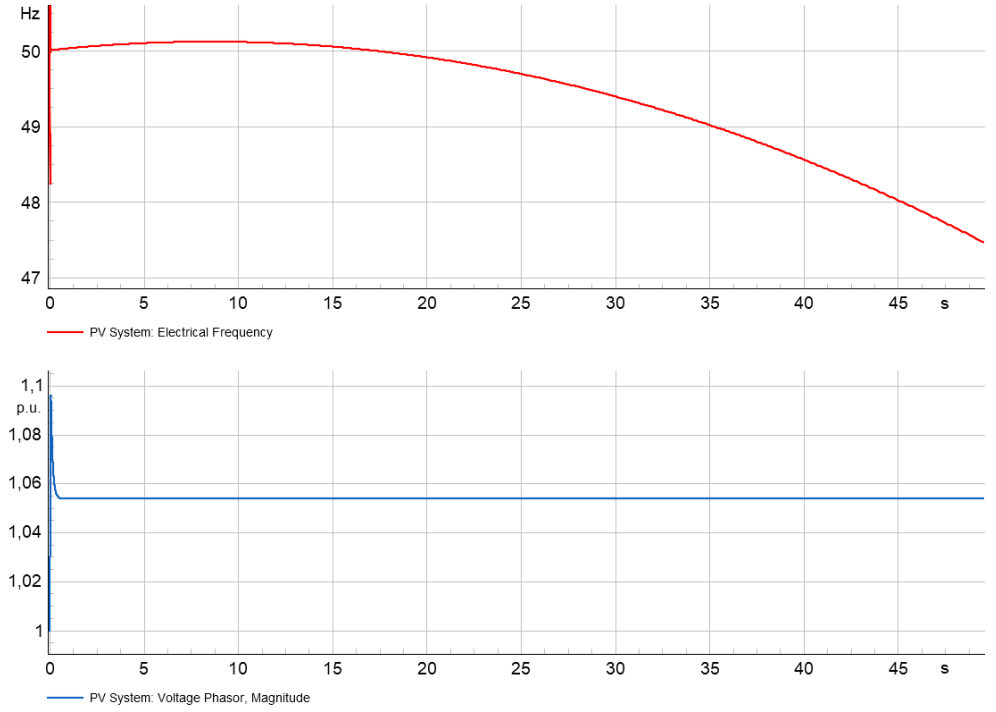


**Figure C.21:** Frequency and voltage magnitude graphs for test -10 % load, break point B.

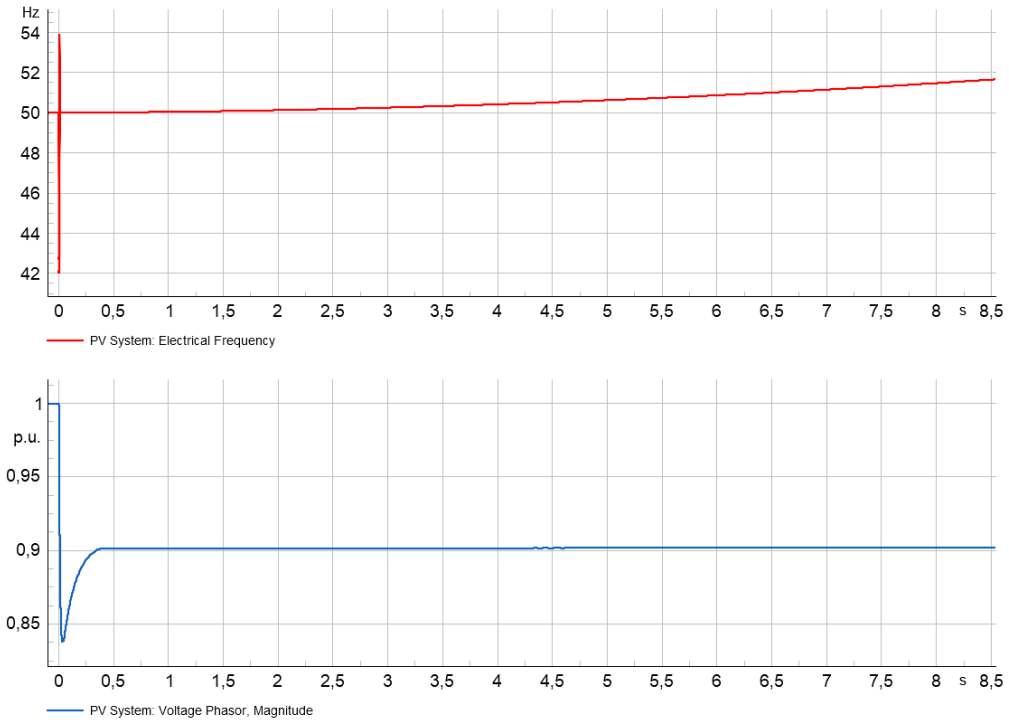


**Figure C.22:** Frequency and voltage magnitude graphs for test +10 % load, break point A.

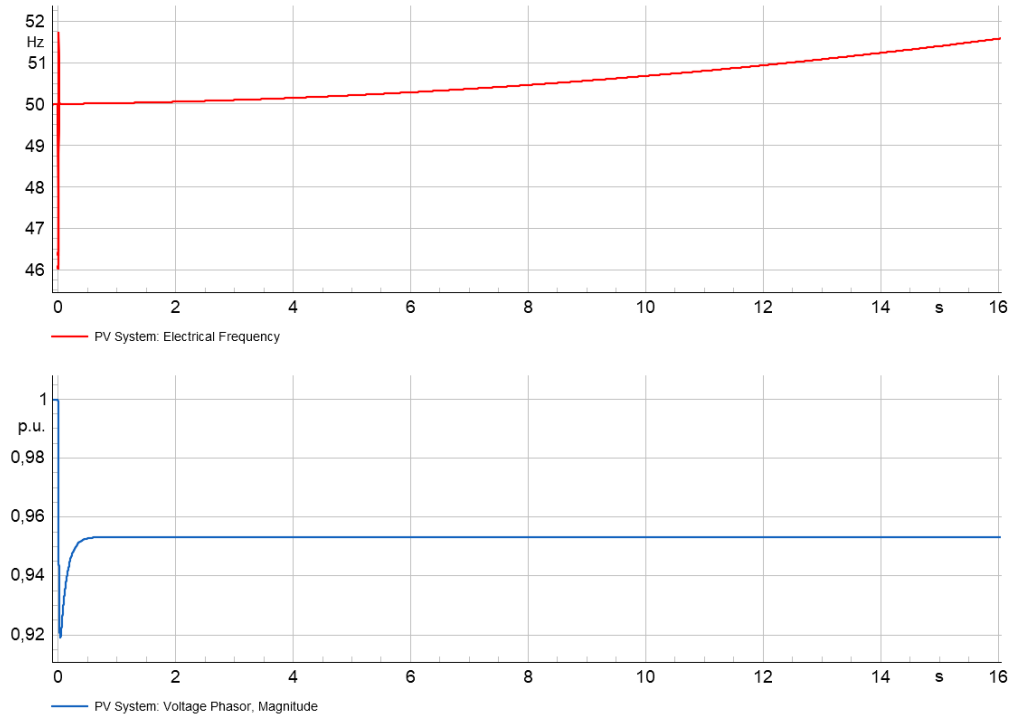


**Figure C.23:** Frequency and voltage magnitude graphs for test +10 % load, break point B.

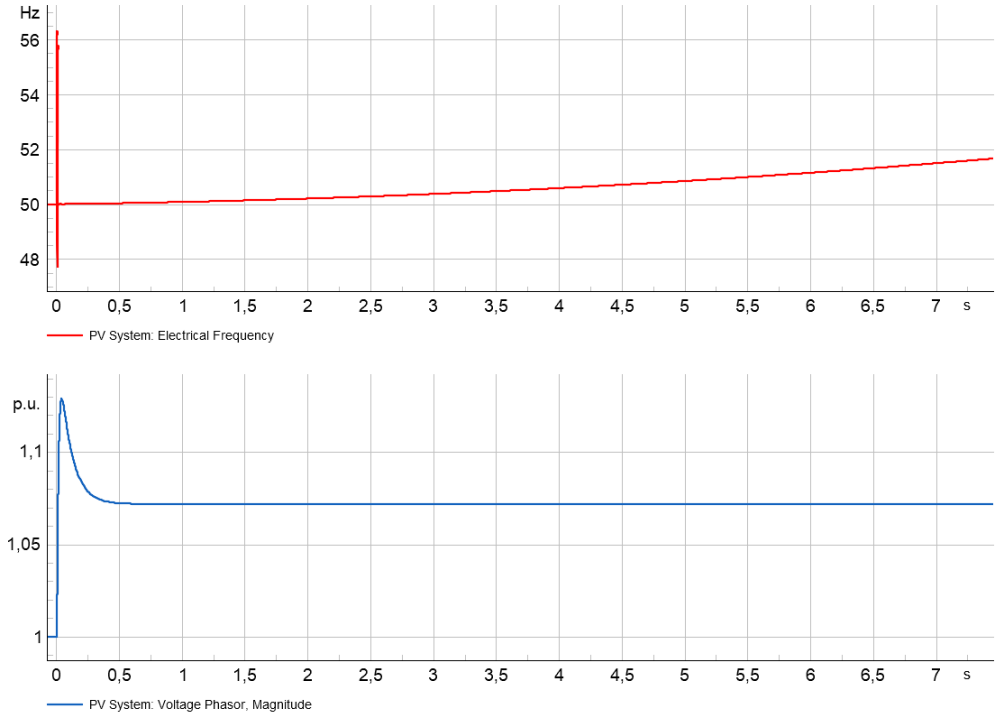


**Figure C.24:** Frequency and voltage magnitude graphs for test -25 % load, break point A.

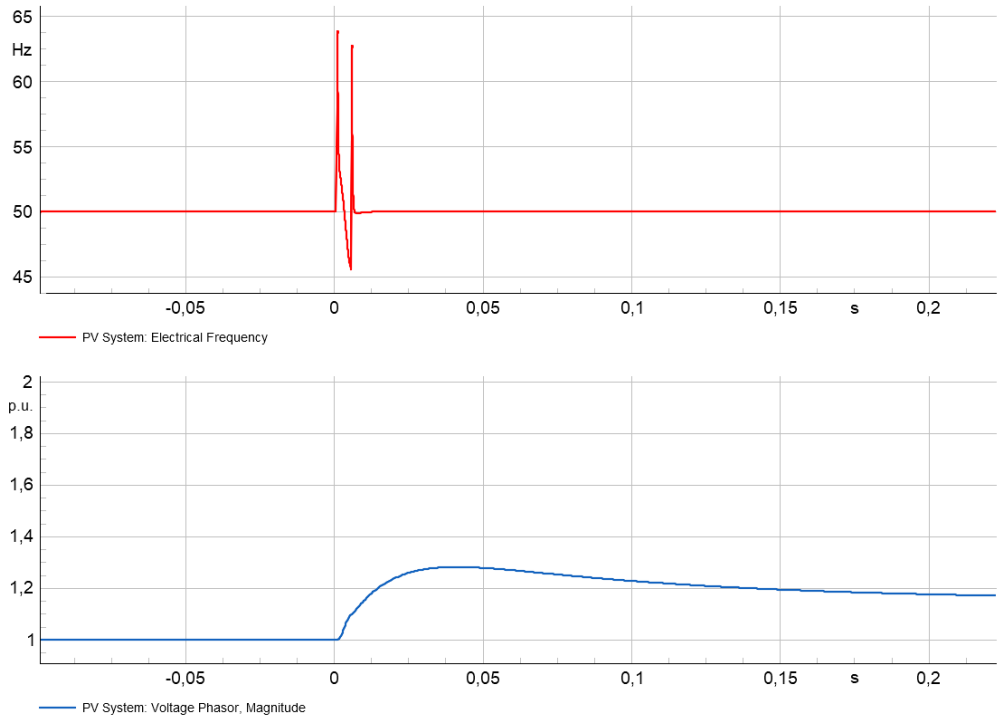


**Figure C.25:** Frequency and voltage magnitude graphs for test -25 % load, break point B.

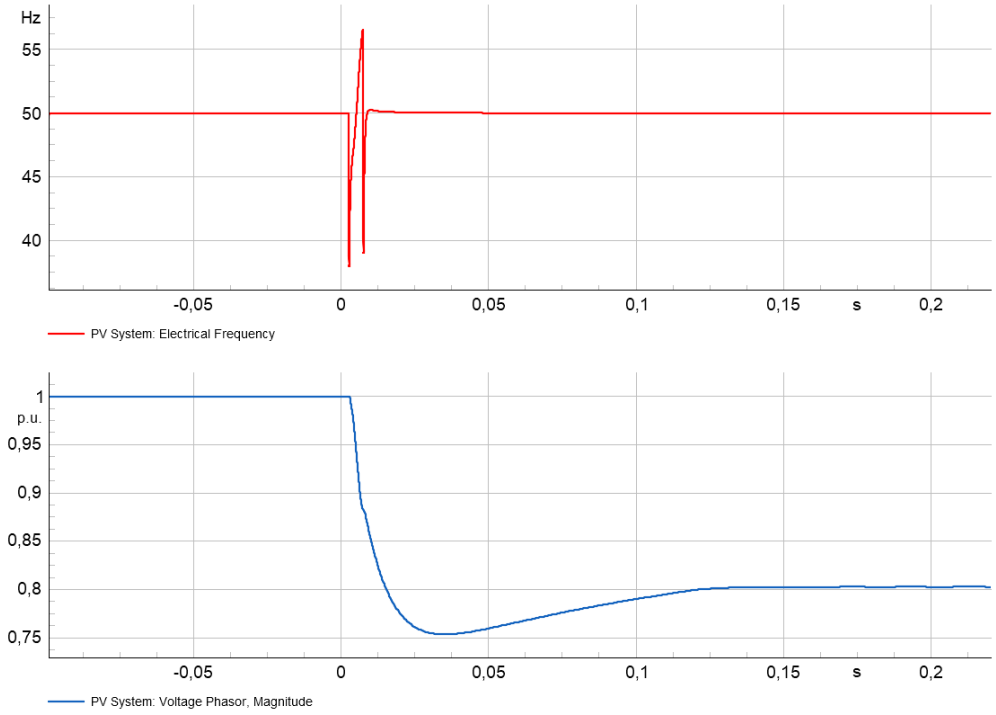


**Figure C.26:** Frequency and voltage magnitude graphs for test +25 % load, break point A.

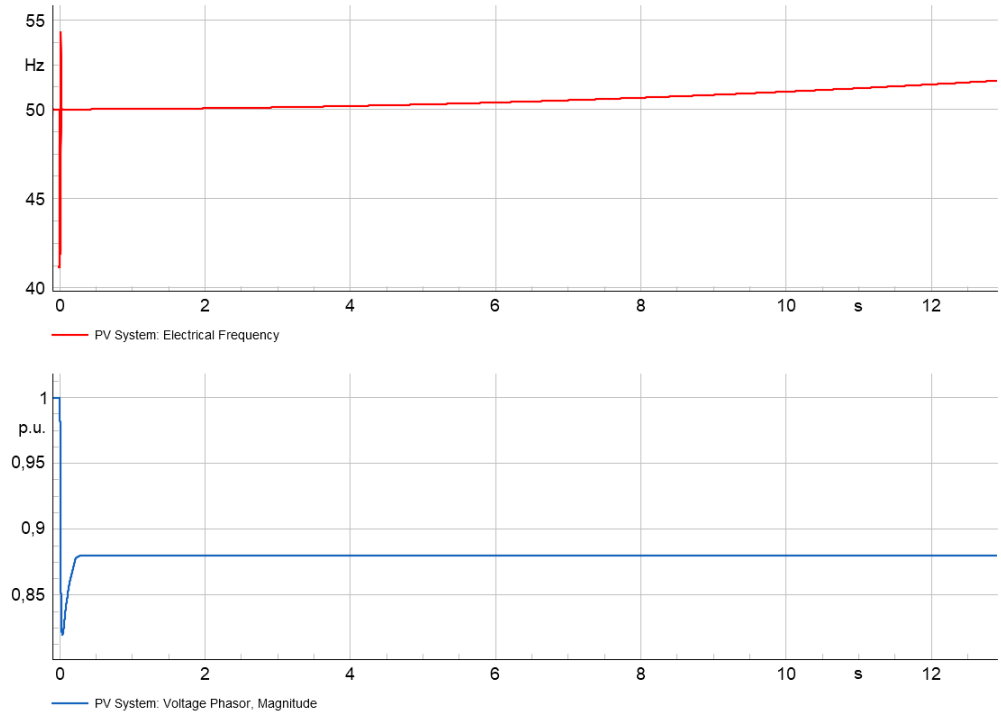


**Figure C.27:** Frequency and voltage magnitude graphs for test +25 % load, break point B.

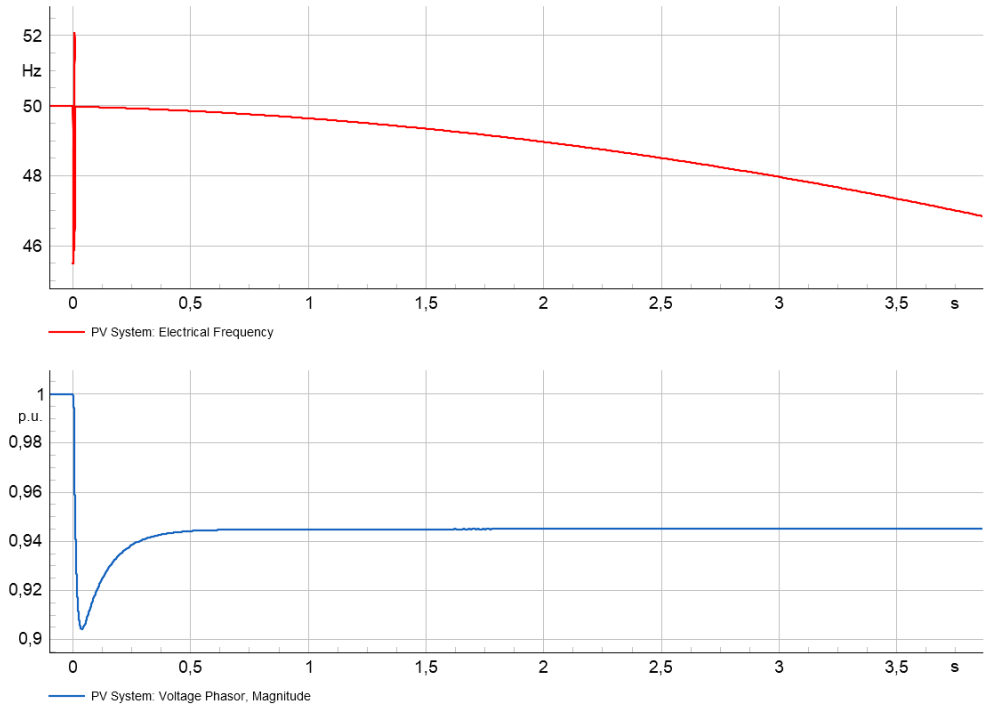


**Figure C.28:** Frequency and voltage magnitude graphs for test -0,1 kVAr load, break point A.

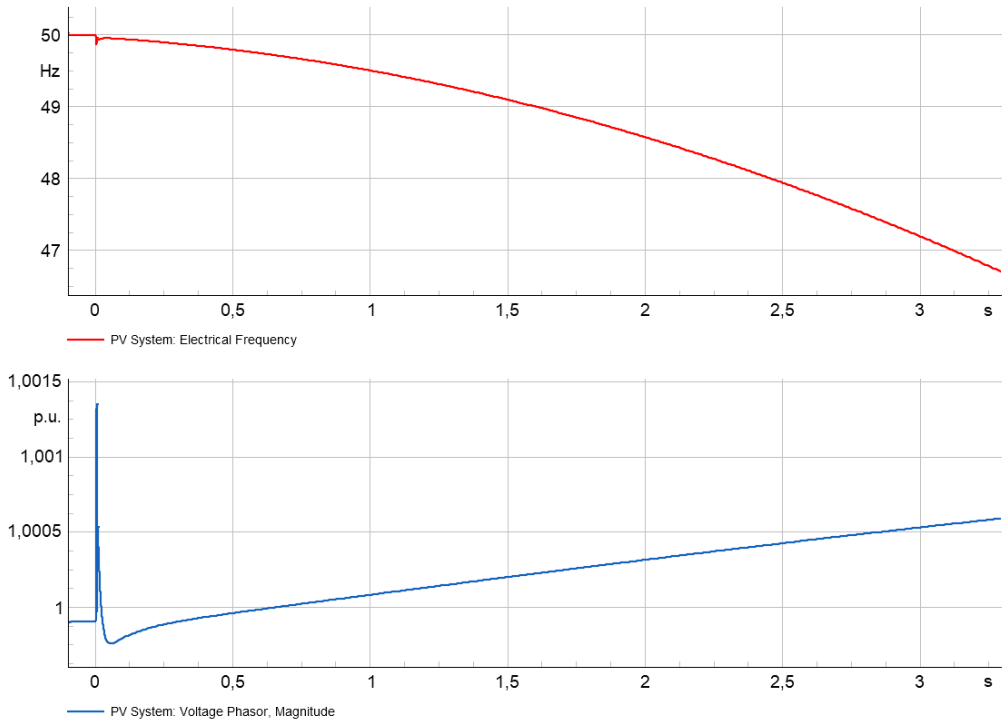


**Figure C.29:** Frequency and voltage magnitude graphs for test -0,1 kVAr load, break point B.

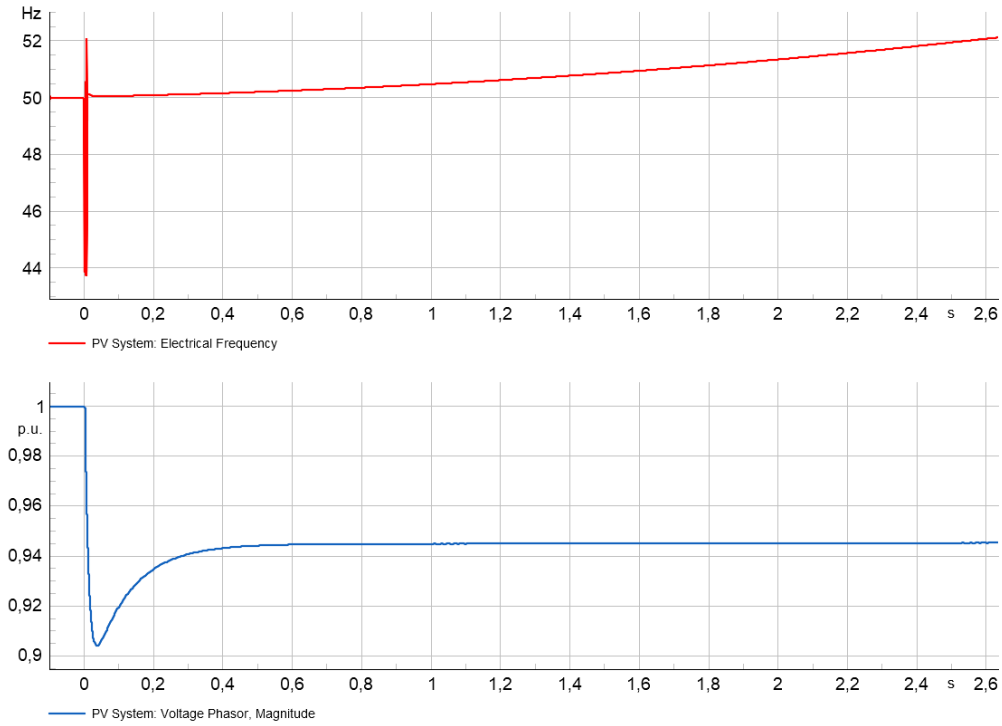


**Figure C.30:** Frequency and voltage magnitude graphs for test +0,1 kVAr load, break point A.

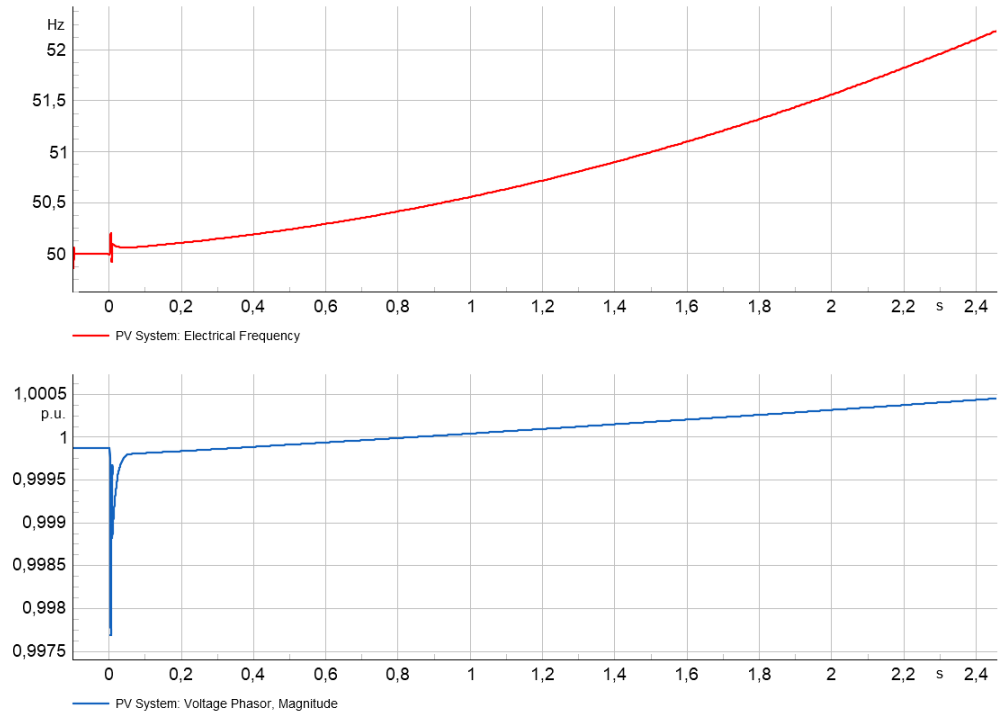


**Figure C.31:** Frequency and voltage magnitude graphs for test +0,1 kVAr load, break point B.

**Table C.1:** Numerical values of the NDZ points depicted in Figure 4.9, with respect to total generation 298.5 kW.

| Active power P, in % of the total generation | Reactive power Q, in % of the total generation | Protection trigger time [s] |
|---|---|---|
| 128.2 | 0 | 0.230 |
| 78.3 | 0 | 0.661 |
| 0 | 0.255 | 5.023 |
| 0 | -0.42 | 4.980 |
| 105 | 0.29 | 4.980 |
| 110 | 0.32 | 4.980 |
| 115 | 0.35 | 5.004 |
| 120 | 0.38 | 5.020 |
| 125 | 0.43 | 5.002 |
| 128.2 | 0.45 | 0.227 |
| 105 | -0.46 | 4.990 |
| 110 | -0.5 | 5.013 |
| 115 | -0.54 | 5.027 |
| 120 | -0.59 | 5.011 |
| 125 | -0.65 | 5.037 |
| 128.2 | -0.67 | 0.230 |
| 95 | 0.23 | 5.000 |
| 90 | 0.20 | 5.042 |
| 85 | 0.18 | 4.982 |
| 80 | 0.16 | 5.036 |
| 95 | -0.38 | 4.990 |
| 90 | -0.34 | 5.022 |
| 85 | -0.31 | 4.982 |
| 80 | -0.29 | 5.021 |
| 78.3 | -0.29 | 0.661 |

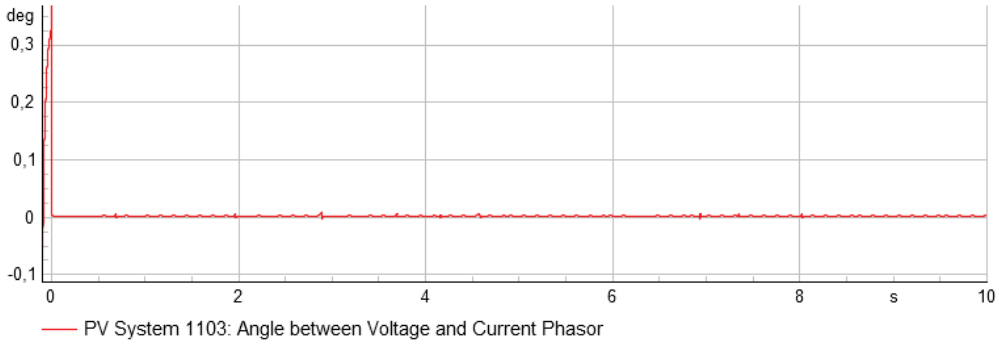


**Figure C.32:** Angle difference between voltage and current when the grid disconnects at 0 seconds, performed in PV-grid model with generation equal load values.

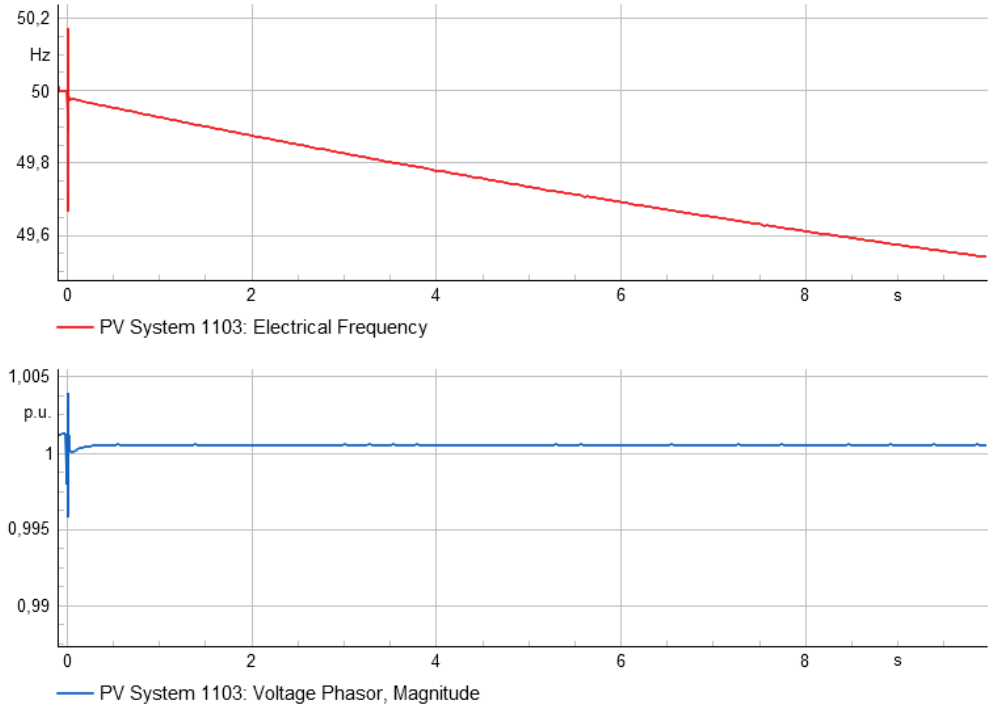


**Figure C.33:** Frequency and voltage magnitude graphs for disconnection at 0 seconds, performed in PV-grid model with generation equal load values.

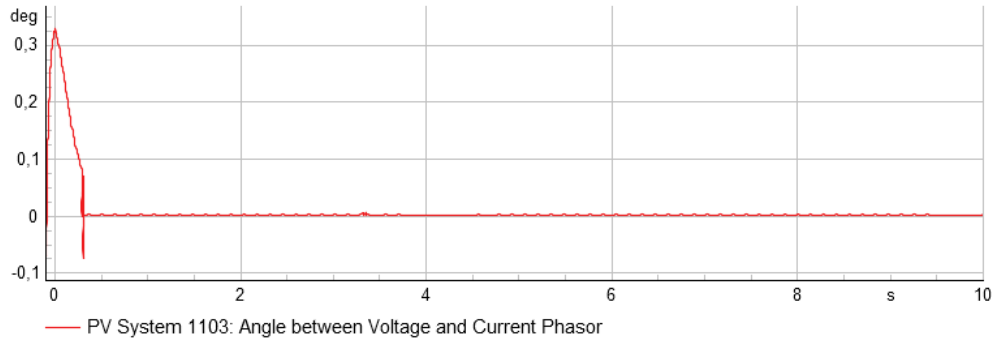


**Figure C.34:** Angle difference between voltage and current when the grid disconnects at 0.3 seconds, performed in PV-grid model with generation equal load values.

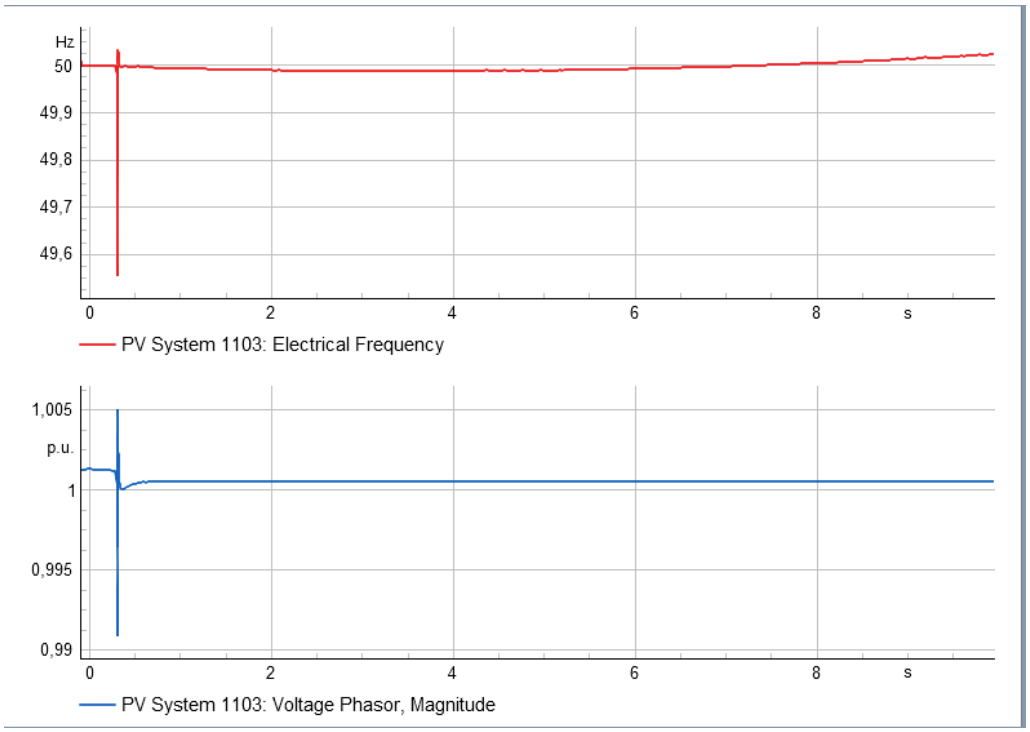


**Figure C.35:** Frequency and voltage magnitude graphs for disconnection at 0.3 seconds, performed in PV-grid model with generation equal load values.

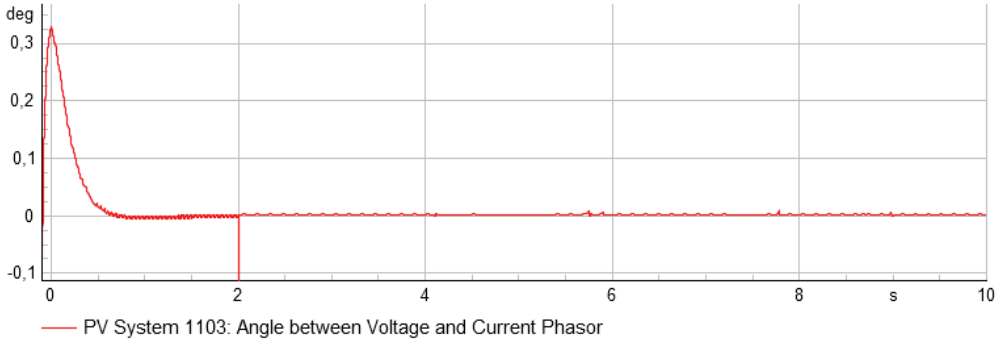


**Figure C.36:** Angle difference between voltage and current when the grid disconnects at 2 seconds, performed in PV-grid model with generation equal load values.

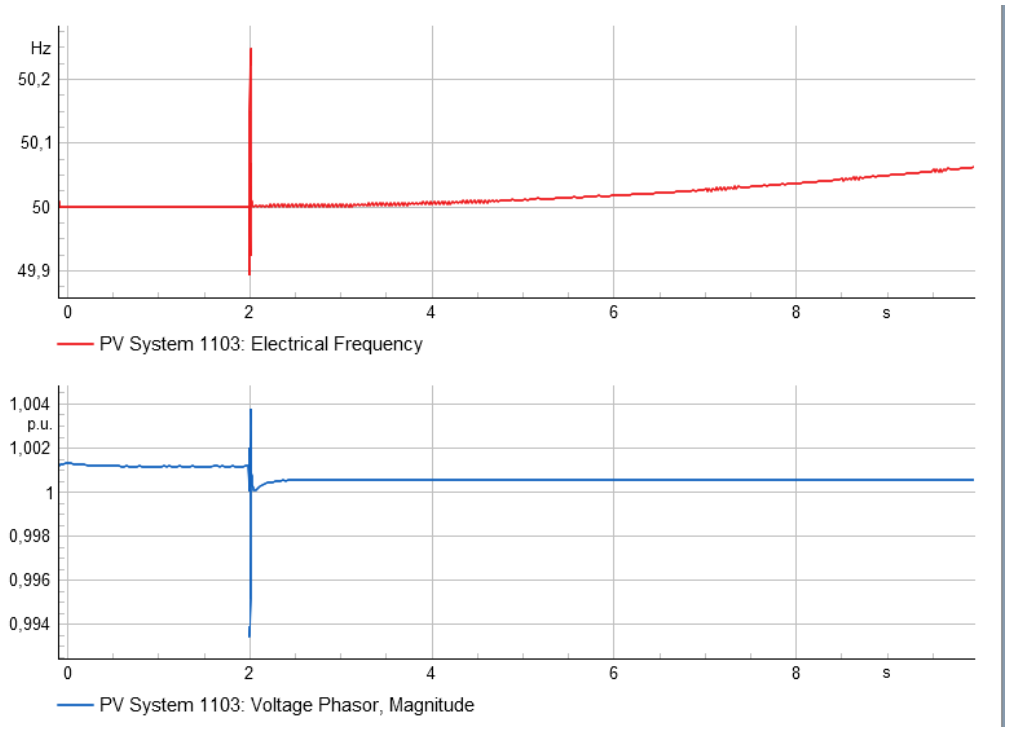


**Figure C.37:** Frequency and voltage magnitude graphs for disconnection at 2 seconds, performed in PV-grid model with generation equal load values.

**DEPARTMENT OF ELECTRICAL ENGINEERING**
**CHALMERS UNIVERSITY OF TECHNOLOGY**
Gothenburg, Sweden
www.chalmers.se


CHALMERS
UNIVERSITY OF TECHNOLOGY